Membranes Based on Metal-Organic Frameworks (MOFs) or Zeolites and New Membrane Concepts for Hydrogen Purification

VON DER NATURWISSENSCHAFTLICHEN FAKULTÄT DER

GOTTFRIED WILHELM LEIBNIZ UNIVERSITÄT HANNOVER

ZUR ERLANGUNG DES GRADES

Doktor der Naturwissenschaften

(Dr. rer. nat.)

genehmigte Dissertation

von

Sebastian Friebe, M. Sc.

2017

Referent: Prof. Dr. rer. nat. Jürgen Caro

Korreferent: Prof. Dr. rer. nat. Armin Feldhoff

Weiterer Korreferent: Prof. Dr. Aisheng Huang

Tag der Promotion: 24.03.2017

Preface

The presented results of this thesis were obtained during my time as Ph.D. candidate in the workgroup of Prof. Caro at the Institute of Physical Chemistry and Electrochemistry at the Gottfried Wilhelm Leibniz University Hannover from January 2014 to January 2017. In this period, I worked as a research assistant for the European project **M^4CO_2** (Energy efficient **M**OF-based **M**ixed-**M**atrix-**M**embranes for **CO_2** capture).

Five research articles - all emerged with my contribution as first author or as co-author, respectively - are presented in this thesis. In addition, I authored several additional publications and one patent, which are not included here but listed in the Appendix. For all these articles, I would like to express my deepest respect for all the valuable comments and stimulating discussions from my coworkers, reviewers and project partners in M^4CO_2, especially Prof. Dr. Jürgen Caro, Prof. Dr. Freek Kapteijn & Prof. Dr. Jorge Gascon (both TU Delft, Netherlands), Prof. Dr. Joaquin Coronas (Unizar, Spain) and Prof. Dr. Christian Serre (CNRS-ILV, France). The following announcement will clarify my made contribution towards the successful publication of those articles.

The first two articles about MOF membranes and corresponding composite membranes (Mixed-Matrix-Membranes (MMMs), multilayer membranes), *"NH_2-MIL-125 as Membrane for Carbon Dioxide Sequestration: Thin Supported MOF Layers Contra Mixed-Matrix-Membranes"* and *"Metal-Organic Framework UiO-66 Layer: A Highly Oriented Membrane with Good Selectivity and Hydrogen Permeance"* in chapter 2 were written by me. I prepared the MOF membranes and the corresponding composite membranes, namely the multilayer membrane and the MMMs. In addition, I performed the corresponding characterizations like infrared spectroscopy (IR), X-ray diffraction (XRD) analysis, scanning electron microscopy (SEM), energy dispersive X-ray spectroscopy (EDXS) and carried out the permeation measurements. Nevertheless, I kindly thank Daniel Unruh, Benjamin Geppert and Frank Steinbach for their support and technical help concerning IR spectroscopy, EDXS and Rietveld-refinement. Furthermore, I appreciate Alexander Mundstock for his support during the experiments and writing, since he helped me to improve the quality of the manuscripts to a high degree.

The third research article in chapter 2, "*Comparative Study of MIL-96(Al) as Continuous Metal-Organic Frameworks Layer and Mixed-Matrix Membrane"* was also written by me. I carried out a great part of the membranes characterization in terms of SEM and permeation measurements. However, I kindly thank Alexander Knebel for all help regarding the preparation and characterization of the membranes, since the results were achieved during his master thesis under my supervision. Furthermore, I appreciate Nadja Bigall, Marvin Benzaqui and Prof. Dr. Christian Serre for stimulating discussions and support during the writing process. They helped me to improve the quality of the manuscript to a valuable degree.

The fourth research article in chapter 2 about zeolites, "*On Comparing Permeation Through Matrimid®-based Mixed Matrix and Multilayer Sandwich FAU Membranes: H_2/CO_2 separation, support functionalization and ion exchange*" was written by my colleague Alexander Mundstock. My contribution was the preparation of the zeolite based MMMs and the multilayer membrane as well as and their characterization in terms of SEM and EDXS. Furthermore, I helped him with the improvement of the manuscript, especially in terms of the evaluation of the gas separation results.

The research article in chapter 3, *"Inverted Fuel Cell: Room-Temperature Hydrogen Separation from an Exhaust Gas by Using a Commercial Short-Circuited PEM Fuel Cell without Applying any Electrical Voltage"* was written by me with the help of Prof. Caro. I built up the setup for the usage of the fuel cell as membrane and membrane reactor and carried out the measurements of the separation performance. However, I would like to appreciate Benjamin Geppert for his help and technical support concerning the measurements with the resistive cascade. Furthermore, I thank SolviCore GmbH & Co. KG in Hanau for supplying the Nafion membranes and Volkswagen Technologiezentrum Isenbüttel for supplying the fuel cell.

Acknowledgement

I would like to give my appreciation to a great number of people, who have supported me during my research time as Ph.D. candidate at the Institute of Physical Chemistry and Electrochemistry at the Gottfried Wilhelm Leibniz University Hannover, since the credit for this thesis does not belong to me alone.

First and foremost, I would like to express my deepest and whole-hearted gratitude to my supervisor Prof. Jürgen Caro for the opportunity to carry out this interesting research in his work group. He helped me a great deal with his insightful guidance and his patient, invaluable support from day one of this work. Furthermore, he provided an atmosphere of trust, passion for science, kindness and friendship in his international working group.

The financial support of the European project M^4CO_2 is acknowledged. Moreover, I am thankful to my project and cooperation partners, particularly Prof. Freek Kapteijn, Prof. Jorge Gascon, Prof. Joaquin Coronas, Prof. Christian Serre, Prof. Marco Daturi, Prof. Franz Renz, Dr. Shuai Cao, Dr. Lars Heinke, Dr. Nadja Bigall, Dr. Dirk Dorfs as well as all their involved coworkers.

Additionally, I would like to express my thanks to all current and former group members in Prof. Caro's group, especially Prof. Armin Feldhoff, Frank Steinbach, Alexander Mundstock, Benjamin Geppert, Michael Bittner, Karsten Lange, Ina Strauß, Alexander Knebel, Dr. Olga Ravkina, Dr. Lisa Diestel and Dr. Kaveh Partovi for the wonderful friendly atmosphere, for stimulating discussions and support during my work as well as for the great time besides the day-to-day life in science.

Yvonne Gabbey-Uebe, Kerstin Janze, Wilfried Becker, Peter Mühr, Markus Köhler and Jan Kuckuck are appreciated for their continuous assistance in terms of administrative or technical things, for solving mundane arising problems and for the humorous working climate.

Moreover, I also thank all other coworkers of the Institute of Physical Chemistry and Electrochemistry.

I appreciate a lot of people from other institutes and workgroups, in addition. Especially, I want to thank Daniel Unruh, who always had a sympathetic ear and accompanied me since the beginning of the study in chemistry.

Furthermore, I would like to thank all supervised student apprentices, bachelor's degree and master's degree candidates for their help in terms of experimental and scientific aspects.

Words fail me to express my sovereign appreciation to my wife Isabell for her solace, her support and her unswerving love during the progress of this work and extending beyond. I also want to thank my family and my friends for diverting me just at the right time.

Abstract

The present thesis is dedicated to the preparation of new Metal-Organic Framework (MOF) and zeolite based membranes as well as the development of new membrane concepts for the purification of hydrogen from simulated waste gases. Different experimental approaches were followed to improve the membrane quality as well as the separation performance of said membranes.

Three new MOF membranes with varying pore sizes and linker functionalities as well as their corresponding composite membranes, such as Mixed-Matrix-Membranes (MMMs) and multilayers were synthesized on ceramic alumina supports for hydrogen purification. As a first candidate, **NH_2-MIL-125** with uncoordinated amino functions in the porous framework allows the adsorption based separation of hydrogen from carbon dioxide as supported MOF layer as well as corresponding MMM with different weight fractions. Furthermore, the partly reaction of these amino functions with the polymer matrix ensures a gapless embedment and, therefore, good separation capabilities of the MMMs. Another candidate for hydrogen purification is the MOF **UiO-66**, which was prepared highly oriented via a modulated synthesis approach and showed a soft molecular sieve separation behavior with increasing gas size, due to the linker flexibility within the framework. By covering this MOF layer with an additional thin polymer layer, the separation capabilities could be drastically enhanced, thus resulting in a membrane with a sharp molecular sieve cut off. The third investigated MOF was **MIL-96**, which features a very narrow pore size as well as a virtual two dimensional pore system as a consequence of the unique pore structure, thus resulting in crystal facet dependent separation capabilities. The corresponding MMMs gave insight in problems occurring during preparation in dependence of the used filler size.

Supported **FAU** membranes and corresponding ion-exchanged powder based MMMs were also prepared to separate hydrogen. The quality of the neat FAU layers showed increased separation performance as a consequence of different support pre-treatments, such as functionalization with APTES (3-aminopropyltriethoxysilane) or PDA (polydopamine). In contrary, the MMM performance could be related to the ionic potential of the cation used for the post-synthetic ion-exchange.

A commercial short-circuited Nafion based proton exchange membrane (PEM) fuel cell was investigated as new concept for the hydrogen purification. By using an inert sweep gas, hydrogen was separated with 100 % selectivity from different simulated waste gases. The proton flux became adjustable by inserting a resistor in the electron's way of migration. The fuel cell was also used as catalytic membrane reactor for olefin hydration.

Keywords: Metal-Organic Framework membrane, Zeolite membrane, Mixed-Matrix-Membrane, hydrogen purification, pre- and post-synthetic modifications, PEM fuel cell

Kurzfassung

Die vorliegende Arbeit behandelt die Herstellung von MOF- und Zeolith-basierten Membranen sowie die Entwicklung neuer Membrankonzepte zur Aufreinigung von Wasserstoff aus simulierten Abgasen. Verschiedene experimentelle Ansätze wurden verfolgt, um die Membranqualität und dadurch deren Trenneigenschaften zu verbessern.

Drei neue trägergestützte MOF-Membranen mit verschiedenen Porengrößen sowie Linkerfunktionalitäten und entsprechende Kompositmembranen, wie *Mixed Matrix Membranen* (MMMs) und Sandwich-Membranen, wurden für die Aufreinigung von Wasserstoff hergestellt. **NH_2-MIL-125** besitzt frei zugängliche Aminogruppen im Gerüst und erlaubt somit die adsorptionskontrollierte Trennung von Wasserstoff und Kohlenstoffdioxid. Zudem stellt die Reaktion der Aminogruppen mit der Matrimid-Polymermatrix eine lückenlose Einbettung und daher gute Trenneigenschaften der MMMs sicher. Der MOF **UiO-66** als weiterer Kandidat zur Wasserstoffaufreinigung wurde mittels modulierter Synthese als orientierte Schicht hergestellt und zeigte, aufgrund der Gerüstflexibilität, nur schwaches Molekularsiebverhalten in der permeativen Trennung unterschiedlich großer Gase. Durch Aufbringen einer dünnen Polymerschicht konnten die Gastrenneigenschaften dieser MOF-Membran drastisch verbessert werden, sodass die Membran nun einen Molekularsiebcharakter aufwies. Der dritte untersuchte MOF, **MIL-96**, besitzt eine geringe Porengröße sowie ein virtuelles zweidimensionales Porensystem. Aufgrund der einzigartigen Porenstruktur resultieren anisotrope Separationseigenschaften, die von der Kristallorientierung, d.h. den Kristallfacetten abhängen. Bei der Präparation der entsprechenden MMMs wurden Probleme wie Sedimentierung, Aggregation und sekundäre Kristallisationsprozesse in Abhängigkeit der Größe des Additivs identifiziert.

Trägergestützte **FAU**(Faujasit)-Membranen und entsprechende MMMs mit ionenausgetauschten FAU-Pulvern wurden hergestellt und hinsichtlich der Wasserstoffabtrennung untersucht. Die Zeolith-Schichten zeigten dabei verbesserte Eigenschaften in Abhängigkeit der Funktionalisierung des Trägers mit APTES (3-Aminopropyltriethoxysilan) oder PDA (Polydopamin). Das Trennverhalten der MMMs konnte mit dem Ionenpotential des ausgetauschten Kations korreliert werden.

Eine kurzgeschlossene Nafion-basierte Protonenaustauschmembran-Brennstoffzelle wurde als neues Membrankonzept zur Wasserstoffabtrennung untersucht. Durch Spülen mit einem inerten Gas konnte Wasserstoff mit 100 % Selektivität aus verschiedenen Abgasen abgetrennt werden. Der Protonenfluss wurde durch den Einbau eines Widerstands in den Pfad der Elektronen einstellbar. Die Brennstoffzelle wurde zudem als katalytischer Membranreaktor für die Olefinhydrierung verwendet.

Keywords: MOF-Membran, Zeolith-Membran, Mixed-Matrix-Membran, Wasserstoffabtrennung, Funktionalisierung, PEM-Brennstoffzelle

Abbreviations

APTES	3-aminopropyltriethoxysilane
CPO	Crystal Preferred Orientation
DFT	Density Functional Theory
DMF	Dimethylformamide
EDXS	Energy Dispersive X-ray Spectroscopy
EXAFS	Extended X-ray Absorption Fine Structure
FAU	Faujasite
IR	Infrared
LTA	Linde Typ-A
MIL	materiauxs de l’institut Lavoisier
MMM	Mixed-Matrix Membrane
MOF	Metal-Organic Framework
PCN	Porous Coordination Network
PCP	Porous Coordination Polymer
PDA	Polydopamine
PEM	Proton Exchange Membrane
PSA	Pressure Swing Adsorption
PSPM	Polymer Stabilized Percolation Membrane
SBU	Secondary Building Unit
SEM	Scanning Electron Microscopy
UiO	Universitetet i Oslo
XRD	X-ray Diffraction
ZIF	Zeolitic Imidazolate Framework

Contents

1. Setting the Scene

1.1 Historical Membrane Development

Earliest investigations on membrane phenomena date back to the 18th century. For instance, in 1748 *Jean-Antoine Nollet* experimented on water permeation through a diaphragm (pig's bladder). He found a direction-dependent mass transport and applied the word "osmosis" for the first time[1]. About a century later (1855), *Adolf Fick* recognized empirically that compounds move from the concentrated to the less concentrated side of an interface, as a result of a gradient in concentration. Therewith, he established the two diffusion laws of molecules in dependence of position and time[2]. Ten years later (1864) *Moritz Traube* developed the first synthetic semipermeable glue-based membrane, which was later used for experiments by other scientists. Furthermore, he suggested the atomic sieve theory for the first time to explain the semipermeable behavior of his artificial membrane[3]. In 1866, for the first time, *Thomas Graham* separated gases via a rubber membrane[4]. It follows from his findings that different gases feature varying diffusion velocities and that the latter is dependent on the molecular mass of the gases[5].

Figure 1: *Scientists, which pioneered the modern membrane science for separation. Jean-Antoine Nollet, Adolf Fick, Moritz Traube, Thomas Graham (from left to right).*

All these scientists were pioneers in the early membrane science and had a formative influence on the later research fields. However, it lasted until the early 1930's, since microporous collodion (nitrocellulose) membranes were commercially available[6,7,8]. From this on to the early 1950's, membranes were tried to bring to the industrial relevant level for separation processes. Despite the availability of versatile polymer materials, useful membranes for separation were non-producible at this time. Ever since the works of *Sidney Loeb & Srinivasa Sourirajan* in the early 1960's, the membrane research was brought to a new level. Their developed process ensured the defect-free production of high-flux reverse osmosis membranes, which consisted of thin selective top layers on much thicker non-selective microporous supports for stability and mechanical strength[9,10]. This breakthrough in membrane fabrication and the following period from 1960 to 1980 brought out a significant change in the status of membrane technology. Progression of the original *Loeb-*

Sourirajan process and the use of composite materials or other membrane geometries led to a lot of high-performance membranes[11,12,13]. However, despite the development of thousands of different materials to yield high-performance membranes during the last four decades, only a few of them are used in practice-relevant separation processes up to now, since roughly 90 % off those membranes are made from less than ten materials[14,15].

1.2 Motivation

Membrane assisted gas separation technology has gained a lot of interest during the last four decades, especially with respect to the conservation of energy and the associated cost reduction in comparison to conventional methods like (cryogenic) distillation or pressure swing adsorption (PSA)[16,17]. Compared to the latter methods, the energy demand of a membrane process is lower, since it gets along without a regeneration step, for instance[18]. In general, a membrane can be simply defined as a discrete material barrier, having lateral dimensions greater than its thickness, which enables a preferential pathway of one species in a mixture of two or more adjacent components under a variety of driving forces[19].

Depending on the aided driving force such as a concentration gradient, membrane technology can be employed on industrial relevant processes like O_2/N_2 separation, H_2 recovery from process gas streams, CO_2 removal from flue gas, hydrocarbon gas separation or dewatering[20]. Nevertheless, if looking at the importance, hydrogen purification seems to be one of the most interesting tasks due the ever-increasing energy consumption and the associated environmental problems[21]. At the moment, hydrogen is mainly produced by steam-gas reforming of fossil fuels (e.g. coal, natural gas, oil) followed by the water-gas shift reaction, thus getting converted to a H_2/CO_2 gas mixture by several partial oxidation and reforming steps[22,23]. However, before the hydrogen is utilizable as energy source for the production of electricity (combustion in a turbine or fuel cell) it has to be de-polluted from the remaining contaminants, such as CO, CO_2 and CH_4[24]. As mentioned above, this purification can be done more economic than compared to other methods like PSA or cryogenic distillation with the help of suitable membranes. Especially the simplicity of installation and operation, low requirements in terms of maintenance and space and the good process flexibility are beneficial versus the traditional methods. Moreover, the possible up scaling or down scaling speak for membrane assisted separation processes[25]. Consequently, the chemical industry has paid a lot of attention to the membrane assisted separation technology recently.

Membranes, in general, can be classified in terms of their chemical composition and their operating principle. The former can be roughly divided into organic (polymeric) and inorganic materials, while the latter is broadly an interplay between diffusion- and adsorption based separation[26].

Due to their mechanical and chemical stability, low costs and their simple processing, polymeric membranes have great potential for industrial relevant processes[25,27]. Consequently, the majority of industrial membrane separation processes is realized with polymeric materials so far. Unfortunately, they may suffer from instability at high temperatures, low fluxes and low selectivities, thus limiting their performance as predicted by Robeson[28,29]. Hence, the interest in new membrane materials as well as new membrane concepts is still continuing.

Inorganic membranes, for example, can be roughly classified in dense (metals or perovskites)[30,31] and porous membranes (zeolites, microporous silica)[32]. However, the classification in dense or porous membranes is solely a matter of the different permeation mechanisms through the materials. Dense membranes transport species (e.g. molecules, protons, oxygen ions) via the solution-diffusion mechanism[33]. Thus the separation is based on the difference in solubility and mobility of the different solutes in the membrane. In contrary, porous membranes can have several diffusion based separation principles such as convective flow, surface diffusion, Knudsen-Diffusion or molecular sieving depending on the pore size of the material[26].

Molecular sieve zeolites, for example, have attracted a lot of interest during the past thirty years, due to their uniform pore structure and their great thermal and chemical stability. Furthermore, the possibility to modify their framework by structure directing agents (SDAs) or post synthetic approaches, such as ion-exchange, and the easy synthesis speak for them as membrane materials[34,35].

However, among all available porous materials, Metal-Organic Frameworks (MOFs) have gained the greater interest during the past two decades. The diversity of MOF chemistry allows the tailored synthesis of an almost unlimited number of microporous structures[36]. Additionally, these structures can be modified with functional linkers or can possess unsaturated accessible metal sites as adsorption centers for different gases[37]. Based on their synthesis via the building block concept and the associated adjustable pore sizes and adsorption properties, MOFs are promising candidates for versatile separation processes[38,39]. However, despite some pioneering activities and plenty work in the development of supported MOF-based membranes, the *scale up* and reproducibility of these defect-free MOF membranes is still a major challenge, due to their fragile nature. Consequently, supported MOF membranes have not yet been used for industrial relevant separation. An interesting approach to overcome this problem is the fabrication of so called Mixed-Matrix-Membranes (MMMs).

MMMs, a combination of a polymer matrix and embedded filler particles (MOFs, zeolites, carbon etc.), combine the good properties of both, the inorganic filler (permselectivity) as well as the polymer (mechanical stability)[40]. Moreover, MMMs may be able to close the gap between neat MOF-layers and neat polymer membranes, due to the combination of all the positive properties of both materials in one composite[41,42]. As a consequence of the latter, they may be applicable for membrane-assisted processes like separation of different gases, pervaporation or removal of undesired contaminants[43,44]. Additionally, by preparing the MMMs as hollow fibers or as coiled modules there is great potential to become competitive to existing techniques and the successful preparation of nano-scale MOFs will allow the preparation of high-permeance MMMs which can compete with polymer membranes.

The aim of this thesis is, therefore, the preparation of new Mixed-Matrix-Membranes based on MOFs or zeolites as well as the development of new membrane concepts for the purification of hydrogen from different simulated waste gases.

1.3 Metal-Organic Frameworks (MOFs)

1.3.1 History and Designation of MOFs

About twenty years ago the appellation Metal-Organic Framework (MOF) appeared for the first time in literature[45]. Since then, the development of new MOFs literally exploded. However, there was no clear definition in terms of their name and consequently they were also called Porous Coordination Polymers (PCPs) or Porous Coordination Networks (PCNs), making a uniform definition inevitable[46]. Following the common zeolite naming system, MOFs were then most frequently classified with three letters plus one number. Nevertheless, due to the lack of a distinct clarification, MOFs with different names often are still quite the same (e.g.: M_2dhtp, MOF-74)[47].

Thus, scientists developed different approaches to categorize MOFs in to different classes. For instance Kitagawa et al. divided the MOFs in terms of their stability upon de-/sorption processes, while others like Férey classified MOFs with respect to the connectivity of the so called secondary building unit (SBU)[36,48]. Until now the classification is commonest based on the university's origin (e.g. UiO: Universitetet i Oslo, MIL: materiauxs de l'institut Lavoisier) or specific similarities, such as topologies (c.f. ZIF: Zeolitic Imidazolate Framework)[49,50]. Since the beginning of MOF research in the year 1995 up to now a huge quantity of new MOF structures have been developed and investigated in terms of their properties and concomitant use for gas purification and several other promising applications.

1.3.2 MOFs: Structure and Properties

Metal-Organic Frameworks (MOFs) are hybrid inorganic-organic materials, consisting of metal-containing clusters or discrete metal ions as inorganic nodes and organic linker molecules, bridging them to well-defined periodic structures[36]. As shown in Figure 2, the network structures of MOF-5 and ZIF-8 were chosen to describe the general buildup of MOFs, consisting of inorganic metal clusters or discrete coordinated metal ions as secondary building unit (SBU) and organic linkers (1,4-benzene-dicarboxylate, 2-methyl-imidazolate)[49,51].

As a result of their building-block construction in a tailor-made fashion, MOFs are one of a kind in terms of their variable properties. They can be designed by well-wrought plans, thus resulting in unique requested properties, such as large specific surface area, adsorption sites or pore sizes[37,39]. Furthermore, by using the right starting materials, MOFs can also work as smart materials, therefore, being applicable as sensors or re-/acting as a consequence of external stimuli[52]. By means of Figure 3, the variability of MOF synthesis for specific applications and the inserting of different exemplary functional groups can be demonstrated.

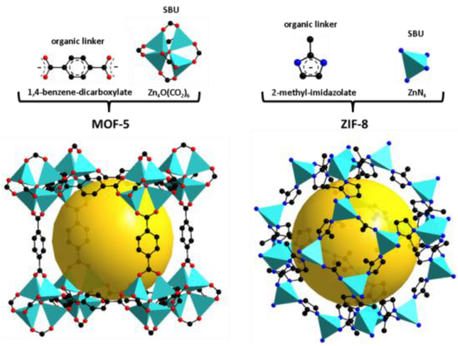

Figure 2: *General construction of MOFs with different kind of linkers. MOF-5 structure, consisting of terephthalate bridged Zn_4O^{6+} clusters, thus forming a cubic structure (left). Zn^{2+} cations coordinated via 2-methylimidazolate, resulting in the sodalite topology of the ZIF-8 framework (right).*

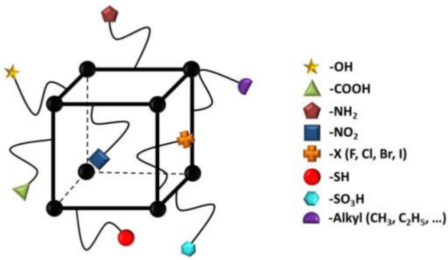

Figure 3: *Exemplary demonstration of inserting different common functional groups during MOF synthesis by using linkers with specific functionalities.*

Due to the unlimited possibility to modify the MOF's properties, they are promising candidates for several applications. For example, they feature potential for gas storage, separation, catalysis, drug release, sensing, or as remote controlled materials[37,39,52]. Consequently, the research area of MOFs has boomed in the past two decades.

1.3.3 Structures and Properties of NH_2-MIL-125, UiO-66 and MIL-96

NH_2-MIL-125 is an example of a MOF structure with a functional linker. It is constructed of cyclic TiO_4 octamers, which are connected via the 2-amino terephthalate linkers and forms a tetragonal structure. The construction results in two different cages, which are connected by windows of round about 6 Å[53,54,55]. The position of the NH_2-function is not precisely defined up to now. However, since it does not coordinate in the structure, the NH_2 group displays an adsorption center[56]. Furthermore, it also decreases the pore size to a reasonable degree. Due to the latter facts and the overall robustness of NH_2-MIL-125 in harsh conditions, it is under intense study as a candidate for adsorption of acidic gases, such as CO_2 or H_2S. For instance, in comparison to the un-functionalized counterpart, NH_2-MIL-125 shows a drastic enhanced adsorption capacity for CO_2, as reported in different works[57,58]. Furthermore, it has been well investigated in terms of the adjustment of particle size and morphology by appropriate modulators[59]. The mentioned facts make NH_2-MIL-125 an interesting material for membrane fabrication as well as filler material for the preparation of composite materials. The latter could benefit from the interactions between amino group and matrix, resulting in a gapless embedment.

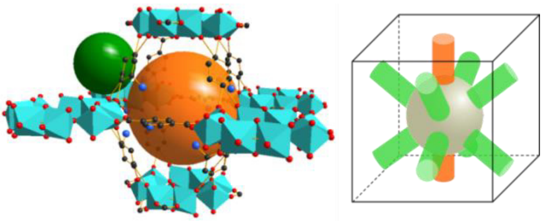

Figure 4: *Structure of NH_2-MIL-125 (left) and schematical representation of the corresponding 3D channel system (right). Each cage (octahedral: orange; tetrahedral: green) is filled with several amino functions (blue spheres).*

The reaction of zirconium chloride and terephthalic acid reveals another MOF structure, which is termed **UiO-66** (Universitetet in Oslo). Like a lot of other zirconium-based MOFs[60,61,62], UiO-66 shows exceptional stability against chemicals, temperature and mechanical stress[63,64]. Therefore, it is a promising material for the fabrication of robust membranes as already shown for CO_2/N_2 separation under harsh conditions recently[65]. Furthermore, it has already been well investigated in terms of the pore functionalization[66,67], different synthesis routes[68,69], flexibility and mechanical properties[70]. Additionally, the structural characteristics including the crystallographic positions of the atoms were investigated in detail via DFT calculations in combination with EXAFS measurements and Rietveld refinements by Lillerud et al. and Lamberti et al.[71,72]. Their works clarified, that the 3D structure of UiO-66 consists of $Zr_6O_4(OH)_4$ nodes as inorganic subunit, which are each twelvefold bridged to other nodes via the benzene 1,4-dicarboxylate linker, resulting in triangular windows with a size of 6 Å [73,74,75] (c.f. Figure 5). These windows connect two types of cages (octahedral: 11 Å Ø, tetrahedral: 8 Å Ø)[76].

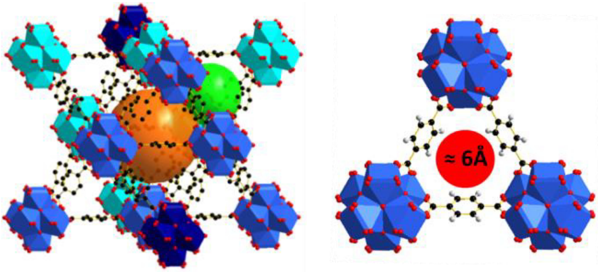

Figure 5: *Structure of UiO-66 (left) and schematical representation of the corresponding windows of about 6 Å (right), which connect both the octahedral (orange) and tetrahedral (green) cages.*

Like the majority of Zr-based MOFs, also a lot of Al-based MOFs show great potential for fabrication of membranes, due to their good stability. For instance, the reaction of $Al(NO_3)_3 \cdot 9H_2O$ with the tridentate linker trimesic acid (1,3,5-benzene-tricarboxylic acid) results in a MOF termed **MIL-96**, which is stable in water and up to 300 °C[77,78,79]. The alumina octahedral building units show a very rare structure, containing corner-sharing chains of metal octahedra bridged by 3µ-oxo centered trinuclear units in the c-direction of the hexagonal unit cell as characteristic element (c.f. Figure 6)[80,81]. The 3D MOF structure has a unique feature, since there is no direct connection between two equal cavities, as a result of the 3µ-oxo clusters baring the passage. Hence, one of the cavities acts as junction between the other ones. Furthermore, the window size in a certain crystallographic direction is very narrow, thus sealing this path gas-tight. The above mentioned idiosyncrasies result in a virtual 2D pore network, which allows solely a "zigzag" gas transport. The latter features a dependence on the crystal morphology, as already shown for other systems[82].

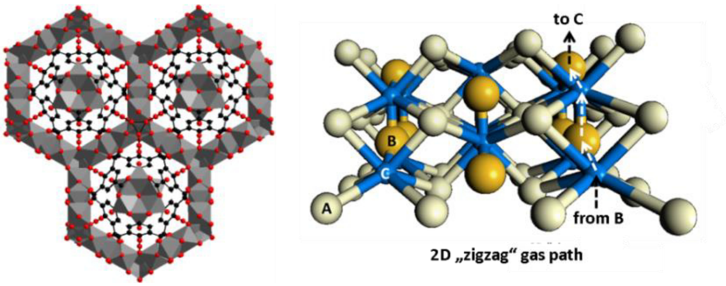

Figure 6: *Structure of MIL-96 in c-direction showing the characteristic 3µ-oxo clusters baring the passage (left). Schematical representation of the corresponding "virtual" 2D pore system, which solely allows a gas transport between cavity B and C.*

1.3.4 Differentiation to Zeolites

In comparison to MOFs, zeolites are sheer inorganic materials. These aluminosilicates are minerals, commonest constructed from connected tetrahedral SiO_4 and AlO_4 units and counter ions, such as alkali metals like Na^+, K^+ or alkaline earth metals like Mg^{2+} or Ca^{2+}, for charge neutrality[83]. By changing the Si/Al ratio, the properties (e.g. hydrophilicity, iconicity, acidity, stability) of the resulting zeolite can be affected[84]. As an example, zeolite faujasite is most often prepared as NaX with a Si/Al ratio of 1.2-1.5. It consists of sodalite cages, which are bridged to a 3D network via 12-membered oxygen ring pores with a size of approximately 7.4 Å. Furthermore, in activated state, NaX features dehydrated metal ions, which affect the adsorptive interactions with different gases (e.g. CO_2, ethylene, propylene)[85,86]. Consequently, despite the longish awareness of zeolites, they are still promising materials for separation approaches or other potential applications such as adsorbents, catalysts or sensors, due to their uniform pore structure, the opportunity for post-synthetic functionalization, such as ion-exchange or grafting, and their overall robustness in harsh conditions and high temperatures.

1.3.5 Introduction to Porous MOF and Zeolite Membranes

Porous membranes of MOFs or zeolites can either be prepared as self-supported (symmetric) or supported (asymmetric) layers. However, so far, there are only some occasional reports of self-supported membranes of both material classes, since they always suffer from mechanical instability[87,88]. Due to the latter, these self-supported layers have become uninteresting for separation applications, since their tough processability and handling go with severe issues. Consequently, MOF and zeolite membranes were merely used as supported layers (e.g. on ceramic alumina disks). But the defect-free, reproducible preparation of such supported membranes is still a challenging task[89,90]. Furthermore, up to now, only a few supported zeolite membranes are applied for an industrial separation process (e.g. LTA for alcohol dewatering)[34], while supported MOF membranes still wait for their turn.

1.4 Mixed-Matrix-Membranes (MMMs)

1.4.1 General Aspects and Opportunities of MMMs

As mentioned above, the defect-free preparation of supported zeolite or MOF membranes is a great issue in terms of their usage for separation processes. Therefore, the success of the future membrane market requires a breakthrough in terms of high-performance membranes, which combine low-costs, easy processability and mechanical stability. The mentioned breakthrough should give rise to a membrane, which can compete with the efficiency of molecular sieve (MOFs and zeolites) and polymer membranes.

All aforementioned may be within reach via the concept of the Mixed-Matrix-Membranes (MMMs)[42,43,91]. The latter is an organic-inorganic hybrid composite material consisting of a continuous polymeric matrix and dispersed/embedded inorganic filler materials (c.f. Figure 7). The incorporated particles can either act as a simple transport barrier or as separation-active filler. Mixed-Matrix-Membranes provide all positive features of both materials. The polymer ensures favorable mechanical properties (flexibility, long-term stability, reproducibility) while the inorganic filler entails high permselectivity[40,91,92]. Hence it is assumed, that MMMs may close the gap between supported inorganic and polymer membranes. Despite all the positive features mentioned above for MMMs, there are still some problems to face. One severe problem is the incompatibility (low interaction) between the polymeric matrix and the embedded filler, due to a mismatch in polarity. Other difficulties to overcome are sedimentation, aggregation or even re-crystallization phenomena, depending on the nature, particle size and shape of the filler, for instance[93,94].

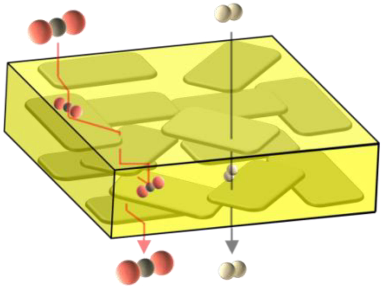

Figure 7: Schematic representation of a Mixed-Matrix-Membrane. The smaller component H_2 (black arrow) can easily pass the filler while the bigger CO_2 (red arrow) has to go the longer way around the molecular sieve particles, thus resulting in a separation of both components.

1.4.2 Classification of MMMs

As mentioned in chapter 1.4.1, a MMM is a composite material consisting of dispersed/embedded filler particles in a polymer matrix. The latter can either be a rubbery or a glassy polymer. The difference between these two types is the operating temperature in relation to the glass transition point and the concomitant transport behavior. Rubbery polymers, like a lot of Siloxanes, operate above their glass transition temperature. This allows an easy rearrangement of the polymer chains, thus affecting the separation performance. Consequently, rubbery polymers generally show great permeabilities at medium or low selectivities. The majority of these polymers separate components as a consequence of their solubility in the polymeric matrix and can, therefore, be used for the sequestration of volatile organic compounds, for example. In contrary to this, glassy polymers, such as Matrimid, operate below their glass transition temperature. Consequently, the polymer rearrangement is very unlikely, resulting in imperfectly packed chains, which goes hand in hand with the formation of excess free volume. Due to the presence of these micro-voids, a lot of glassy polymers work diffusion controlled. As a result of the facts mentioned above, glassy polymers often show great selectivities but medium or low permeabilities. They might, therefore, be utilizable for the separation of light gases[95,96,97,98].

Besides the polymeric matrix, also the filler can be classified into two different classes, namely inorganic and inorganic-organic fillers. Examples for the former class are silica, carbon or zeolites, for instance. A lot of these materials were already used in dense as well as porous form to investigate their capabilities as transport barrier or separation active filler[92]. For instance, the incorporation of zeolites has attracted a great interest for the preparation of MMMs in the past two decades, due to the combination of the molecular sieve properties of the filler with the mechanical features of the polymer[99]. However, as mentioned above, a severe intermittent issue with sheer inorganic materials is their incompatibility with the polymer matrix. Although there are measures to overcome these problems, such as the post-synthetic grafting with appropriate silanes[100,101], zeolite based MMMs show a declining tendency.

In contrary to this, MOFs as inorganic-organic materials feature a hybrid nature. Furthermore, by using appropriate linker molecules, MOFs can be functionalized during the synthesis[102] or even post-synthetic with diamines or other bidentate bridging components, for instance, to ensure a good interaction with the polymeric matrix and to increase their compatibility with their surroundings[103,104]. Thus, the formation of voids between the filler and the polymer can be avoided to a great degree. The reasons mentioned above go hand in hand with the fact, that the trend is towards MOF based MMMs and that they will more and more corner the market[105].

1.4.3 Limitations of MMMs

As mentioned in chapter 1.4.1, there are several problems to overcome, depending on the size, shape and nature of the used filler materials. For instance, if µm-sized crystals are used for preparation, the MMMs may suffer from precipitation and the formation of remaining unselective voids. In contrary, if the particles are nm-sized, they can form aggregates and even recrystallize to bigger crystals during conditioning, thus also leading to voids inside the polymer matrix[106,107]. These problems lead to inhomogeneous MMMs and non-optimal separation performances. As mentioned in chapter 1.4.2, one measure to eliminate these problems is the adjustment of the filler-polymer matching, thus increasing their compatibility by covalent or direct coupling[108,109]. A second important parameter to solve this issue is the viscosity of the casting solution. However, it turns out a difficult task to find and adjust the right viscosity for every casting approach and every polymer-filler pair anew.

Other effects affecting the MMM performance are the polymer rigidification around the embedded fillers or partial pore blockage due to polymer chains penetrating the filler's pore system. All these mentioned limitations affect the separation performance of the MMMs to a great degree but with different impacts. Figure 8 schematically demonstrates the mentioned theoretical problems and the concomitant effects on the gas separation capabilities of the MMMs.

Case I is the ideal MMM interfacial morphology, since the filler is embedded without any voids or changes in the polymeric structure. This is the most desired case, since it results in increased permeability as well as enhanced selectivity. Cases II and III belong to the same family of interfacial effects where the filler is not embedded ideally, resulting in huge (case II) or very small Å-sized – roughly the size of gaseous penetrants - voids (case III). These effects can be attributed to a weak polymer-filler interaction and result in increased permeability at constant or slightly reduced selectivity. However, it is very difficult to distinguish between both cases, since the transmembrane transport can also be a consequence of overlaying effects. Also cases IV-VI belong to the same origin of interfacial morphologies. While case IV and V can be attributed to a reduced permeability region in the whole zeolite (case IV) or the outer layer of the zeolite (case V), the origin of case VI is a rigidified and more structured polymer layer around the filler. All described phenomena result in decreased permeability and un/-modified selectivity. Nevertheless, as mentioned earlier, the determination of the exact interfacial effects is very hard, due to overlaying transport phenomena of the components through the membrane[92,93,94,110,111].

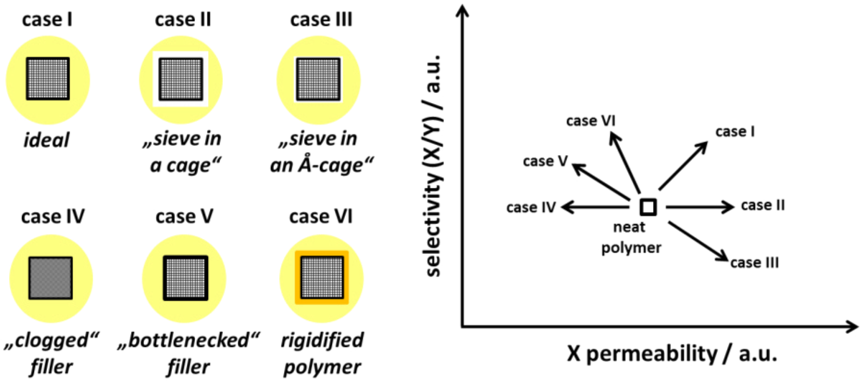

Figure 8: *Non-ideal effects & interfacial morphologies (left) and their corresponding theoretical result on the separation performance of MMMs with respect to the neat polymer membrane (right).*

1.5 Mass Transport in Membranes

1.5.1 General Aspects and Important Parameters

The quality of a membrane can be assessed by the overall mass transport properties, namely the amount of the permeated components and their resulting ratio at the permeate side. The former can be categorized in three general termini: 1) flux F, 2) permeance Π and 3) permeability P[19]. The flux F (Eq. 1) is the permeated amount n of a gas species i divided by time t and membrane area A. The permeance Π can be calculated by division of the flux by the pressure difference Δp between retentate and permeate side, while the permeability P is the product of the permeance with the membrane thickness d (c.f. Eqs. 2 & 3). The permeability is the fairest and commonest parameter to describe the transport properties of a membrane, since it reveals the material's intrinsic capabilities.

$$F = \frac{n_i}{t \cdot A} \qquad \text{(Eq. 1)}$$

$$\Pi = \frac{n_i}{t \cdot A} \cdot \frac{1}{\Delta p} \qquad \text{(Eq. 2)}$$

$$P = \frac{n_i}{t \cdot A \cdot \Delta p} \cdot d \qquad \text{(Eq. 3)}$$

The membrane selectivity in terms of the permeated components i and j can be expressed with the mixture separation factor $\alpha_{i,j}$, which is the fraction of the component's (i, j) molar ratio in the permeate, divided by the molar ratio of these components at the retentate side[19]. The latter can roughly be approximated with the feed composition, since only a small amount permeates through the membrane, resulting in a neglectable change in the retentate composition (Eq. 4).

$$\alpha_{i,j} = \frac{n_{i,p}/n_{j,p}}{n_{i,r}/n_{j,r}} \qquad \text{(Eq. 4)}$$

With the help of the aforementioned parameter pool, the membrane quality can be rated by permeation measurements. However, to generate a mass transport across a membrane, the presence of a driving force such as a partial pressure difference and the concomitant concentration gradient is inevitable. Therefore, the next two chapters introduce the permeation behavior in porous and dense membranes as well as some insight in diffusion and adsorption for said systems.

1.5.2 Mass Transport in Porous Membranes

The permeation across a membrane, except for molecular sieving, is always the interplay of diffusion and adsorption[112,113]. Therefore, the mass transport of components runs through different stages in general. First, the components adsorb on the outer surface of the porous membrane, followed by surface diffusion and bulk diffusion through the porous system. Lastly, after effusion from the porous system, the components desorb from the membrane surface again[114]. Figure 9 schematically displays the different separation mechanisms, namely molecular sieving as well as diffusion and adsorption controlled separation.

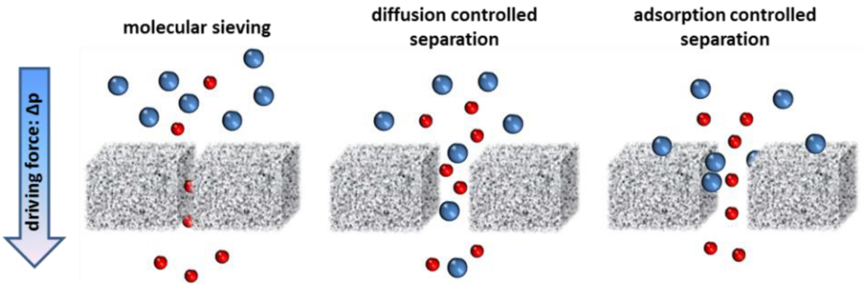

Figure 9: *Different separation mechanisms for porous membranes as a consequence of an outer driving force such as a pressure difference.*

As a rule of thumb, the overall membrane selectivity can be roughly predicted by multiplication of the diffusion selectivity with the adsorption selectivity[112,113]. Diffusion can generally be described as the enrichment of a component at a certain region and the depletion of the component density at the starting point. It can be expressed in the easiest form by Fick's first law (Eq. 5),

$$J_i = -D_i \nabla c_i \quad \text{with} \quad \nabla c_i = \frac{\partial c_i}{\partial x} \qquad \text{(Eq. 5)}$$

where J_i and D_i are the material flux and the Fickian diffusion coefficient, respectively, while ∇c_i is the concentration gradient in x direction. Based on Eq. 5, the material flux is assumed to be proportional to the concentration gradient, if the latter is not too high[115]. Following Fick's law, which is also utilizable for multi-component systems by some modifications including the mixture component diffusivity and the assumption, that one component is liquid, the diffusion is a consequence of the concentration gradient on the diffusion rate. The latter is formally right, however, the correct driving force is the chemical potential gradient $\nabla \mu_i$[116], which is implied by another diffusion law, namely the Maxwell-Stefan model. If the diffusion is considered as a mass transport driven by the chemical potential gradient and a frictional force, evoked by the diffusive velocity of another component, the easiest case - a two component system - can be described by the following equation 6

$$-\nabla\mu_i = RTx_j\left(\frac{\vartheta_i - \vartheta_j}{\mathfrak{D}_{ij}^{mix}}\right) \quad \text{with} \quad \nabla\mu_i = \frac{\partial\mu_i}{\partial x} \qquad \text{(Eq. 6)}$$

where R, $T$and x are the ideal gas constant, the temperature and the molar fraction of component j, while ϑ are the gas velocities of components i *and* j. $\mathfrak{D}_{ij}^{m}$ is the mixture Maxwell-Stefan diffusion coefficient[117,118]. For single component Maxwell-Stefan diffusion, the resulting physical law can be written in similar style as Fick's law of diffusion, if the chemical potential gradient is expressed with the help of the relationship between chemical potential and partial pressure p as well as the concentration gradient, like in equation 7.

$$J_i = \vartheta_i \cdot c_i = -\mathfrak{D}_i^s \cdot \left(\frac{\partial ln p_i}{\partial ln c_i}\right) \cdot \nabla c_i \qquad \text{(Eq. 7)}$$

where $\mathfrak{D}_i^s$ is the single gas Maxwell-Stefan diffusion coefficient of component i. If comparing Eqs. 5 and 7, the relation between the Fickian and the Maxwell-Stefan diffusivity can be expressed as follows:

$$D_i = \mathfrak{D}_i^s \cdot \left(\frac{\partial ln p_i}{\partial ln c_i}\right) \qquad \text{(Eq. 8)}$$

As mentioned earlier, the second important parameter to describe the mass transport through a porous membrane is the adsorption. The latter is a thermodynamic process, since there is an equilibrium with specific kinetic constants for adsorption k_{ads} and desorption k_{des}. In principle, the adsorption can result from chemical (chemisorption) or physical (physisorption) interaction of gaseous species with a surface. However, since chemisorption is a rather seldom phenomenon, the physisorption is more popular to describe adsorption processes[119]. At isothermal (constant temperature) conditions, the amount of adsorbed molecules at the surface is solely a function of pressure. A very feasible model to describe the adsorption of a single component on a surface is the Langmuir-Model[120], according to equation 9

$$\theta_i = \frac{K_i \cdot p_i}{1 + K_i \cdot p_i} \quad \text{with} \quad K_i = \frac{k_{ads}}{k_{des}} \qquad \text{(Eq. 9)}$$

where θ_i is the degree of coverage for component i, while K_i is the equilibrium constant. The Langmuir model can also be used for multi-component, multi side adsorption. For instance, the degree of coverage for component j in a binary mixture with component i can be expressed with equation 10.

$$\theta_j = \frac{K_j \cdot p_j}{1 + K_i \cdot p_i + K_j \cdot p_j} \quad \text{(Eq. 10)}$$

When looking at Eqs. 9 and 10, the linear relationship for the degree of coverage θ in dependence of the partial pressure becomes obvious, if the partial pressure is small. At higher feed pressures, the Langmuir isotherm runs into saturation[120]. Despite the presence of several other isotherms and models for the explanation of adsorption phenomena, the Langmuir model is sufficient enough to describe the adsorption processes and their impact on mass transport in porous membranes.

1.5.3 Mass Transport in Dense Membranes

Similar to porous membranes, the separation performance of polymeric membranes or MMMs also depend on the interplay of diffusion and adsorption. The diffusion in these membranes can be described with the same physical laws as discussed in chapter 1.5.2. However, the impact of adsorption on the separation performance is slightly different, since these types of membranes separate components via the solution-diffusion mechanism[33]. Consequently, the amount of adsorption for a specific gas molecule depends on the ability to be "soluted" in the polymeric matrix. This solubility strongly depends on interactions - like van der Waals forces - of the gaseous species with the polymer. As a rule of thumb, the solubility can be approximated with the help of the condensability of a gas (e.g. $C_4H_{10} > C_3H_8 > C_2H_6 > CH_4 > N_2 > H_2$), which goes roughly hand in hand with the molecular size[121]. Thus, large more condensable molecules are favored in terms of sorption selectivity. That is why CO_2, for instance, shows preferable sorption in polyimides in comparison to hydrogen. However, the solubility of components is strongly dependent on the temperature (after van't Hoff). Consequently, H_2/CO_2 separation should be done at higher temperatures to suppress the CO_2 adsorption. The permeability for polymer membranes and MMMs can then be written as the product of a diffusivity/mobility term *D* and solubility/sorption term *S* (equation 11)[26].

$$P = D \cdot S \quad \text{(Eq. 11)}$$

Equation 11 can be used as a first benchmark for the prediction of the MMMs' separation performance. However, the balance between the mobility term *D* and the solubility term *S* is different for glassy and rubbery polymers. For instance, the diffusivity in glassy polymers decreases far more drastically with increasing molecule size in comparison to rubbery polymers. Also the solubility shows different behaviors for the two polymer types. For glassy polymers the mobility term is usually dominant in comparison to the sorption term. Consequently, small molecules permeate preferentially. In contrary to the latter, in rubbery polymers the sorption term is usually dominant. Thus, larger molecules permeate preferentially, in general[122].

1.5.4 Dense Membranes: Subgroup Conductive Membranes

A specific type of dense membranes are conductive membranes, which generally separate components with infinite selectivity, since only one mixture component is able to permeate through the material of choice. For instance, conductive ceramics such as perovskites were already investigated as oxygen ion or proton conducting materials[123,124]. But also polymeric materials are known to be able for the use as conductive membranes. For example, Nafion as a sulfonated polytetrafluoroethylene is known to be an anion barrier but a cation conductor. Therefore, it is utilizable for proton transport[125,126]. Nonetheless, all these mentioned materials have in common, that the mass transport is based on ion conduction. Thus, the separation with these materials runs through different stages as compared to those mentioned in chapter 1.5.2. First, the gas molecules adsorb on the membrane surface, followed by splitting into ions and electrons with the help of an appropriate catalysts, if necessary. The ions then migrate through the membrane materials by various possible mechanisms (vacancy diffusion, Grotthus-mechanism, etc.)[127,128]. The electrons can either go the same way through the membrane (e.g. dual phase perovskites) or have to take a detour, if the membrane material is insulating for electrons (Nafion). At the permeate side, the gases recombine and desorb from the surface for further use.

For instance, the overall material flux of hydrogen through a proton conducting material such as Nafion in a fuel can then be described as

$$J_{H_2} = \frac{\sigma_{H^+}}{z_{H^+} \cdot e \cdot d} \cdot \nabla\emptyset \qquad \text{(Eq.12)}$$

where σ_{H^+} and z_{H^+} are the proton conductivity and charge, while e and d are the elementary charge and the membrane thickness, respectively. The term $\nabla\emptyset$ is the electrostatic potential gradient across the membrane, which is generated by the oxidation of hydrogen at the anode side as well as the reaction of hydrogen with oxygen at the cathode side. Altogether, the ion transport through the membrane material is also affected by a concentration gradient ∇c as well as a pressure gradient Δp, since both the latter affect the electrostatic potential gradient $\nabla\emptyset$ to a certain degree[129] (Eqs. 13 & 14). Thus, all above mentioned gradients are more or less the driving force of the transport through conductive membranes. However, concerning the transport through Nafion, the proton conductivity is the rate-determining step, which is solely influenced by the electrostatic potential gradient[129].

$$\nabla\emptyset \propto \nabla c \qquad \text{(Eq.13)}$$

$$\nabla\emptyset \propto \Delta p \qquad \text{(Eq.14)}$$

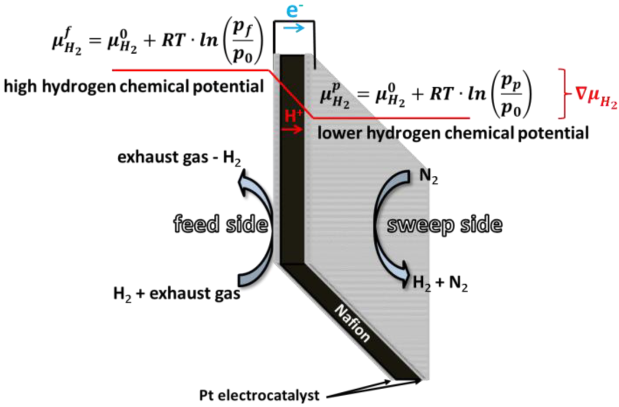

Figure 10: *Schematic representation of the generalized proton transport through a Nafion membrane as a consequence of the chemical potential gradient $\nabla\mu_{H_2}$ between feed and sweep side. Herein, $\mu^0_{H_2}$, $\mu^f_{H_2}$ and $\mu^p_{H_2}$ denote the standard chemical potential as well as the chemical potential at the feed side and the permeate side, respectively. p_0, p_f and p_p denote the standard pressure, the partial pressure of hydrogen at the feed side and the partial pressure of hydrogen at the sweep side.*

The generalized case of a hydrogen transport through a proton conducting material such as Nafion is shown in Figure 10. Therein, platinum is used as catalysts for the splitting as well as the recombination of hydrogen. By using oxygen or simply air at the sweep side, the normal operating mode of a fuel cell can be set up. The electrons have to take the detour, since Nafion is insulating for electrons. However, following the above mentioned principle, also the separation of hydrogen from a simulated waste gas should be possible, by using an inert sweep gas (e.g. Nitrogen, Argon) instead of a reactive one (e.g. air, oxygen).

1.6 References

(1) J. A. (Abbé) Nollet, Investigation of the Causes for the Ebullition of Liquids. *J. Membr. Sci.* **1995**, 100, 1. (reprinted from Histoire de Lacademie Royale des Science **1748**, 57-104, 1752).
(2) A. Fick, Ueber Diffusion. *Ann. Phys.* **1855**, 170, 59.
(3) M. Traube, Experimente zur Theorie der Zellenbildung und Endosmose. *Arch. Anat. Physiol. u. wiss. Med*. **1867** 87.
(4) T. Graham, On the Absorption and Dialytic Separation of Gases by Colloid Septa. *Philosophical Transactions*, **1866**, 235.
(5) T. Graham, Über die Bewegung der Gase. *Lieb. Ann*. **1850**, 76, 138.
(6) R. Zsigmondy, W. Bachmann, Über neue Filter. *Z. Anorg. Chem*, **1918**, 103, 119.
(7) J. D. Ferrey, Ultrafilter Membranes and Ultrafiltration. *Chem. Rev*, **1936**, 18, 373.
(8) W. J. Elford, Principles Governing the Preparation of Membranes Having Graded Porosities. The Properties of 'Gradocol' Membranes as Ultrafilters. *Trans. Faraday Soc.*, **1937**, 33, 1094.
(9) S. Loeb, S. Sourirajan, Sea Water Deminerilization by Means of a Semipermeable Membrane. (**1961**) Dept. Eng, UCLA, Los Angeles, CA, USA, Report No.60-60.
(10) S. Loeb, S. Sourirajan, Sea Water Deminerilization by Means of an Osmotic Membrane. *Advances in Chemistry Series 38*, **1962**, 117.
(11) R. L. Riley, H.K. Lonsdale, C. R. Lyons, Composite Membranes for Seawater Desalination by Reverse Osmosis. *J. Appl. Pol. Sci.* **1971**, 15, 1267.
(12) O. Kutowy, S. Sourirajan, Cellulose Acetate Ultrafiltration Membranes. *J. Appl. Pol. Sci.* **1975**, 19, 1449.
(13) J. M. S. Henis, M. K. Tripodi, A novel Approach to Gas Separation using Hollow Fiber Membranes. *Sep. Sci. Tech.*, **1980**, 15, 1059.
(14) R. W. Baker, Furure Directions of Membranes Gas Separation Technology. *Ind. Eng. Chem. Res.* **2002,** *41,* 1393.
(15) R. W. Baker, B. T. Low, Gas Separation Materials. A Perspective. *Macromolecules*, **2014**, 47, 6999.
(16) R. D. Noble, S. A. Stern, Membrane science and technology series 2: Membrane separation technology, principles and applications. *Elsevier 1st edition* **1995**.
(17) M. Mulder, Basic principles of membrane technology. *Kluwer Academic 2nd edition* **1996**.
(18) R.W. Baker, K. Lokhandwala, Natural gas processing with membranes: An overview. *Ind. Eng. Chem. Res*. **2008**, 47, 2109.
(19) W. J. Koros, Y. H. Ma, T. Shimidzu, Terminology for membranes and membrane processes. *Pure & Appl. Chem.*, **1996**, 68, 1479.

(20) P. Bernardo, E. Drioli, G.Golemme, Membrane Gas Separation. A Review/State of the Art. *Ind. Eng. Chem. Res.* **2009**, 48, 4638.
(21) P. Nejat, F. Jomehdazeh, M. M Taheri, M. Gohari, M. Z. Abd. Zahid, A global review of energy consumption, CO_2 emissions and policy in the residential sector (with an oveview of the top ten CO_2 emitting countries). *Renew. Sust. Energ. Rev.* **2015**, 43, 843.
(22) M. Kanniche, R. Gros-Bonnivard, P. Jaud, J. Valle-Marcos, J.-M. Amann, C. Bouallou, Pre-combustion, post-combustion and oxy-combustion in thermal power plant for CO_2 capture. *Appl. Therm. Eng.* **2010**, 30, 53.
(23) J.-M. Amann, M. Kanniche, C. Bouallou, Reforming natural gas for CO_2 pre-combustion capture in combined cycle power plant. *Clean Techn. Environ. Policy*, **2009**, 11, 67.
(24) J. R. Rostrup-Nielsen, T. Rostrup-Nielsen, Large-scale Hydrogen Production. *CATTECH*, **2002**, 6, 150.
(25) M. Ulbricht, Advanced functional polymer membranes. *Polymer*, **2006**, 47, 2217.
(26) Y. Yampolski, B. Freeman, Membrane gas separation. *John Wiley & Sons*, **2010**.
(27) D. F. Sanders, Z. P. Smith, R. Guo, L.M Robeson, J. E. McGrath, D. R. Paul, B. D. Freeman, Energy-efficient polymeric gas separation membranes for a sustainable future: A review. *Polymer*, **2013**, 54, 4729.
(28) L. M. Robeson, Polymer membranes for gas separation. *Curr. Opin. Solid State Mater. Sci.*, **1999**, 4, 549.
(29) L. M. Robeson, The upper bound revisited. *J. Membr. Sci.*, **2008**, 320, 390.
(30) N.A. Al-Mufachi, N.V. Rees, R. Steinberger-Wilkens, Hydrogen selective membranes: A review of palladium-based dense metal membranes. *Renew. Sust. Energ. Rev.*, **2015**, 47, 540.
(31) D. D. Athayde, D. F. Souza, A. M. A. Silva, D. Vasconcelos, E. H. M. Nunes, J. C. Diniz da Costa, W. L. Vasconcelos, Review of perovskite ceramic synthesis and membrane preparation methods. *Ceram. Int.*, **2016**, 42, 6555.
(32) M. Pera-Titus, Porous Inorganic Membranes for CO_2 Capture: Present and Prospects. *Chem. Rev.*, **2014**, 114, 1413.
(33) J. G. Wijmans, R. W. Baker, The solution-diffusion model: a review. *J. Membr. Sci.*, **1995**, 107, 1.
(34) N. Rangnekar, N. Mittal, B. Elyassi, J. Caro, Zeolite membranes – a review and comparison with MOFs. *Chem. Soc. Rev.*, **2015**,44, 7128.
(35) C. Feng, K. C. Khulbe, T. Matsuura, R. Franood, A. F. Ismail, Recent progress in zeolite/zeotype membranes. *J. Membr. Sci.*, **2015**, 1, 49.
(36) G. Ferey, Hybrid Porous Solids: Past, Present, Future. *Chem. Soc. Rev.*, **2008**, *37*, 191.

(37) J.-R. Li, R. J. Kuppler, H.-C. Zhou, Selective Gas Adsorption and Separation in Metal–organic Frameworks. *Chem. Soc. Rev.,* **2009**, *38*, 1477.
(38) J. Gascon, F. Kapteijn, Metal-Organic Framework Membranes - High Potential, Bright Future? *Angew. Chem. Int. Ed.,* **2010**, *49*, 1530.
(39) J.-R. Li, J. Sculley, H.-C. Zhou, Metal-organic frameworks for separations. *Chem. Rev*., **2011**, *112*, 869.
(40) B. Seoane, J. Coronas, I. Gascon, M. Etxeberria Benavides, O. Karvan, J. Caro, F. Kapteijn, J. Gascon, Metal-organic framework based mixed matrix membranes: a solution for highly efficient CO_2 capture? *Chem. Soc. Rev.,* **2015**, 44, 2421.
(41) T. Rodenas, M. van Dalen, E. García-Pérez, P. Serra-Crespo, B. Zornoza, F. Kapteijn, J. Gascon, Visualizing MOF Mixed Matrix Membranes at the nanoscale: towards structure-performance relationships in CO_2/CH_4 separation over NH_2-MIL-53(Al)@PI. *Adv. Funct. Mat*., **2014**, 24 249.
(42) T. Rodenas, I. Luz, G. Prieto, B. Seoane, H. Miro, A. Corma, F. Kapteijn, F. Llabrés i Xamena, J. Gascon, Metal-organic-framework nanosheets in polymer composite materials for gas separation applications. *Nat. Mater.*, **2014**, 14, 48.
(43) B. Zornoza, P. Serra-Crespo, C. Tellez, J. Coronas, J. Gascon, F. Kapteijn, Functionalized flexible MOFs as fillers in mixed matrix membranes for highly selective separation of CO_2 from CH_4 at elevated pressures. *Chem. Commun*., **2011**, 47, 9522.
(44) L. Lin, A. Wang, L Zhang, M. Dong, Y. Zhang, Novel mixed matrix membranes for sulfur removal and for fuel cell apllications. *J. Power Sources*, **2012**, 220, 138.
(45) O. M. Yaghi, H. L. Li, Hydrothermal Synthesis of a Metal-Organic Framework Containing Large Rectangular Channels. *J. Am. Chem. Soc*., **1995**, 117, 10401.
(46) S. R. Batten, N. R. Champness, X.-M. Chen, J. Garcia-Martinez, S. Kitagawa, L. Öhrström, M. O'Keeffe, M. P. Suh, J. Reedijk, Terminology of metal–organic frameworks and coordination polymers (IUPAC Recommendations 2013). *Pure Appl. Chem*., **2013**, 85, 1715.
(47) C. Chmelik, A. Mundstock, P. D. C. Dietzel, J. Caro, Idisyncrasies of Co_2(dhtp): In situ annealing by methanol. *Micropor. Mesopor. Mater*, 2014, 183, 117.
(48) S. Kitagawa, S. Kitaura, S. Noro, Functional porous coordination polymers. *Angew. Chem. Int. Ed.*, **2004**, 14, 3001.
(49) K. S. Park, Z. Ni, A. P. Cote, J. Y. Choi, R. Huang, F. J. Uribe-Romo, H. K. Chae, M. O'Keeffe, O. M. Yaghi, Exceptional chemical and thermal stability of zeolitic imidazolate frameworks. *Proc. Natl. Acad. Sci. USA,* **2006**, 103, 10186.
(50) A. Huang, H. Bux, F. Steinbach, J. Caro, Molecular-Sieve Membrane with Hydrogen Permselectivity: ZIF-22 in LTA Topology Prepared with 3-Aminopropyltriethoxysilane as Covalent Linker. *Angew. Chem*., **2010**, *122*, 5078.

(51) O. M. Yaghi, C. E. Davis, G. Li, H. Li, Selective Guest Binding by Tailored Channels in a 3-D Porous Zinc(II)-Benzenetricarboxylate Network. *J. Am. Chem. Soc*., **1997**, 119, 2861.

(52) Z. Wang, A. Knebel, S. Grosejan, D. Wagner, S. Bräse, C. Wöll, J. Caro, L. Heinke, Tunable molecular separation by nanoporous membranes. *Nature Commun*., **2016**, 7, 13872.

(53) M. Dan-Hardi, C. Serre, T. Frot, L. Rozes , G. Maurin, C. Sanchez, G. Ferey A new photoactive crystalline highly porous titanium(IV) dicarboxylate. *J. Am. Chem. Soc.*, **2009**, 131, 10857.

(54) C. Zlotea, D. Phanon, M. Mazaj, D. Heurtaux, V. Guillerm, C. Serre, P. Horcajada, T. Devic, E. Magnier, F. Cuevas, G. Ferey, P.L. Llewellyn, M. Latroche, Effect of NH_2 and CF_3 functionalization on the hydrogen sorption properties of MOFs. *Dalton Trans*., **2011**, 40, 4879.

(55) M. A. Moreira, J. C. Santos, A. F. P. Ferreira, J. M. Loureiro, F. Ragon, P. Horcajada, P. G. Yot, C. Serre, A. E. Rodrigues, Toward understanding the influence of ethylbenzene in p-xylene selectivity of the porous titanium amino terephthalate MIL-125(Ti): adsorption equilibrium and separation of xylene isomers. *Langmuir*, **2012**, 28, 3494.

(56) R. Vaidhyanathan, S. S. Iremonger, G. K. H. Shimizu, P. G. Boyd, S. Alavi, T. K. Woo, Direct observation and quantification of CO_2 binding in an amine-functionalized nanoporous solid. *Science,* **2010**, 330, 650.

(57) S.-N. Kim, J. Kim, H.-Y. Cho, W.-S. Ahn, Adsorption/catalytic properties of MIL-125 and NH_2-MIL-125. *Catal. Today,* **2013**, 204, 85.

(58) B. Arstad, H. Fjellvåg, K. Kongshaug, O. Swang, R. Blom, Amine functionalised metal organic frameworks (MOFs) as adsorbents for carbon dioxide, *Adsorption*, **2008**, 14 755.

(59) S. Hu, M. Liu, K. Li, Y. Zuo, A. Zhang, C. Song, G. Zhang, X. Guo, Solvothermal synthesis of NH_2-MIL-125(Ti) from circular plate to octahedron. *CrystEngComm*, **2014**, 16 9645.

(60) O. V. Gutov, W. Bury, D.A. Gomez-Gauldron, V. Krungleviciute, D. Fairen-Jimenez, J. E. Mondloch, A. A. Sarjeant, S. S. Al-Juaid, R. Q. Snurr, J. T. Hupp, T. Yildrim, O.K. Farha, Water-stable Zirconium-based Metal-organic Framework Material with High-surface Area and Gas-storage Capacities. *Chem. Eur. J*., **2014**, 20, 12389.

(61) V. Guillerm, F. Ragon, M. Dan-Hardi, T. Devic, M. Vishnuvarthan, B. Campo, A. Vimont, G. Clet, Q. Yang, G. Maurin, G. Ferey, A. Vittadini, S. Gross, C. Serre, A Series of Isoreticular, Highly Stable, Porous Zirconium Oxide Based Metal–Organic Frameworks. *Angew. Chem*., **2012**, 124, 9401; *Angew. Chem. Int. Ed*., **2012**, 51, 9267.

(62) B. Van de Voorde, D. D. Borges, F. Vermoortele, R. Wouters, B. Bozbiyik, J. Denayer, F. Taulelle, C. Martineau, C. Serre, G. Maurin, D. De Vos, D. Isolation of Renewable Phenolics by Adsorption on Ultrastable Hydrophobic MIL-140 Metal–Organic Frameworks. *ChemSusChem,* **2015**, 8, 3159.
(63) M. Kandiah, M. H. Nielsen, S. Usseglio, S. Jakobsen, U. Olsbye, M. Tilset, C. Larabi, E. A. Quadrelli, F. Bonino, K. P. Lillerud, Synthesis and Stability of Tagged UiO-66 Zr-MOFs. *Chem. Mater*., **2010**, 22, 6632.
(64) C.G. Piscopo, A. Polyzoidis, M. Schwarzer, S. Loebbecke, Stability of UiO-66 Under Acidic Treatment: Opportunities and Limitations for Post-synthetic Modifications. *Micropor. Mesopor. Mater*., **2015**, 208, 30.
(65) J. Liu, N. Canfield, W. Liu, W., Preparation and Characterization of a Hydrophobic Metal−Organic Framework Membrane Supported on a Thin Porous Metal Sheet. *Ind. Eng. Chem. Res.,* **2016**, 55, 3823.
(66) M. J. Katz, Z. J. Brown, Y. J. Colon, P. W. Siu, K. A. Scheidt, R. Q. Snurr, J. T. Hupp, O. K. Farha, A Facile Synthesis of UiO-66, UiO-67 and Their Derivatives. *ChemComm,* **2013**, 49, 9449.
(67) F. Vermoortele, R. Ameloot, A. Vimont, C. Serre, D. De Vos, An Amino-modified Zr-terephthalate Metal–organic Framework as an Acid–base Catalyst for Cross-aldol Condensation. *ChemComm,* **2010**, 47, 1521.
(68) I. Stassen, M. Styles, T. Van Assche, N. Campagnol, J. Fransaer, T. Denayer, J.-C. Tan, P. Falcaro, D. De Vos, R. Ameloot, Electrochemical Film Deposition of the Zirconium Metal–Organic Framework UiO-66 and Application in a Miniaturized Sorbent Trap. *Chem. Mater.*, **2015**, 27, 1801.
(69) C. Zhang, Y. Zhao, Y. Li, X. Zhang, L. Chi, G. Lu, G. Defect-Controlled Preparation of UiO-66 Metal–Organic Framework Thin Films with Molecular Sieving Capability. *Chem. Asian J.* **2016**, 11*,* 207.
(70) H. Wu, T. Yildrim, W. Zhou, Exceptional Mechanical Stability of Highly Porous Zirconium Metal–Organic Framework UiO-66 and Its Important Implications. *J. Phys. Chem. Lett.,* **2013**, 4, 925.
(71) L. Valenzano, B. Civalleri, S. Chavan, S. Bordiga, M. H. Nilsen, S. Jakobsen, K. P. Lillerud, C. Lamberti, Disclosing the Complex Structure of UiO-66 Metal Organic Framework: A Synergic Combination of Experiment and Theory. *Chem. Mater*., **2011**, 23, 1700.
(72) S. Øien, D. Wragg, H. Reinsch, S. Svelle, S: Bordiga, C. Lamberti, K. P. Lillerud, Detailed Structure Analysis of Atomic Positions and Defects in Zirconium Metal–Organic Frameworks. *Cryst. Growth Des*., **2014**, 14, 5370.

(73) J. H. Cavka, S. Jakobsen, U. Olsbye, N. Guillou, C. Lamberti, S. Bordiga, K. P. Lillerud, A New Zirconium Inorganic Building Brick Forming Metal Organic Frameworks with Exceptional Stability. *J. Am. Chem. Soc*., **2008**, 130, 13850.

(74) S. Devautour-Vinot, G. Maurin, C. Serre, P. Horcajada, D. Paula da Cunha, V. Guillerm, E. de Souza Costa, F. Taulelle, C. Martineau, Structure and Dynamics of the Functionalized MOF Type UiO-66(Zr): NMR and Dielectric Relaxation Spectroscopies Coupled with DFT Calculations. *Chem. Mater*., **2012**, 24, 2168.

(75) M. J. Cliffe, W. Wan, X. Zou, P. A. Chater, A. K. Kleppe, M. G. Tucker, H. Wilhelm, N. P. Funnell, F.-X. Coudert, A. L. Goodwin, Correlated Defect Nanoregions in a Metal–organic Framework. *Nat. Commun*., **2014**, 5, 1.

(76) P. S. Barcia, P. Guimaraes, P. A. P. Mendes, J. A. C. Silva, V. Guillerm, H. Chevreau, C. Serre, A. E. Rodrigues, Reverse Shape Selectivity in the Adsorption of Hexane and Xylene Isomers in MOF UiO-66. *Micropor. Mesopor. Mater*., **2011**, 139, 67.

(77) T. Loiseau, L. Lecroq, C. Volkringer, J. Marrot, G. Ferey, M. Haouas, F. Taulelle, S. Bourrelly, P. L. Llewellyn, M. Latroche, MIL-96 a Porous Aluminium Trimesate 3D Structure Constructed from a Hexagonal Network of 18-Membred Rings and μ_3-Oxo-Centred Trinuclear Units. *J. Amer. Chem. Soc.,* **2006**, 128, 10223.

(78) T. Ahnfeldt, N. Guillou, D. Gunzelmann, I. Margiolaki, T. Loiseau, G. Ferey, J. Senker, N. Stock, $[Al_4(OH)_2(OCH_3)_4(H_2N\text{-bdc})_3] \cdot x\, H_2O$: A 12-Connected Porous Metal-Organic Framework with an Unprecedented Aluminium-Containing Brick. *Angew. Chem*., **2009**, 121, 5265.

(79) T. Loiseau, C. Serre, C. Huguenard, G. Fink, F. Taulelle, M. Henry, T. Bataille, G. Ferey, A Rationale for the Large Breathing of the Porous Aluminium Terephthalate (MIL-53) Upon Hydration. *Chem. Eur. J*., **2004**, 10, 1373.

(80) C. Volkringer, T. Loiseau, A new indium metal-organic 3D framework with 1,3,5-benzenetricarboxylate, MIL-96 (In), containing μ_3-oxo-centred trinuclear units and a hexagonal 18-ring network. *Mater. Res. Bull.,* **2006**, 41, 948.

(81) C. Volkringer T. Loiseau, G. Ferey, C. M. Morais, F. Taulelle, V. Montouillout, D. Massiot, Synthesis, crystal structure and ^{71}Ga solid state NMR of a MOF-type gallium trimesate (MIL-96) with μ_3-oxo bridged trinuclear units and a hexagonal 18-ring network. *Micropor. Mesopor. Mater.,* **2007**, 105, 111.

(82) Y. Mao, B. Su, W. Cao, J. Li, Y. Ying, W. Ying, Y. Hou, L. Sun, X. Peng, Specific Oriented Metal–Organic Framework Membranes and Their Facet-Tuned Separation Performance. *ACS Appl. Mater. Interfaces,* **2014**, 6, 15676.

(83) M. E. Davis, R. F. Lobo, Zeolite and molecular sieve synthesis. *Chem. Mater.*, **2002**, 4, 756.

(84) L. Shirazi, E. Jamshidi, M. R. Ghasemi, The effect of Si/Al ratio of ZSM-5 zeolite on its morphology, acidity and crystal size. *Cryst. Res. Technol.*, **2008**, 43, 1300.

(85) A. Huang, N. Wang, J. Caro, Seeding-free synthesis of dense zeolite FAU membranes on 3-aminopropyltriethoxysilane-functionalized alumina supports. *J. Membr. Sci*., **2012**, 389, 272.
(86) A. Mundstock, N. Wang, S. Friebe, J. Caro., Propane/propene permeation through Na-X membranes: The interplay of separation performance and pre-synthetic support functionalization. *Micropor. Mesopor. Mater*., **2015**, 215, 20.
(87) Y. Zhang, Q. Gao, Z. Lin, T. Zhang, J. Xu, Y. Tan, W. Tian, L. Jiang, Constructing Free Standing Metal Organic Framework MIL-53 Membrane Based on Anodized Aluminum Oxide Precursor. *Sci. Rep*., **2014**, 4, 1.
(88) T. Ben, C. Lu, C. Pei, S. Xu, S. Qiu, Polymer-Supported and Free-Standing Metal-Organic Framework Membrane. *Chem. Eur. J*., **2012**,18, 10250.
(89) J. Coronas, Present and future synthesis challenges for zeolites. *Chem. Eng. J*., **2010**, 156, 236.
(90) J. Caro, Are MOF membranes better in gas separation than those made of zeolites? *Curr. Opin. Chem. Eng*., **2011**, 1, 77.
(91) G. Dong, H. Li, V. Chen, Challenges and opportunities for mixed-matrix-membranes for gas separation. *J. Mater. Chem. A*, **2013**, 1, 4610.
(92) T.-S. Chung, L. Y. Liang, Y. Li, S. Kulprathipanja, Mixed matrix membranes (MMMs) comprising organic polymers with dispersed inorganic fillers for gas separation. *Prog. Polym. Sci*., **2007**, 32, 483.
(93) R. Mahajan, R. Burns, M. Schaeffer, W. J. Koros, Challenges in Forming Successful Mixed Matrix Membranes with Rigid Polymeric Materials. *J. Appl. Pol. Sci.,* **2002**, 86, 881.
(94) J. B. Hooper, K. S. Schweizer, Contact Aggregation, Bridging, and Steric Stabilisation in Dense Polymer-Particle Mixtures. *Macromolecules,* **2005,** 38, 8858.
(95) R. D. Noble, Perspectives on Mixed matrix membranes. *J. Membr. Sci*., **2011**, 378, 393.
(96) S. Wang, X. Li, H. Wu, Z. Tian, Q. Xin, G. He, D. Peng, S Chen, Y. Yin, Z. Jiang, M. D. Guiver, Advances in high permeability polymer-based membrane materials for CO_2 separations. *Energy Environ. Sci*., **2016**, 9, 1863.
(97) Y. Yampolski, Polymeric gas separation membranes. *Macromolecules,* **2012**, 45, 3298.
(98) I. Pinnau, A. Morisato, Z. He, Influence of Side-Chain Length on the Gas Permeation Properties of Poly(2-alkylacetylenes). *Macromolecules*, **2004**, 37, 2823.
(99) D. Bastani, N. Esmaeili, M. Asadollahi, Polymeric mixed matrix membranes containing zeolites as a filler for gas separation applications: A review. *J. Ind. Eng. Chem*., **2013**, 19, 375.

(100) A. E. Amooghin, M. Omidkhah, A. Kargari, The effects of aminosilane grafting on NaY zeolite-Matrimid®5218 mixed matrix membranes for CO_2/CH_4 separation. *J. Membr. Sci*., **2015**, 490, 364.
(101) O. G. Nik, X. Y. Chen, S. Kaliaguine, Amine-functionalized FAU/EMT-polyimide mixed matrix membranes for CO_2/CH_4 separation. *J. Membr. Sci*., **2011**, 379, 468.
(102) H. Deng, C. J. Doonan, H. Furukawa, R. B. Ferreira, J. Towne, C. B. Knobler, B. Wang, O. M. Yaghi, Multiple Functional Groups of Varying Ratios in Metal-Organic Frameworks. *Science*, **2010**, 327, 846.
(103) S. M. Cohen, Postsynthetic Methods for the Functionalization of Metal Organic Frameworks. *Chem. Rev.*, **2012**, 112, 970.
(104) Z. Wang, S. M. Cohen, Postsynthetic modification of metal–organic frameworks. *Chem. Soc. Rev*., **2009**, 38, 1315
(105) B. Zornoza, C. Tellez, J. Coronas, J. Gascon, F. Kapteijn, Metal organic framework based mixed matrix membranes: an increasingly important field of research with a large application potential. *Micropor. Mesopor. Mater*., **2013**, 166, 67.
(106) S. Friebe, L. Diestel, A. Knebel, A. Wollbrink, J. Caro, MOF-based Mixed Matrix Membranes in gas separation – Mystery and reality. *Chem. Ing. Tech*., **2016**, 88, 1788.
(107) A. Knebel, S. Friebe, N. C. Bigall, M. Benzaqui, C. Serre, J. Caro, Comparative Study of MIL-96(Al) as Continuous MOF-Layer and Mixed-Matrix-Membrane. *ACS Appl. Mater. Interf.* **2016**, 8, 7536.
(108) S. Friebe, A. Mundstock, D. Unruh, F. Renz, J. Caro, NH_2-MIL-125 as membrane for carbon dioxide sequestration: Thin supported MOF layers contra Mixed-Matrix-Membranes. *J. Membr. Sci.*, **2016**, 516, 185.
(109) L. Diestel, N. Wang, A. Schulz, F. Steinbach, J. Caro, Matrimid-Based Mixed Matrix Membranes: Interpretation and Correlation of Experimental Findings for Zeolitic Imidazolate Frameworks as Fillers in H_2/CO_2 Separation. *Ind. Eng. Chem. Res*. **2015**, 54, 1103.
(110) T. T. Moore, W. J. Koros, Non-ideal effects in organic–inorganic materials for gas separation membranes. *J. Mol. Struct*., **2005**, 87.
(111) M. A. Aaron, A. F. Ismail, T. Matsuura, M. M. Montazer-Rahmati, Performance studies of mixed matrix membranes for gas separation: A review. *Sep. Purif. Tech.,* **2010**, 75, 229.
(112) J. Caro, M. Noack, P. Kölsch, Zeolite membranes: From the laboratory scale to technical applications. *Adsoprtion*, **2005**, 11, 215.
(113) J. Caro, M. Noack, P. Kölsch, R. Schäfer, Zeolite membranes - state of their development and perspective. *Micropor. Mesopor, Mater*., **2000**, 38,3.
(114) R. M. Barrer, Porous crystal membranes. *J. Chem. Soc. Farady Trans*., **1990**, 86, 1123.

(115) J. Kärger, S. Vasenkov, S. M. Auerbach, Diffusion in zeolites. *Marcel-Dekker Inc*., New York, **2003**.
(116) J. Kärger, D. M. Ruthven, Diffusion in zeolites and other microporous materials. *John Viley & Sons*, New York, **1992**.
(117) R. Krishna, J. A. Wesselingh, The Maxwell-Stefan approach to mass transfer. *Chem. Eng. Sci.*, **1997**, 52, 861.
(118) F. Kapteijn, J. A. Moulijn, R. Krishna, The generalized Maxwell-Stefan model for diffusion in zeolites: Sorbate molecules with different saturation loadings. *Chem. Eng. Sci.*, **2000**, 55, 2923.
(119) K. S. W. Sing, D.H. Everett, R. A. W. Haul, L. Moscou, R. A. Pierotti, J. Rouquerol, T. Siemieniewska, Reporting physisorption data for gas/ solid systems with special reference to determination of surface area and porosity. *Pure Appl. Chem*., **1985**, 57, 603.
(120) I. Langmuir, The adsorption of gases on plane surfaces of glass, mica and platinum. *J. Am. Chem. Soc*., **1918**, 40, 1361.
(121) T. C. Merkel, V.I. Bondar, K. Nagai, B. D. Freeman, I. Pinnau, Gas sorption, diffusion, and permeation in Poly(dimethylsiloxane). *J. Polym. Sci. B Polym. Phys.,* **2000**, 38, 415.
(122) A. Javaid, Membranes for solubility-based gas separation applications. *Chem. Eng. J*., **2005**, 112, 219.
(123) X. Chen, L. Huan, Yanying Wei, H. Wang, Tantalum stabilized $SrCoO_3$−perovskite membrane for oxygen separation. *J. Membr. Sci*., **2011**, 368, 159.
(124) S. Ricote, A. Manerbino, N. P. Sullivan, Preparation of dense mixed electron- and proton-conducting ceramic composite materials using solid-state reactive sintering: $BaCe_{0.8}Y_{0.1}M_{0.1}O_{3-\delta}$–$Ce_{0.8}Y_{0.1}M_{0.1}O_{2-\delta}$ (M=Y, Yb, Er, Eu). *J Mater. Sci*., **2014**, 49, 4332.
(125) W.-k. Lee, C.-H. ho, J. W. Van Zee, M. Murthy, The effects of compression and gas diffusion layers on the performance of a PEM fuel cell. *J. Power Sources,* **1999**, 84, 45.
(126) V. Mehta, J. S. Cooper, Review and analysis of PEM fuel cell design and manufacturing. J. Power Sources, 2003, 114, 32.
(127) J. E. ten Elshof, H. J. M. Bouwmeetser, H. Verweij, Oxygen transport through $La_{1-x}Sr_xFeO_{3-\delta}$ membranes. I. Permeation in air/He gradients, *Solid State Ionics*, 1995, 81, 97.
(128) K. D. Kreuer, On the development of proton conducting polymer membranes for hydrogen and methanol fuel cells, *J. Membr. Sci.,* 2001, 15, 29.
(129) S. T. Revankar, P. Majumdar, Fuel cells: Principles, design and analysis, *Taylor & Francis Group*, **2014**.

2. Membranes for Hydrogen Separation based on Metal-Organic Frameworks (MOFs) and Zeolites

2.1 Summary

Due to the ever-increasing energy consumption and the close-knitted demand for clean energy, hydrogen purification is a crucial task for industry. In relation to the common methods like cryogenic distillation or PSA, membrane based hydrogen purification can be done more economical and is, therefore, an interesting alternative. Zeolite or MOFs and membranes resting upon their composites such as MMMs have become famous for this separation task in the last ten years, due to their tailorable pore size and their adjustable properties. The first three publications in this chapter introduce three novel MOF based membranes, which can be applied for hydrogen purification. The fourth publication reports on the usage FAU as supported membranes and ion-exchanged FAU particles as filler for MMM fabrication.

The publication in chapter 2.2 reports a supported NH_2-MIL-125 membrane and corresponding MMMs with different filler content and good H_2/CO_2 selectivity. Although the 3D framework of NH_2-MIL-125 features pore sizes of about 6 Å, the non-coordinating amino functions in the framework possess good potential for retaining CO_2 in a gas mixture, thus resulting in improved selectivity. Furthermore, in the MMMs some of these amino functions can react directly with the carbonyl functions of the Matrimid via a ring opening polymerization reaction, thus ensuring good filler embedding inside the polymeric matrix.

A highly oriented UiO-66 membrane with large hydrogen permeance is introduced in chapter 2.3. The latter membrane was prepared by a benzoic acid modulated synthesis and went in accordance with the van-der Drift growth model, thus resulting in a high crystal preferred orientation. Furthermore, by covering this membrane with a thin polymer layer, the “soft” molecular sieve UiO-66 was transferred into a system with a sharp cut off, most likely due to suppressed linker mobility in this multilayer membrane.

The publication in chapter 2.4 outlines two MIL-96 MOF membranes with different crystal habits and corresponding MMMs with five different filler sizes for gas separation. Since the 3D framework of MIL-96 has transport limiting paths in some directions, resulting in a virtually 2D framework, the corresponding supported MOF membranes show interesting transport properties in dependence of their crystal habit. Additionally, the publication reports filler size dependent problems in terms of the MMM fabrication such as aggregation, segregation or recrystallization inside the polymeric matrix.

Supported FAU membranes and ion-exchanged FAU based Mixed-Matrix-Membranes are reported in the publication in chapter 2.5. It highlights the separation performance in dependence of the support pre-treatment as well as the used filler material for MMM fabrication. The separation performance is in accordance with the ionic potential of the used metal ions, thus explaining the varying separation capabilities.

2.2 NH_2-MIL-125 as Membrane for Carbon Dioxide Sequestration: Thin Supported MOF Layers contra Mixed-Matrix-Membranes

S. Friebe, A. Mundstock, D. Unruh, F. Renz, J. Caro

Journal of Membrane Science **2016**, 516, 185-193.

Journal of Membrane Science 516 (2016) 185–193

Contents lists available at ScienceDirect

Journal of Membrane Science

journal homepage: www.elsevier.com/locate/memsci

NH_2-MIL-125 as membrane for carbon dioxide sequestration: Thin supported MOF layers contra Mixed-Matrix-Membranes

S. Friebe [a,*], A. Mundstock [a], D. Unruh [b], F. Renz [b], J. Caro [a]

[a] Institute of Physical Chemistry and Electrochemistry, Leibniz University Hannover, Callinstraße 3A, D-30167 Hannover, Germany
[b] Institute of Inorganic Chemistry, Leibniz University Hannover, Callinstraße 9, D-30167 Hannover, Germany

ARTICLE INFO

Article history:
Received 16 February 2016
Received in revised form
31 May 2016
Accepted 10 June 2016
Available online 15 June 2016

Keywords:
Hydrogen (H_2)/carbon dioxide (CO_2) separation
Supported NH_2-MIL-125 membrane
Mixed-Matrix-Membrane (MMMS)
Van-der-Waals interaction
Amine-functionalization

ABSTRACT

A novel supported thin NH_2-MIL-125 MOF layer has been prepared and evaluated as a new membrane in the separation of an equimolar hydrogen (H_2)/carbon dioxide (CO_2) mixture at different temperatures. Additionally, Mixed-Matrix-Membranes (MMMs), consisting of the NH_2-MIL-125 MOF powder and Matrimid as continuous polymer matrix, were prepared and investigated for the same separation process. Permeation measurements were performed at 150 °C and varying feed pressures (3, 4, 5 bar), thus simulating the pre-combustion process for CO_2 sequestration. Since NH_2-MIL-125 has free amine groups in its pore system, the attractive interaction with the polar acidic molecule CO_2 is expected to retain it in comparison to H_2, resulting in an enhanced separation performance. For the neat supported NH_2-MIL-125 membrane, the H_2 permeability is indeed by the factor of 8 larger than that of CO_2 at room temperature. In case of the MMMs, the addition of the MOF powder enhances both the permeability and the selectivity in comparison to the neat polymer Matrimid.

1. Introduction

Currently, one of the main environmental problems is the global climate change, due to the emission of greenhouse gases (e.g. CO_2) through human activities. As a result of this, the research field of environmentally friendly, economical and energy efficient carbon dioxide capture technologies gains more and more attention [1–4]. At the moment, three main carbon capturing processes (post-combustion, pre-combustion and oxy-fuel combustion) are of interest [5]. Post-combustions aim is the separation and capture of CO_2 from flue gases. The oxy-fuel process uses oxygen instead of air in the energy conversion, which results in a high purity CO_2 stream as flue gas [6–8]. In the pre-combustion process, fossil fuels (e.g. coal, natural gas, oil) are transformed into a H_2/CO_2 gas mixture (synthesis gas) by several partial oxidation and reforming steps [1,9]. The separated hydrogen can be used as energy source for the production of electricity (combustion in a turbine or fuel cell). Consequently, the development of new materials for gas storage and gas separation is a rapidly growing field of material science. Metal Organic Frameworks (MOFs) with their large surface area, high porosity and the possibility to tailor their pore system by combining various types of metal ions and linkers, have recently become attractive for gas storage and separation [10]. Concerning the CO_2 capture, especially amine-functionalized MOF structures gained a lot of interest, due to their affinity for CO_2 molecules. This approach to develop NH_2-containing adsorbents is based on the fact, that the most prevalent industrial process for CO_2 separation is the absorption in aqueous solutions of alkanolamines [11,12]. However, one drawback of the washing method is the formation of strong bonds between the amine containing solvents and the CO_2. Therefore, the regeneration of the solution suffers from parasitic costs and so alternatives are inevitable. The adsorptive separation by porous adsorbents may be one of the suitable alternatives. For instance, amine containing MOF-structures allow a reversible CO_2 capture with good selectivity. Herein the amine function not only decreases the pore size of the framework but also shows an affinity for CO_2, due to van-der-Waals forces [13]. Additionally, the regeneration of the porous sorbent is easy to achieve by heating, evacuation or simple nitrogen flush. Several works have already shown the potential of amine containing MOF-structures for CO_2 adsorption [14–16]. Their results indicated, that amine containing MOF structures show higher adsorption uptake due to van-der-Waals forces between CO_2 and the amine functional groups in comparison to their unfunctionalized counterparts. For instance, one study clarified, that NH_2-MIL-125 has a CO_2 uptake of around 125 mg g^{-1} at ambient conditions, whereas the N_2 uptake is just around 10 mg g^{-1} at the same conditions [14,15]. There is some pioneering work for CO_2 separation by using MOF membranes. However, the preparation of MOFs or zeolites as continuous defect-free layers is a challenging

* Corresponding author.
E-mail address: sebastian.friebe@pci.uni-hannover.de (S. Friebe).

http://dx.doi.org/10.1016/j.memsci.2016.06.015
0376-7388/

task since their reproducibility and up-scalability are still a huge bottleneck [17,18]. Since these MOF films are not self-supporting, they are usually prepared on graded ceramic tubular or monolithic supports. Hence the cost of the membrane is dominated by relative expensive supports [19]. Recent preparations of MOF membrane layers on polymer supports look promising [20–22].

Consequently, the majority of industrial membrane separation processes is realized with polymer membranes, due to their mechanical stability, low costs and their simple processing [23]. From the variety of polymers for MMM fabrication, the use of Matrimid seems to be a good choice for the separation of H_2/CO_2 mixtures. Matrimid features high thermal and chemical stability, easy processability and an appropriate overall selectivity for several gas pairs [24]. In addition, it is compatible to a huge number of filler materials, adheres excellent on several different substrate surfaces (metal, steel, alumina) and does not require a complicated treatment after the MMM fabrication.

For polymers, H_2/CO_2 separation can be described by the solution-diffusion model. This model describes the separation process with two major effects: (i) diffusion (favors the smaller H_2) and (ii) solubility (favors the better adsorbed CO_2) [25]. As a result of these contradicting effects, the separation of the gas pair H_2/CO_2 is more complicated compared to other ones and has to be done at higher temperatures to minimize the CO_2 adsorption. A general problem with polymer membranes for gas separation is their low permselectivity. MMMs, a combination of a polymer matrix and embedded filler particles (MOFs, zeolites etc.) [26], are an appropriate alternative to overcome this problem, since they combine the good properties of both, the inorganic filler (permselectivity) as well as the polymer (mechanical stability) [27,28], which was recently clearly indicated in ref. [29]. In summary, MMMs may be able to close the gap between neat MOF-layers and neat polymer membranes, due to the combination of all the positive properties of both materials in one composite. Due to their unique features, they may be applicable for membrane-assisted processes like gas separation of different gases [30–32], pervaporation [33] or removal of undesired contaminants [34,35]. However, it turns out a practical problem that MMMs cannot be easily made as sub-micron thick membrane layers like polymer membranes. The successful preparation of nano-scale MOFs [26,36,37] will allow the preparation of high-permeance MMMs which can compete with polymer membranes.

MOFs, as thin supported layer or as filler in MMMs, can separate gases via size exclusion (molecular sieve) or adsorption interaction, depending on their pore size and their functional groups inside the porous framework. Our study focuses on the MOF NH_2-MIL-125, which features a high thermal stability (up to 300 °C) and also remains stable in water or heptane [14]. It is isostructural to the non-functionalized MIL-125 and has a three dimensional tetragonal framework with octahedral and tetrahedral cages, which are connected via three-cornered windows with a size of approximately 6 Å [38–40]. The octahedral cages, in which a majority of the amine-functions (cf. Fig. 1A and C) is located, are accessible from all directions through the 3D channel network (cf. Fig. 1B). The position and geometry of the amine groups in the structure are not yet precisely defined. Nevertheless, since the kinetic diameters of hydrogen (2.9 Å) and carbon dioxide (3.3 Å) are both smaller than the pore size of the NH_2-MIL-125, one cannot expect molecular sieving but adsorption based separation, due to the attractive interaction of CO_2 with the NH_2-functionalized framework. This adsorptive interaction can have an opposite influence on the permeation behavior of a H_2/CO_2 mixture through an NH_2-MIL-125 membrane: The presence of NH_2 groups increases the adsorption of CO_2 but it reduces its diffusivity.

To the best of our knowledge, both the neat NH_2-MIL-125 MOF layer and the NH_2-MIL-125 MMMs are prepared and evaluated as membrane for the first time. The adsorptive interaction of CO_2 with the amine functions in the framework and the partly cross-linkage between the MOF and the polymer chains of Matrimid were characterized by IR-spectroscopy. Additionally, the textural properties of the powder and the membrane were investigated with X-ray diffraction (XRD) and scanning electron microscopy (SEM). We proposed a ring opening polymerization reaction to be responsible for the good interaction between the filler material and the polymer matrix with NH_2-MIL-125 as nodes. Further investigations were considered on the effect of filler content, feed pressure and operating temperature on the H_2/CO_2 separation capabilities of both membrane types. Lastly, the results were brought into relation to the predicted membrane performance (Maxwell-Modell) and to the Robeson upper bound for state-of-the art composite membranes.

2. Experimental section

2.1. Materials

The chemicals in this work were obtained from commercial vendors at a reagent grade purity or higher and used without further purification.

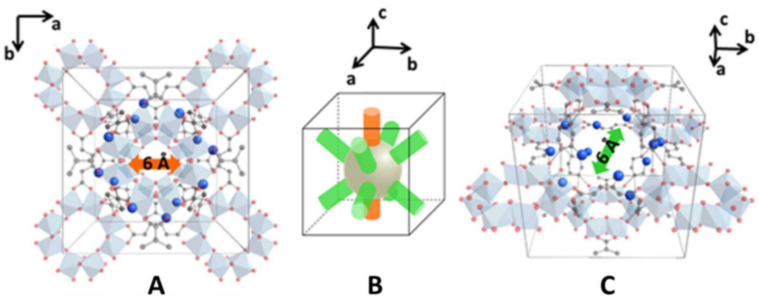

Fig. 1. Schematic structure of NH_2-MIL-125 in viewing direction of the different windows, which connect (A) the octahedral cages and (C) both cage types. Blue (non-transparent) balls show the free amine groups inside the framework schematically. B demonstrates the schematic connection between all cages in the 3D porous network. (For interpretation of the references to color in this figure legend, the reader is referred to the web version of this article.)

2.2. Preparation of NH_2-MIL-125 powder

The preparation of the powder was done following a recipe reported elsewhere [14]. For a typical synthesis, 0.355 mL tetrapropylorthotitanate (TPOT) was dissolved in 10 mL methanol (solution 1). Additionally a second solution, consisting of 0.434 g aminoterephthalic acid (NH_2-bdc) in 10 mL dimethylformamide (DMF), was prepared (solution 2). Both solutions were heated up to 70 °C. After heating, the solutions were combined in a Teflon lined microwave autoclave and heated up to 150 °C for 30 min (heating rate: 24 °C/min). After the synthesis, the autoclave was cooled down in an ice bath and the resulting yellowish powder was washed with methanol several times and activated in an oven at 80 °C. After activation the powder was stored under Argon atmosphere for further use.

2.3. Preparation of supported NH_2-MIL-125 layer

The NH_2-MIL-125 layer was prepared by a hydrothermal synthesis following a recipe reported elsewhere with slight modifications [14,37]. Therefore a solution of 10 wt% NH_2-MIL-125 powder in ethanol was produced. This solution was used to get a layer of seeding crystals on top of the α-Al_2O_3 supports (2.5 μm pores; Fraunhofer IKTS, former Hermsdorfer HITK, Germany) by coating. After the coating the seeded support was dried for an adequate time. For the growth process, 0.434 g NH_2-bdc and 0.355 mL TPOT were solved in a mixture of 7.5 mL methanol and 7.5 mL DMF. This solution was filled in a 23 mL Teflon lined autoclave. One of the seeded supports was put on the bottom of the autoclave in face-up orientation. The autoclave was heated in a conventional oven at 150 °C for 24 h. After the autoclave was cooled down to room temperature, the membrane was washed with methanol several times, stored in dichloromethane (DCM) for one day and kept subsequently overnight at 70 °C in an drying oven.

2.4. Preparation of supported MMMs

The supported MMMs were produced by a simple casting approach. Therefore the evacuated NH_2-MIL-125 powder and the Matrimid 5218 were weighed in a glass bottle under inert gas atmosphere. After that, 1 mL dichloromethane (DCM) was added, the glass bottle was closed and the resulting mixture was stirred overnight. At the following day the mixture was first thickened and then casted on an α-Al_2O_3 supports (2.5 μm pores; Fraunhofer IKTS, former Hermsdorfer HITK, Germany) with the help of an Eppendorf-Pipette. After casting, the MMMs were stored in an atmosphere of DCM to allow a slow solvent evaporation. At the end the membranes were activated at 150 °C in a nitrogen flush for several hours.

2.5. Characterization techniques

2.5.1. X-Ray diffraction

The XRD measurements were done on a Bruker D8 Advance Diffractometer with Cu-Kα-radiation in a range between 5° and 30°.

2.5.2. FTIR

FTIR spectra were recorded on a Tensor 27 (Bruker) spectrometer. Each sample was scanned 15 times with a resolution of 4 cm^{-1} and averaged to obtain the final spectrum. The measurement in activated state was done in an evacuated sample chamber (vacuum pump: Pfeiffer Hi Cube, Model TC 110, $p \approx 10^{-5}$ mbar), whereas the measurement in low CO_2 atmosphere was done by flushing the previously evacuated chamber with a corresponding amount of pure CO_2 before measurement start.

2.5.3. Scanning electron microscopy

The scanning electron microscopy (SEM) studies of the samples were done with a field-emission electron microscope (JEOL JSM-6700F). Concerning the powder analysis, the accelerating voltage was set to 2 kV and the working distance was 8 mm. For the SEM investigation of the membranes and MMMs the parameters were set to 10 kV and 15 mm. Energy dispersive X-Ray spectroscopy (EDXS) was done at 10 kV accelerating voltage at a working distance of 15 mm with an INCA 300 energy-dispersive X-Ray-spectrometer.

2.5.4. Gas permeation measurements

Our assumptions of the permeation properties were evaluated by mixed gas separation measurements. The membranes were sealed in the permeation cell with Viton O-rings (FKM 70 Vi 370). Gas separation measurements were carried out by feeding an equimolar mixture of H_2/CO_2 (25/25 mL/min) by means of two flow-mass controllers, while the permeate side of the membrane was swept with a controlled stream of N_2 at 1 bar by means of another mass-flow controller (MOF membrane: 50 mL/min; MMMs: 1 mL/min). The NH_2-MIL-125 layer was investigated in a temperature range between room temperature and 150 °C. The MMMs were used at a constant temperature of 150 °C and varying feed over pressures (0, 3, 4 and 5 bar), thus simulating the practice-relevant pre-combustion conditions. Concentrations of H_2 and CO_2 in the permeate were analyzed by an Agilent Technologies 7890B online gas chromatograph equipped with a thermal conductivity detector.

3. Results and discussion

3.1. Structure analysis

The X-Ray diffraction patterns of NH_2-MIL-125 as powder and as thin continuous supported layer, together with a simulated XRD from a cif-file (CCDC 751157) are shown in Fig. 2. Obviously, the characteristic reflexes of the NH_2-MIL-125 powder are in good accordance with the simulated XRD. The main reflexes can clearly be assigned to the (011), (002) and (121) planes. These characteristic reflexes can also be observed for the membrane, indicating the successful preparation of a supported NH_2-MIL-125 layer. Additionally, the comparison between the powder with a statistic orientation of the crystallites and the MOF layer show, that the NH_2-MIL-125 membrane has grown without preferential orientation relative to the support.

3.2. Investigation of filler-CO_2 and filler-polymer interaction

The FT-IR spectra of NH_2-MIL-125 in activated state and in CO_2 atmosphere are recorded in Fig. 3. By comparing the two spectra, the difference in the region between 1400–1600 cm^{-1} and 3300–3500 cm^{-1} is obvious. The IR spectrum in the activated state exhibits more detailed and also more split peaks in the specified regions. This means, that the specific peaks of the amine shear vibration (1400–1600 cm^{-1}) and the amine stretching vibration (3300–3500 cm^{-1}) are suppressed, indicating the adsorptive interaction of NH_2-MIL-125 with CO_2 if the latter is present [13–15].

The FT-IR spectra of a neat Matrimid film and a 10 wt% NH_2-MIL-125 MMM are displayed in Fig. 4. By comparison of the specific peaks for the symmetric/asymmetric C=O stretching vibrations (1650–1800 cm^{-1}) and the symmetric/asymmetric aliphatic C–H stretching vibrations (2850–3000 cm^{-1}), one can see, that the signal intensities for the MMM are much lower. The reduced intensity of the carbonyl functions may be a hint for a partly cross-linkage between the polymer chains and the NH_2-MIL-125 particles (cf. grey balls in upper inset Fig. 4) via a ring-opening polymerization reaction as already shown for several polyimides with diamines as cross-linkers [41,42].

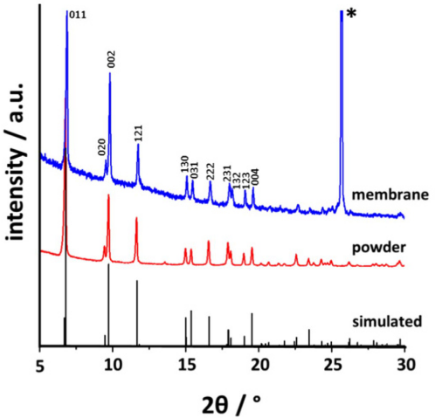

Fig. 2. X-Ray-diffractograms of the synthesized NH_2-MIL-125 powder (red line), the thin supported NH_2-MIL-125 layer (blue line) and a simulated XRD pattern from the cif-file of MIL-125 (black line). * reflex from the α-Al_2O_3 support. The measured XRDs have been normalized to the (011) reflex for better comparison. (For interpretation of the references to color in this figure legend, the reader is referred to the web version of this article.)

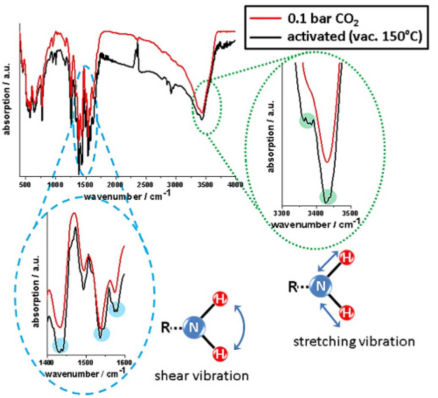

Fig. 3. IR-spectra of NH_2-MIL-125 powder in CO_2 enriched atmosphere (10% CO_2, 90% N_2) and in the activated state. Inset shows characteristic shear vibrations (blue dashed line) and stretching vibrations (green spotted line) for the free amine. (For interpretation of the references to color in this figure legend, the reader is referred to the web version of this article.)

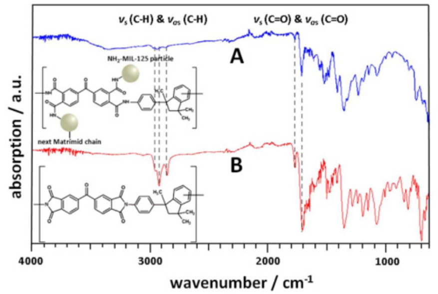

Fig. 4. Comparative IR-study of a neat Matrimid film (B) and Matrimid containing 10 wt% NH_2-MIL-125 particles (A). The dashed lines indicate the specific peaks for the symmetric/asymmetric C=O stretching vibrations and the symmetric/asymmetric aliphatic C-H stretching vibrations, respectively. The two small insets clarify the ring opening polymerization with the NH_2-MIL-125 particles as nodes between the polymer chains.

A possible explanation for the suppressed signal intensity of the aliphatic C-H vibrations is a hindrance of the polymer chain mobility within the cross-linked bulk material.

3.3. SEM analysis

The morphological properties of the thin continuous NH_2-MIL-125 layer (sawn and polished) and the MMMs with NH_2-MIL-125 as embedded filler were observed by SEM analysis. The cross-sectional image of the NH_2-MIL-125 layer is shown in Fig. 5A. It indicates a thin MOF layer of approximately 2 μm thickness on the α-Al_2O_3 support (2.5 μm pores; Fraunhofer IKTS, former Hermsdorfer HITK, Germany). Fig. 5B–D shows the EDXS results of the cross-sectional image and the elemental maps of Al and Ti, respectively. Looking at the elemental maps one can see, that the Ti-Kα signal can not only be found in the continuous layer on top but also in the pores of the rough support. One can assume, therefore, that the NH_2-MIL-125 synthesis solution infiltrated the support and most probably NH_2-MIL-125 growth started in the pores of the support and then continued to crystallize to a thin top layer. In conclusion, from SEM investigation one can expect an appropriate gas separation performance, since the neat supported NH_2-MIL-125 layer shows no recognizable defects or cracks.

As an example for the MMMs, Fig. 6 shows an SEM of a 10 wt% NH_2-MIL-125@Matrimid MMM. The powder used for the MMM preparation (cf. Fig. 6A) shows a circular/tetragonal plate-like crystal shape, which was previously reported for NH_2-MIL-125 prepared in a DMF/methanol solvent mixture [43]. These crystals have a maximum diameter of approximately 800 nm and a thickness of around 200 nm. Fig. 6B and C shows the cross-sectional images of a 10 wt% NH_2-MIL-125@Matrimid in low and high magnification. They indicate, that the MMM has a thickness of nearly 120 μm (cf. Fig. 6B) and that the particles are embedded very well in the polymer Matrimid, thus revealing a good polymer-filler interaction (cf. Fig. 6C). The good embedding can be assigned to the partly cross-linkage between the NH_2-MIL-125 particles and the Matrimid chains as mentioned above (cf. Fig. 4). As recognizable from the EDXS mapping in Fig. 6D and E, the distribution of the filler is homogeneous in the polymer and there is no sign of agglomeration. Consequently, one can also expect a good separation performance for the MMMs.

3.4. Gas separation performance

A thin supported membrane of type NH_2-MIL-125 and Mixed-Matrix-Membranes (MMMs) of the corresponding powder and Matrimid in weight ratios 10/20 wt% have been evaluated in the H_2/CO_2 separation. We expect an adsorption based separation because of the interaction of carbon dioxide with the free amine groups (cf. Fig. 3) in the MOF framework rather than molecular sieving (pore sizes, neglecting framework flexibility are

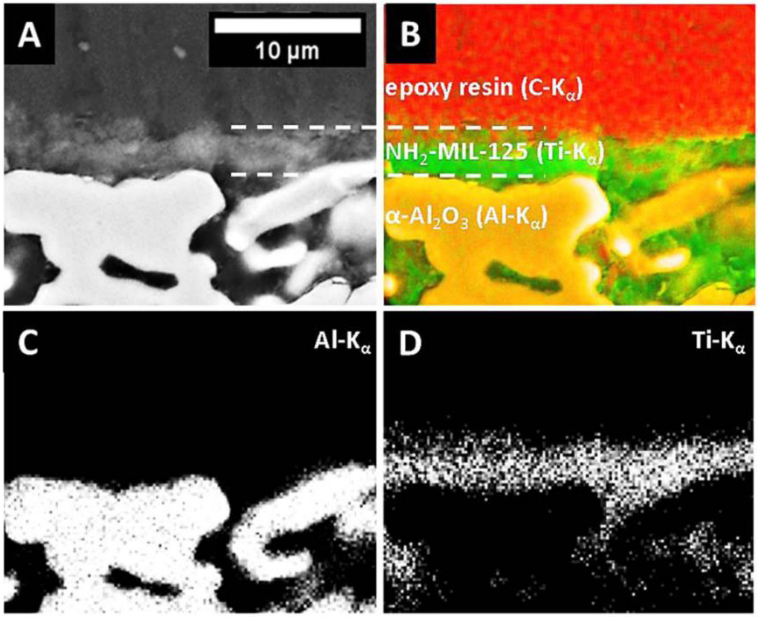

Fig. 5. SEM (A) and EDXS image (B) of the NH_2-MIL-125 membrane cross section. Color code: epoxy resin (red), NH_2-MIL-125 layer (green), α-Al_2O_3 support (yellow). (C) and (D) show the EDXS element distributions of the support (Al-K$_\alpha$) and the MOF-layer (Ti-K$_\alpha$). (For interpretation of the references to color in this figure legend, the reader is referred to the web version of this article.)

approximately 6 Å). As indicated in Fig. 7A, the hydrogen permeability through the thin supported NH_2-MIL-125 layer is indeed approximately eight times higher than those of CO_2 at room temperature. Obviously, the permselectivity decreases with higher temperature, due to a weaker interaction of CO_2 with the amine groups, thus counteracting the impact of the NH_2-functionalization. To get additional information on the permeation mechanism, we also conducted single gas permeation measurements (cf. Fig. 7B). Comparing Fig. 7A and B, we can state that the hydrogen permeability as single gas is slightly increased, but more or less the same as the mixed gas permeability, indicating that there is no strong adsorptive interaction. In contrary to this finding, the single gas CO_2 permeability is remarkably enhanced (roughly doubled) compared to mixed gas permeation. This surprising finding ought to be a result of the interaction of CO_2 with the limited number of NH_2 groups. In the single gas permeation experiment, the CO_2 partial pressure is identical with the total pressure and a large number of adsorbed CO_2 molecules are in interaction with a limited number of NH_2 groups. In the equimolar mixture, the CO_2 partial pressure is 50% of the total pressure. Now less CO_2 interact with the limited number of NH_2 groups, they are stronger adsorbed and their translational mobility is reduced. Our results are in fair accordance to other investigations with deviations between single and mixed gas permeation measurements [44,45], due to the interplay of adsorption and diffusion.

The mixed gas separation results of MMMs containing 10 and 20 wt% NH_2-MIL-125 and a neat Matrimid membrane are shown in Fig. 8. In comparison to the neat Matrimid membrane, both MMMs exhibit a better gas separation performance, that is to say higher hydrogen permeability and higher H_2/CO_2 separation factor. The 10 wt% NH_2-MIL-125@Matrimid MMM shows an increased permeability by approximately 40%, while the selectivity increased by around 25%. At higher feed pressures the permeability increased even more at a constant (H_2/CO_2) selectivity of about 7. Regarding the 20 wt% NH_2-MIL-125@Matrimid MMM, the permeability increased (60%) at a slightly decreased selectivity (10%) in comparison to the neat Matrimid membrane. The performance of the 20 wt% NH_2-MIL-125@Matrimid MMM may be a result of the formation of aggregates and unselective pathways through the composite, thus lowering the overall performance. However, as a result of the elevated temperature (T = 150 °C), the hydrogen permeability is enhanced due to a higher diffusion of the penetrants, while CO_2 adsorption on the MOF and solution in the polymer is suppressed, resulting in a good separation performance. Our finding of an enhanced membrane performance through embedding amine-functionalized fillers is in good accordance with recently published works [46–50].

The major parameters to describe the gas separation performance of a membrane are the permeability of a specific component in the gas mixture and the mixture separation factor, which are related to each other to a high degree. In general, a higher permeability of a specific gas mixture component results in a decreased gas mixture separation factor. As a result of this trade-off relationship, each gas pair has a limited upper bound of the

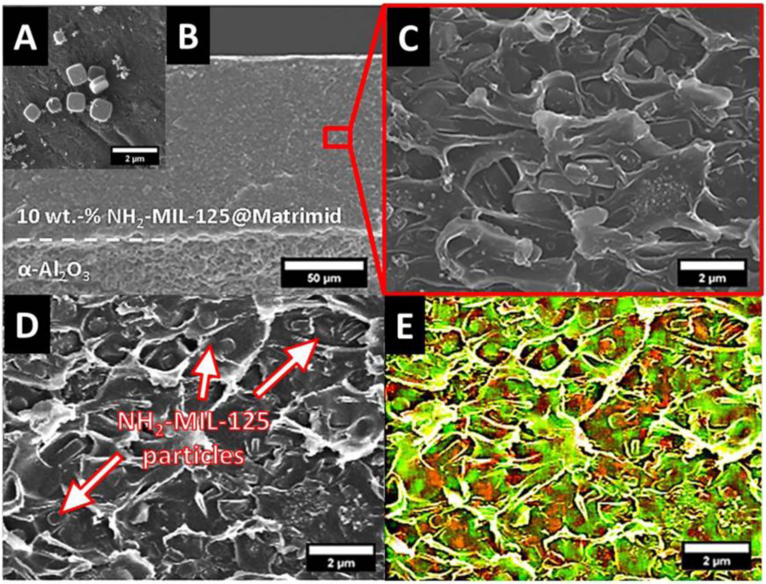

Fig. 6. SEM image of the NH_2-MIL-125 powder (A) and the cross section of a 10 wt% NH_2-MIL-125@Matrimid MMM in low (B) and high (C) magnification. Image D and E show the homogeneous distribution of the powder inside the MMM cross section (same image section). Color code: polymer (green), NH_2-MIL-125 (red). (For interpretation of the references to color in this figure legend, the reader is referred to the web version of this article.)

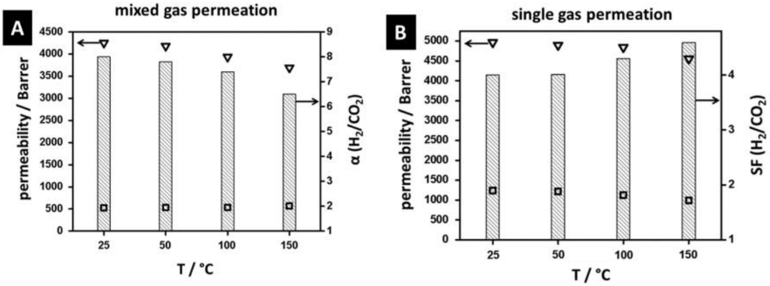

Fig. 7. Mixed (A) and single gas permeabilities (B) for H_2 (▽) and CO_2 (□) and ideal/real separation factors (columns) for an equimolar mixture of H_2/CO_2 at different temperatures for the neat supported NH_2-MIL-125 membrane.

separation factor at a given permeability for one gas component. This so called Robeson upper bound indicates a trendline for the separation of an equimolar H_2/CO_2 mixture [51]. To bring the above mentioned gas separation results of all membranes under study in relation to this Robeson upper bound, we plotted the logarithmic mixture separation factor versus the logarithmic hydrogen permeability (cf. Fig. 9). In summary, all membranes under study show a better performance than the upper bound at these practice-relevant measurement conditions, which was also previously shown for MMMs based on ZIF-8 in Matrimid for similar loadings [52,53].

3.5. Prediction and evaluation of MMM performance with the Maxwell-Model

The Maxwell-model was originally designed to describe the electrical conductivity through heterogeneous media [54], which is very similar to the permeation through a MMM with a polymer as continuous phase (P_C) and embedded MOF as dispersed phase (P_D) [55,56]. Following Eq. (1), the Maxwell-model can be used to predict the effective permeability (P_{eff}) for an MMM, when the permeabilities for the neat continuous (i) polymer (P_C) and (ii) MOF (P_D) phase are known [57]:

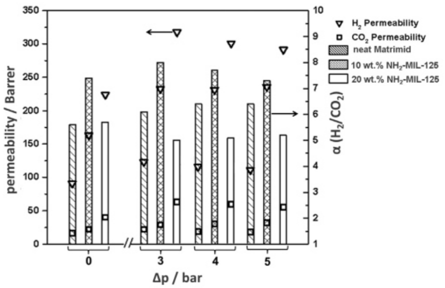

Fig. 8. Mixed gas permeabilities and separation factors α for an equimolar mixture of H_2/CO_2 at different feed pressures and 150 °C for 10/20 wt% NH_2-MIL-125@Matrimid MMMs. The used thicknesses for permeability calculations were 54 μm (neat Matrimid), 122 μm (10 wt% NH_2-MIL-125) and 131 μm (20 wt% NH_2-MIL-125), respectively.

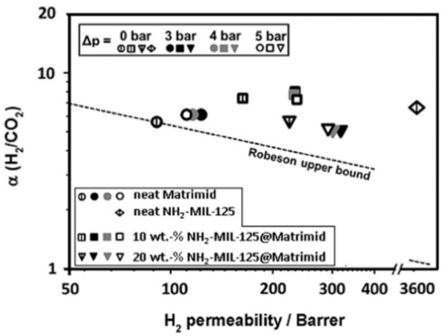

Fig. 9. Hydrogen permeabilities and separation factors α (H_2/CO_2) for all membranes under study at 150 °C for different permeation conditions relative to the Robeson upper bound [51]. Material code: Matrimid (circle), 10 wt% NH_2-MIL-125@Matrimid (square), 20 wt% NH_2-MIL-125@Matrimid (triangle), neat supported NH_2-MIL-125 (diamond).

$$P_{eff} = P_C\left[\frac{P_D + 2P_C - 2\left(\frac{wt\%}{100}\right)_D (P_C - P_D)}{P_D + 2P_C + \left(\frac{wt\%}{100}\right)_D (P_C - P_D)}\right] \quad (1)$$

Hereafter, we will use the Maxwell model for a quantitative interpretation and correlation of the MMM permeation data. Normally, this model is valid for spherical particles and does not account for particle size-distribution, particle shape, and aggregation of particles [58]. Unfortunately, the NH_2-MIL-125 particles are neither spherical nor monodisperse (cf. Fig. 6A) and the particle distribution seems to be homogeneous (cf. Fig. 6D and E) but is probably not ideal. Furthermore, the influence of (i) a suppressed framework flexibility and (ii) the polymer-filler coupling via a ring opening polymerization (c.f. Fig. 4) are also ambiguous. These above mentioned facts may affect the MMM performance and lead to an underestimation of the MMM capabilities as shown in Fig. 10. Obviously there seems to be an optimal weight fraction for the filler material (approximately 10 wt%). Concerning the 20 wt% NH_2-MIL-125@Matrimid MMM, the bigger deviation from the predicted permeability may be the result of an increased

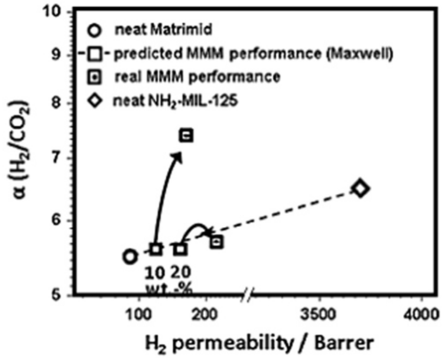

Fig. 10. Predicted (Maxwell-model) and experimentally found separation factors α (H_2/CO_2) for the 10 and 20 wt% NH_2-MIL-125 in Matrimid MMMs at 150 °C and atmospheric pressure. Wicke-Kallenbach measurement with both feed and permeate side at 1 bar.

agglomeration tendency of the filler material, thus forming more unselective pathways through the MMM, as already mentioned above. This experimental finding is in complete accordance with our previous finding on ZIF-8/Matrimid MMMs [53]. However, we believe that all, the limited validity of the Maxwell-model as described above, the suppressed framework flexibility by the surrounding polymer phase as described in [52,59] and the covalent coupling between the polymer phase and the filler material contribute to the deviating performance of the MMMs.

4. Conclusions

The present study demonstrates the high performance of the amine-functionalized MOF NH_2-MIL-125 as continuous supported layer as well as corresponding Matrimid-based MMMs in the separation of equimolar H_2/CO_2 mixtures at various temperatures and feed pressures. IR-spectroscopy clearly shows the adsorptive interaction of CO_2 with the amine functionalities of NH_2-MIL-125. Furthermore, via IR-spectroscopy, the partly cross-linkage of the NH_2-MIL-125 particles with the Matrimid chains was experimentally verified. The adsorptive interactions of CO_2 with NH_2-MIL-125 are assumed to be responsible for the high separation performance of this material as neat MOF membrane as well as filler material for MMMs. Regarding the thin supported MOF layer, higher temperatures led to a decrease of the permselectivity, due to the weakened (compared to lower temperatures) adsorptive interaction between the amine groups and CO_2, thus reducing the retention of the latter. Considering the MMMs, the amount of 10 wt% filler seems to be optimal, since both the permeability and the selectivity are enhanced in comparison to the neat polymer membrane, whereas 20 wt% MOF loading only further increased the permeability. The separation factor of both MMMs (10 and 20 wt% loading) remained nearly constant with increasing the feed pressures. Lastly, if bringing the performance of both the supported thin NH_2-MIL-125 layer and the Matrimid-based MMMs in relation to the Robeson upper bound and evaluating the performance of the MMMs with the Maxwell- model, all membranes under study exceeded the Robeson upper bound.

Acknowledgements

The authors of this work are grateful for the financial support from the EU 7th Framework Project M_4CO_2 (Grant Agreement No 608490), organized by F. Kapteijn and J. Gascon. D. Unruh acknowledges support from Hannover School of Nanotechnology. F. Renz is thankful for financial support from Deutsche Forschungsgemeinschaft (RE1627/1-3).

References

[1] M. Kanniche, R. Gros-Bonnivard, P. Jaud, J. Valle-Marcos, J.-M. Amann, C. Bouallou, Pre-combustion, post-combustion and oxy-combustion in thermal power plant for CO_2 capture, Appl. Therm. Eng. 30 (2010) 53–62.
[2] N. Casas, J. Schell, L. Joss, M. Mazzotti, A parametric study of a PSA process for pre-combustion CO_2 capture, Sep. Purif. Technol. 104 (2013) 183–192.
[3] J. Davison, Performance and costs of power plants with capture and storage of CO_2, Energy 32 (2007) 1163–1176.
[4] B. Belaissaoui, Y. Le Moullec, H. Hagi, E. Favre, Energy efficiency of oxygen enriched air production technologies: cryogeny vs membranes, Sep. Purif. Technol. 125 (2014) 142–150.
[5] J.C.M. Farla, C.A. Hendriks, K. Blok, Carbon dioxide recovery from industrial processes, Clim. Change 29 (1995) 439–461.
[6] P.H.M. Feron, C.A. Hendriks, CO_2 Process Capture Principles and Costs, Oil & Gas Science and Technology – Rev. IFP, (2005) 451–459.
[7] J. Gibbins, H. Chalmers, Carbon capture and storage, Energy Policy 36 (2008) 4317–4322.
[8] R. Stanger, T. Wall, R. Spörl, M. Paneru, S. Grathwohl, M. Weidmann, G. Scheffknecht, D. McDonald, K. Kyöhänen, J. Ritvanen, S. Rahiala, T. Hyppänen, J. Mletzko, A. Kather, S. Santos, Oxyfuel combustion for CO_2 capture in power plants, Int. J. Greenh. Gas Control 40 (2015) 55–125.
[9] J.-M. Amann, M. Kanniche, C. Bouallou, Reforming natural gas for CO_2 pre-combustion capture in combined cycle power plant, Clean Technol. Environ. Policy 11 (2009) 67–76.
[10] S.R. Batten, N.R. Champness, X.-M. Chen, J. Garcia-Martinez, S. Kitagawa, L. Ohrstrom, M. O'Keffe, M.P. Suh, J. Reedijk, Coordination polymers, metal-organic frameworks and the need for terminology guidelines, CrystEngComm 14 (2012) 3001–3004.
[11] G.T. Rochelle, Amine Scrubbing for CO_2 Capture, Science 325 (2009) 1652–1654.
[12] J. Yang, H.Y. Tan, Q.X. Low, B.P. Binks, J.M. Chin, CO_2 capture by dry alkanolamines and an efficient microwave regeneration process, J. Mater. Chem. A 3 (2015) 6440–6446.
[13] R. Vaidhyanathan, S.S. Iremonger, G.K.H. Shimizu, P.G. Boyd, S. Alavi, T.K. Woo, Direct observation and quantification of CO_2 binding in an amine-functionalized nanoporous solid, Science 330 (2010) 650–653.
[14] S.-N. Kim, J. Kim, H.-Y. Cho, W.-S. Ahn, Adsorption/catalytic properties of MIL-125 and NH_2-MIL-125, Catal. Today 204 (2013) 85–93.
[15] B. Arstad, H. Fjellvåg, K. Kongshaug, O. Swang, R. Blom, Amine functionalised metal organic frameworks (MOFs) as adsorbents for carbon dioxide, Adsorption 14 (2008) 755–-7762.
[16] N. Wang, A. Mundstock, Y. Liu, A. Huang, J. Caro, Amine-modified Mg-MOF-74/CPO-27-Mg membrane with enhanced H_2/CO_2 separation, Chem. Eng. Sci. 124 (2015) 27–36.
[17] J. Coronas, Present and future synthesis challenges for zeolites, Chem. Eng. J. 156 (2010) 236–242.
[18] J. Caro, Are MOF membranes better in gas separation than those made of zeolites? Curr. Opin. Chem. Eng. 1 (2011) 77–83.
[19] J. Caro, M. Noack, Zeolite Membranes – Status and Perspective, in: S. Ernst (Ed.), Advances in Nanoporous Materials, 1, Elsevier, Amsterdam, 2009, pp. 58–62.
[20] A.J. Brown, J.R. Johnson, M.E. Lydon, W.J. Koros, C.W. Jones, S. Nair, Continuous Polycrystalline Zeolitic Imidazolate Framework-90 Membranes on Polymeric Hollow Fibers, Angew. Chem. 124 (2012) 10767–10770.
[21] H.-J. Kim, N.A. Brunelli, A.J. Brown, K.-S. Jang, W.G. Kim, F. Rashidi, J.R. Johnson, W.J. Koros, C.W. Jones, S. Nair, Silylated mesoporous silica membranes on polymeric hollow fiber supports: synthesis and permeation properties, ACS Appl. Mater. Interfaces 6 (2014) 17877-1788.
[22] H.-J. Kim, W. Chaikittisilp, K.-S. Jang, S.A. Didas, J.R. Johnson, W.J. Koros, S. Nair, C.W. Jones, Aziridine-functionalized mesoporous silica membranes on polymeric hollow fibers: synthesis and single-component CO_2 and N_2 permeation properties, Ind. Eng. Chem. Res. 54 (2015) 4407–4413.
[23] M. Ulbricht, Advanced functional polymer membranes, Polymer 47 (2006) 2217–2265.
[24] S. Shishatskiy, C. Nistor, M. Popa, S. Pereira Nunes, K.V. Peinemann, Polyimide asymmetric membranes for hydrogen separation: influence of formation conditions on gas transport properties, Adv. Eng. Mater. 8 (2008) 390–397.
[25] J.G. Wijmans, R.W. Baker, The solution-diffusion model: a review, J. Membr. Sci. 107 (1995) 1–21.
[26] T. Rodenas, I. Luz, G. Prieto, B. Seoane, H. Miro, A. Corma, F. Kapteijn, F. Llabrés i Xamena, J. Gascon, Metal-organic-framework nanosheets in polymer composite materials for gas separation applications, Nat. Mater. 14 (2014) 48–55.
[27] T.-S.- Chung, L.Y. Liang, Y. Li, S. Kulprathipanja, Mixed matrix membranes (MMMs) comprising organic polymers with dispersed inorganic fillers for gas separation, Prog. Polym. Sci. 32 (2007) 483–507.
[28] G. Dong, H. Li, V. Chen, Challenges and opportunities for mixed-matrix-membranes for gas separation, J. Mater. Chem. A 1 (2013) 4610–4630.
[29] B. Seoane, J. Coronas, I. Gascon, M. Etxeberria Benavides, O. Karvan, J. Caro, F. Kapteijn, J. Gascon, Metal-organic framework based mixed matrix membranes: a solution for highly efficient CO_2 capture? Chem. Soc. Rev. 44 (2015) 2421–2454.
[30] B. Zornoza, C. Tellez, J. Coronas, J. Gascon, F. Kapteijn, Metal organic framework based mixed matrix membranes: an increasingly important field of research with a large application potential, Microporous Mesoporous Mater. 166 (2013) 67–78.
[31] B. Zornoza, P. Serra-Crespo, C. Tellez, J. Coronas, J. Gascon, F. Kapteijn, Functionalized flexible MOFs as fillers in mixed matrix membranes for highly selective separation of CO_2 from CH_4 at elevated pressures, Chem. Commun. 47 (2011) 9522–9524.
[32] P. Gorgojo, S. Uriel, C. Tellez, J. Coronas, Development of mixed matrix membranes based on zeolite Nu-6(2) for gas separation, Microporous Mesoporous Mater. 115 (2008) 85–92.
[33] A. Kudasheva, S. Sorribas, B. Zornoza, C. Tellez, J. Coronas, Pervaporation of water/ ethanol mixtures through polyimide based mixed matrix membranes containing ZIF-8, ordered mesoporous silica and ZIF-8-silica core-shell spheres, J. Chem. Technol. Biotechnol. 90 (2015) 669–677.
[34] L. Lin, A. Wang, L. Zhang, M. Dong, Y. Zhang, Novel mixed matrix membranes for sulfur removal and for fuel cell applications, J. Power Sources 220 (2012) 138–146.
[35] A. Zirehpour, A. Rahimpour, M. Jahanshani, M. Peyravi, Mixed matrix membrane application for olive oil wastewater treatment: Process optimization based on Taguchi design method, J. Environ. Manag. 132 (2014) 113–120.
[36] J. Cravillion, R. Nayuk, S. Springer, A. Feldhoff, K. Huber, M. Wiebcke, Controlling zeolitic imidazolate framework nano- and microcrystal formation: insight into crystal growth by time-resolved in situ static light scattering, Chem. Mater. 23 (2011) 2130–2141.
[37] T. Li, Y. Pan, K.-V. Peinemann, Z. Lai, Carbon dioxide selective mixed matrix composite membrane containing ZIF-7 nano-fillers, J. Membr. Sci. 425–426 (2013) 235–242.
[38] M. Dan-Hardi, C. Serre, T. Frot, L. Rozes, G. Maurin, C. Sanchez, G. Ferey, A new photoactive crystalline highly porous titanium(IV) dicarboxylate, J. Am. Chem. Soc. 131 (2009) 10857–10859.
[39] C. Zlotea, D. Phanon, M. Mazaj, D. Heurtaux, V. Guillerm, C. Serre, P. Horcajada, T. Devic, E. Magnier, F. Cuevas, G. Ferey, P.L. Llewellyn, M. Latroche, Effect of NH_2 and CF_3 functionalization on the hydrogen sorption properties of MOFs, Dalton Trans. 40 (2011) 4879–4881.
[40] M.A. Moreira, J.C. Santos, A.F.P. Ferreira, J.M. Loureiro, F. Ragon, P. Horcajada, P. G. Yot, C. Serre, A.E. Rodrigues, Toward understanding the influence of ethylbenzene in p-xylene selectivity of the porous titanium amino terephthalate MIL-125(Ti): adsorption equilibrium and separation of xylene isomers, Langmuir 28 (2012) 3494–3502.
[41] C.E. Powell, X.J. Duthie, S.E. Kenthish, G.G. Qiao, G.W. Stevens, Reversible diamine cross-linking of polyimide membranes, J. Membr. Sci. 291 (2007) 199–209.
[42] S. Kuper, A. Embrechts, H.A. Every, T. de Vries, L.C.P.M. de Smet, Matrimid aerogels by temperature-controlled, solution-based crosslinking, Macromol. Mater. Eng. 298 (2013) 868–875.
[43] S. Hu, M. Liu, K. Li, Y. zuo, A. Zhang, C. Song, G. Zhang, X. Guo, Solvothermal synthesis of NH_2-MIL-125(Ti) from circular plate to octahedron, CrystEngComm 16 (2014) 9645–9650.
[44] F. Zhang, X. Zou, X. Gao, S. Fan, F. Sun, H. Ren, G. Zhu, Hydrogen selective NH_2-MIL-53(Al) MOF membranes with high permeability, Adv. Funct. Mater. 22 (2012) 3583–3590.
[45] Q. Liu, T. Wang, H. Guo, C. Liang, S. liu, Z. Zhang, Y. Cao, D.S. Su, J. Qiu, Controlled synthesis of high performance carbon/zeolite T composite membrane materials for gas separation, Microporous Mesoporous Mater. 120 (2009) 460–466.
[46] T. Rodenas, M. van Dalen, E. García-Pérez, P. Serra-Crespo, B. Zornoza, F. Kapteijn, J. Gascon, Visualizing MOF Mixed Matrix Membranes at the nanoscale: towards structure-performance relationships in CO_2/CH_4 separation over NH_2-MIL-53(Al)@PI, Adv. Funct. Mater. 24 (2014) 249–256.
[47] T. Rodenas, M. van Dalen, P. Serra-Crespo, F. Kapteijn, J. Gascon, Mixed matrix membranes based on NH_2-functionalized MIL-type MOFs: influence of structural and operational parameters on the CO_2/CH_4 separation performance, Microporous Mesoporous Mater. 192 (2014) 35–42.
[48] A.E. Amooghin, M. Omidkhah, A. Kargari, The effects of aminosilane grafting on NaY zeolite-Matrimid®5218 mixed matrix membranes for CO_2/CH_4 separation, J. Membr. Sci. 490 (2015) 364–379.
[49] O.G. Nik, X.Y. Chen, S. Kaliaguine, Amine-functionalized FAU/EMT-polyimide mixed matrix membranes for CO_2/CH_4 separation, J. Membr. Sci. 379 (2011) 468–478.
[50] X.Y. Chen, H. Vinh-Thang, D. Rodrigue, S. Kaliaguine, Amine-functionalized Mil-53 metal-organic framework in polyimide mixed matrix membranes for CO_2/CH4 separation, Ind. Eng. Chem. Res. 51 (2012) 6895–6906.
[51] L.M. Robeson, The upper bound revisited, J. Membr. Sci. 320 (2008) 390–400.
[52] L. Diestel, N. Wang, B. Schwiedland, F. Steinbach, U. Giese, J. Caro, MOF based MMMs with enhanced selectivity due to hindered linker distortion, J. Membr. Sci. 492 (2015) 181–186.
[53] L. Diestel, N. Wang, A. Schulz, F. Steinbach, J. Caro, Matrimid-based mixed

matrix membranes: Interpretation and correlation of experimental findings for zeolitic imidazolate frameworks as fillers in H_2/CO_2 separation, Ind. Eng. Chem. Res. 54 (2015) 1103–1112.
[54] J. Maxwell, A Treatise on Electricity & Magnetism, Dover Publications, New York, 1954.
[55] R. Mahajan, W. Koros, Mixed matrix membrane materials with glassy polymers. Part 2, Polym. Eng. Sci. 42 (2002) 1432–1441.
[56] Z. Huang, Y. Li, R. Wen, M. Teoh, S. Kulprathipanja, Enhanced gas separation properties by using nanostructured PES Zeolite 4 A mixed matrix membranes, J. Appl. Polym. Sci. 101 (2006) 3800–3805.
[57] D.Q. Vu, W.J. Koros, S.J. Miller, Mixed matrix membranes using carbon molecular sieves II. Modeling permeation behavior, J. Membr. Sci. 211 (2003) 335–348.
[58] R. Pal, Permeation models for mixed matrix membranes, J. Colloid Interf. Sci. 317 (2008) 191–198.
[59] R. Mueller, V. Hariharan, C. Zhang, R. Lively, R. Vasenkov, J. Membr. Sci. 499 (2016) 12–19.

2.3 Metal-Organic Framework UiO-66 Layer: A Highly Oriented Membrane with Good Selectivity and Hydrogen Permeance

S. Friebe, B. Geppert, F. Steinbach, J. Caro

ACS Applied Materials and Interfaces **2017**, 9, 12878-12885.

ACS APPLIED MATERIALS & INTERFACES
Research Article
www.acsami.org

Metal–Organic Framework UiO-66 Layer: A Highly Oriented Membrane with Good Selectivity and Hydrogen Permeance

Sebastian Friebe,* Benjamin Geppert, Frank Steinbach, and Jürgen Caro

Institute of Physical Chemistry and Electrochemistry, Leibniz Universität Hannover, Callinstraße 3A, D-30167 Hannover, Germany

Supporting Information

ABSTRACT: The 3D metal–organic framework (MOF) structure UiO-66 $[Zr_6O_4(OH)_4(bdc)_6]$, featuring triangular pores of approximately 6 Å, has been successfully prepared as a thin supported membrane layer with high crystallographic orientation on ceramic α-Al_2O_3 supports. The adhesion of the MOF layer to the ceramic support was investigated in different taxing conditions. Furthermore, by coating this UiO-66 membrane with a thin polyimide (Matrimid) top layer, we prepared a multilayer composite. Said membranes have been evaluated in the separation of hydrogen (H_2) from different binary mixtures at room temperature. H_2 as the smallest molecule (2.9 Å) should pass the UiO-66 membrane preferably since the kinetic diameters of all the other gases under study are larger. The gas mixture separation factors for the neat UiO-66 membrane were indeed found to be H_2/CO_2 = 5.1, H_2/N_2 = 4.7, H_2/CH_4 = 12.9, H_2/C_2H_6 = 22.4, and H_2/C_3H_8 = 28.5. The coating with Matrimid led to a sharp cutoff for gases with kinetic diameters greater than 3.7 Å, resulting in increased separation performance.

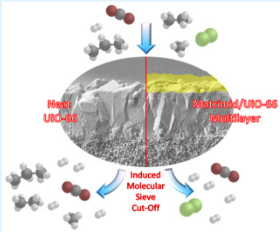

KEYWORDS: *UiO-66, MOF membrane, stability, crystallographic orientation, hydrogen separation, polymer coating*

1. INTRODUCTION

The diversity of metal–organic framework (MOF) chemistry allows the tailored synthesis of an almost unlimited number of microporous structures.[1−3] Additionally, these structures can feature functional groups or unsaturated accessible metal sites as adsorption centers for different gases.[4−7] These two facts speak for MOFs as candidates for high-quality molecular sieve membranes. Consequently, this versatile material class is particularly attractive for membrane assisted separation processes like hydrogen purification from waste gases, CO_2 removal from flue gases, olefin paraffin separation, or removal of unwanted components (e.g., dewatering or desulfurization).[8−10]

Despite some pioneering activities and plenty of work in the development of supported MOF-based membranes, the *scale up* and reproducibility of defect-free MOF membranes are still major challenges.[11,12] Nevertheless, there are several publications with promising approaches to enhance the reproducibility and membrane quality by synthesis modifications or new membrane architectures.[13−17] When looking at the diversity of available MOFs, structures with 3D geometry and pore apertures of a few Å are of particular interest, since they allow an unhindered gas permeation regardless of the crystal orientation within the membrane[18] unlike 1D geometries.[19] Our group already published results with MOF layers as molecular sieve membranes prepared by microwave synthesis,[14] by reactive seeding,[20] or by covalent bonding to the support.[21]

Nevertheless, for application in membrane-based separation processes, the materials have to feature a good mechanical and chemical stability. Especially, the poor hydrothermal stability of most MOFs limits their application under harsh conditions.[22] However, like a lot of other zirconium-based MOFs,[23−26] UiO-66 (Universitet i Oslo) shows exceptional stability against chemicals, temperature, and mechanical stress.[27,28] Therefore, it is a promising material for the fabrication of robust membranes as recently shown for CO_2/N_2 separation under harsh conditions.[29] Furthermore, it has already been well investigated in terms of the pore functionalization,[30] different synthesis routes,[31,32] reaction kinetics,[33] flexibility, and mechanical properties.[34] Additionally, the structural characteristics including the crystallographic positions of the atoms were investigated in detail via DFT calculations in combination with EXAFS measurements and Rietveld refinements by Lillerud, Lamberti, and co-workers.[35,36] Their works clarified that the 3D structure of UiO-66 (Figure 1A) consists of $Zr_6O_4(OH)_4$ nodes as inorganic subunits, which are each 12-fold bridged to other nodes via the benzene 1,4-dicarboxylate linker, resulting in triangular windows with a size of 6 Å (Figure 1B).[37,38] These windows connect two types of cages (octahedral: 11 Å Ø; tetrahedral: 8 Å Ø).[39]

Another study by Jobic and co-workers[40] explored the idiosyncracies of the benzene ring motion via ^{2}H NMR spectroscopy and quasi-elastic neutron scattering (QENS). They pointed out that the aromatic rings feature the lowest rotational energy barrier (≈30 kJ·mol^{-1}) in comparison to other MOFs.[41,42] Additionally, they proved that the rotational

Received: February 13, 2017
Accepted: March 20, 2017
Published: March 20, 2017

DOI: 10.1021/acsami.7b02105
ACS Appl. Mater. Interfaces 2017, 9, 12878−12885

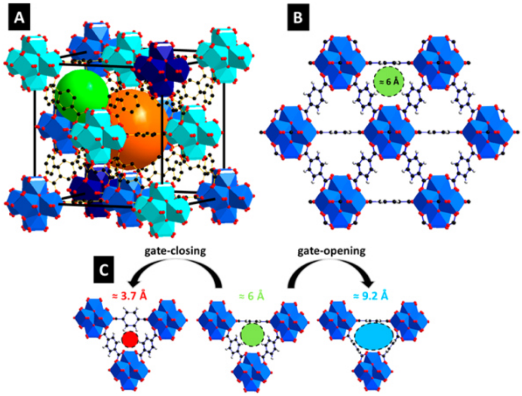

Figure 1. (A) Illustration of the 3D UiO-66 structure showing the octahedral cage (orange ball) and the tetrahedral cage (green ball). (B) Triangular windows between the octahedral and tetrahedral cages with a pore size of 6 Å as found experimentally from Rietveld analysis,[36,39] resulting from the 12-fold terephthalate bridging between the $Zr_6O_4(OH)_4$ nodes. (C) Change of pore entrance size as a result of the 3 orientable benzene rings performing flips around the C_2 symmetry axis. The resulting pore size fluctuates between 3.7 and 9.2 Å. Used cif-file: cm1022882_si_001.cif.[35] Software used: Diamond 3.2.

benzene ring motion shows a temperature dependent behavior. For instance, at room temperature, roughly 7% of the benzene rings are "static", whereas the rest perform "flips" ("slow flips": ≈37%; "fast flips": ≈56%), which can affect the pore entrance size as demonstrated in Figure 1C. We expect the above-mentioned overall robustness of UiO-66 and the benzene ring rotation, thus affecting the pore size entrance, to be an ideal model system to investigate the effect of an additional Matrimid polymer top layer, which should modify the gas separation capabilities of the MOF layer to a certain degree.

Here, we present the synthesis and evaluation of an oriented UiO-66 layer on flat ceramic alumina supports as membrane for the separation of hydrogen from several other gases. The orientation of the octahedral crystals relative to the support is characterized by different crystallographic preferred orientations (CPOs) by comparing the statistically oriented powder and the supported membrane layer. Further, we prepared a multilayer membrane with a polyimide (Matrimid) top layer on the UiO-66 membrane. We expect this polymer layer either to heal present microdefects or to interact with the neat MOF layer at the interface to a certain degree, thus giving modified gas separation capabilities. The separation performance of the prepared membranes has been tested in mixed gas separation.

2. MATERIALS AND METHODS

2.1. Materials. The chemicals and reagents used for the preparation or investigation include zirconium chloride ($ZrCl_4$, anhydrous, 98%, Alfa Aesar), terephthalic acid (H_2bdc, 98%, Sigma-Aldrich), benzoic acid (C_7H_6O, ≥99.5%, Sigma-Aldrich), dimethylformamide (DMF, 99.8% anhydrous, Sigma-Aldrich), methanol (MeOH, ≥99.8%, Sigma-Aldrich), dichloromethane (DCM, 99.8%, Carl Roth), hydrochloric acid (HCl, 37%, Sigma-Aldrich), and Matrimid (Matrimid 5218, Huntsman). All these chemicals were obtained from commercial vendors at reagent grade purity or higher and used without further purification.

2.2. Preparation of Oriented UiO-66 Membrane and UiO-66/Matrimid Multilayer. The supported oriented UiO-66 layer was synthesized via a benzoic acid modulated hydrothermal synthesis following a slightly modified recipe reported elsewhere.[43] For a typical approach, 0.28 g of H_2bdc and 4.4 g of benzoic acid were dissolved in 10 mL of DMF and heated up to 150 °C. In parallel, a second solution of 0.42 g of $ZrCl_4$ in 4.5 mL of DMF was prepared and also heated up to 150 °C. The two solutions were combined in a Teflon lined autoclave. A ceramic α-Al_2O_3 support (70 nm pores in top layer, Fraunhofer IKTS, former Hermsdorfer HITK, Germany), previously modified by seeding with 300 nm octahedral crystals (10 wt % ethanolic suspension; see Figures S1−S3), was placed in the solution in a face down orientation. Subsequently, the autoclave was placed in a conventional oven at 180 °C for 24 h. After cooling down to room temperature the membrane was washed several times with MeOH and then stored in DCM overnight. The membrane was then dried at 80 °C for 24 h.

The UiO-66/Matrimid multilayer was prepared by coating Matrimid dissolved in DCM on top of the neat MOF layer. This composite was subsequently stored in a DCM atmosphere (Petri dish) to allow a slow evaporation of the solvent.

2.3. Characterization. *2.3.1. X-ray Diffraction.* The XRD measurements were done on a Bruker D8 Advance Diffractometer with Cu Kα radiation in a range between 6° and 20°. The CPOs were calculated manually while the orientation expressed as a percentage was calculated with the software Topas 4.1.

2.3.2. Scanning Electron Microscopy. The scanning electron microscopy (SEM, EDXS) studies of the samples were done with a field-emission electron microscope (JEOL JSM-6700F) at 20 kV accelerating voltage and 15 mm working distance.

2.3.3. Gas Permeation Measurements. Our assumptions of the separation capabilities were evaluated by mixed gas separation measurements of different equimolar binary mixtures (H_2/CO_2, H_2/N_2, H_2/CH_4, H_2/C_2H_6, and H_2/C_3H_8). Therefore, the membrane was sealed in the permeation cell with Viton O-rings (FFKM 70 Vi 370). The following measurements were carried out by feeding an equimolar mixture of H_2/X (25/25 cm^3(STP)/min) at room temperature by means of two mass flow controllers (MFCs). The permeate side of the membrane was swept with a controlled N_2 stream by means of another MFC (MOF membrane: 50 cm^3(STP)/min; multilayer membrane: 1 cm^3(STP)/min) and both feed and sweep side at 1 bar (Wicke-Kallenbach technique). Gas chromatography

DOI: 10.1021/acsami.7b02105
ACS Appl. Mater. Interfaces 2017, 9, 12878−12885

ACS Applied Materials & Interfaces — Research Article

(Agilent Technologies 7890B) was applied to investigate the permeated mixture.

3. RESULTS AND DISCUSSION

3.1. Structure Analysis. Figure 2A shows the XRD patterns of UiO-66 powder, a supported UiO-66 membrane,

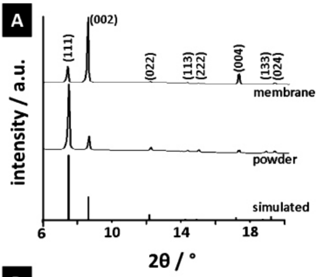

reflection (X/Y)	CPO (X/Y)
002/111	41
002/022	20

Figure 2. (A) X-ray diffractograms of the synthesized UiO-66 powder, the thin supported highly oriented UiO-66 layer, and a simulated XRD pattern from the cif-file. The measured XRDs have been normalized for better comparison. (B) CPOs of (002) vs the (111) and (022) reflections indicating the high orientation of the octahedrons in relation to the perpendicular line to the support (see Figure 3B).

and a simulated XRD from a cif-file.[35] It is obvious that the powder XRD is in accordance with the simulated XRD. Evidently, the membrane has grown with a high orientation, as indicated by the huge intensity change of the (002) and (111) reflections in comparison to the statistically oriented powder, meaning that the corresponding layer was grown with high orientation of the octahedrons relative to the support. Similar findings of oriented layers have already been published for several other MOF and zeolite membranes.[44,45] The orientation of the UiO-66 layer was most likely achieved by presynthetic support seeding followed by a van der Drift growth mechanism[46] and the favorable face down support orientation during the synthesis in combination with the so-called coordination modulation mechanism due to the presence of benzoic acid, proposed by Kitagawa and co-workers.[47,48] The degree of the orientation can be characterized by the so-called crystallographic preferred orientation (CPO) via the following eq 1, where I stands for the intensity of a reflection X or Y and M and P belong to the investigated membrane (M) or the statistically oriented powder (P), respectively:[49]

$$\mathrm{CPO}\frac{(X)}{(Y)} = \frac{((I_M^{(X)}/I_M^{(Y)}) - (I_P^{(X)}/I_P^{(Y)}))}{(I_P^{(X)}/I_P^{(Y)})} \quad (1)$$

For CPO values ≥1, the membrane exhibits a preferred orientation along the direction of (X), whereas a CPO value of 0 means that the membrane shows no specific orientation. To investigate the orientation of the UiO-66 membrane under study, we compared the intensities of the major (002) reflection with the intensities of the (111) and (022) reflections (see Figure 2B).

As shown in Figure 2B, the CPO values for the dominant investigated reflections are CPO (002/111) = 41 and CPO (002/022) = 20, respectively. This clearly exhibits the alignment of the (002) planes in parallel to the support, which is in good accordance with the model of the van der Drift growth.[46] Following the latter, the growth starts from randomly oriented seed crystals until they contact each other. From this point, the crystals grow along the direction with the highest growth rate, thus building the top layer of the membrane. Consistent with this, the highest growth rate of the UiO-66 crystals takes place in the (002) direction. Additionally, this above-mentioned finding was also qualitatively proven by a Rietveld analysis, which roughly resulted in an 85% fraction of preferred (002) orientation for the UiO-66 membrane[50] (see Figure S4).

3.2. Morphological Analysis. Figure 3 shows the SEM images of the UiO-66 membrane in top view (A), the cross

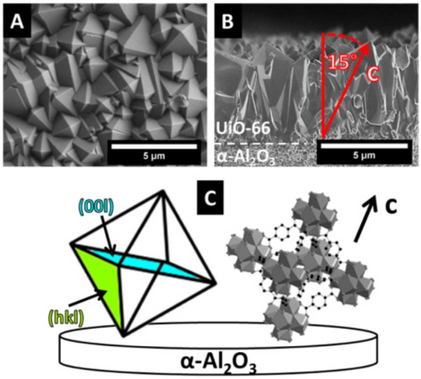

Figure 3. Exemplary SEM images of the supported UiO-66 membrane in (A) top view and (B) cross section. (C) Schematic representation of the octahedrons orientation within the UiO-66 layer and their orientation to the support surface.

section (B), and a schematic illustration for the orientation of the octahedrons and the resulting structure tilting to the support (C). The top view (A) indicates well intergrown crystals, which show the tips of the octahedrons. The taken cross section images of the UiO-66 membrane (B) reveal a 5 μm thick layer with a high orientation across the whole ceramic support (tilting angle of the octahedrons ≈15°). The obvious tilting angle from Figure 3B was confirmed by measuring the c-axis tilt angle for 25 different crystals inside the layer (see Figure S5). Furthermore, the average tilting angle of the latter seems to be in good accordance to the approximated preferred crystal orientation from Rietveld refinement and the concomitant calculation (see Figure S4). From SEM, one can expect a good gas separation performance, since the supported UiO-66 layer shows no recognizable major defects or cracks.

3.3. Stability Analysis. As reported in the literature, the growth of MOFs on polymer fibers such as polyamides or polypropylenes can be facilitated by specific buffer layers (e.g.,

DOI: 10.1021/acsami.7b02105
ACS Appl. Mater. Interfaces 2017, 9, 12878−12885

ACS Applied Materials & Interfaces Research Article

ZnO, TiO_2 or Al_2O_3) fabricated via atomic layer deposition. However, some of these layers show a certain incompatibility to MOFs, thus leading to stability issues.[51,52] Since we also used α-Al_2O_3 supports for the crystallization of our MOF membrane, we analyzed, therefore, the adhesion of the prepared MOF layers to the ceramic support under different (taxing) conditions. The prepared membranes were (i) stored in distilled water for 24 h, (ii) stored in HCl (10%) for 24 h, (iii) sonicated in distilled water for 1 h, and (iv) sonicated in HCl (10%) for 1 h. Said membranes were then investigated via SEM and compared to the pristine MOF layer (c. f. Figure 4A–C). The storage in water did not change the appearance of the UiO-66 layer or the adhesion to the ceramic support. Consequently, the membrane looked like the pristine membrane (cf. Figure 3B), which is in good accordance with stability results reported by several other groups.[53,54] On the contrary to the latter, the storage in HCl (10%) affected the appearance of the layer, as shown in Figure 4 A. The spent membrane shows fewer edges and a smoothed surface, as if some material was abrased through this treatment. However, the contact with the support is still present. The membrane after sonication in water is shown in Figure 4B and also looks like the pristine membrane. Nevertheless, the sonication resulted in a loss of contact to the α-Al_2O_3 disk, thus showing a huge crack between the interface of MOF and support. The sonication in HCl (10%), which displays the most taxing condition, stressed the membrane to the greatest degree (cf. Figure 4C). Hence, the UiO-66 layer not only lost almost all contact with the support but also was destroyed into several small slices.

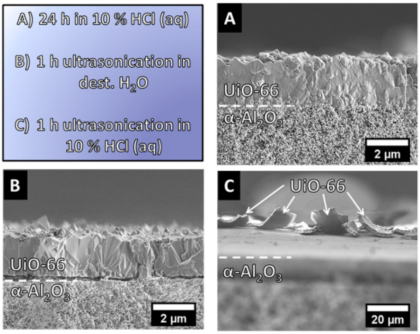

Figure 4. SEM images of the supported UiO-66 membrane after adhesion tests in three different taxing conditions: (A) after storage in 10% HCl (aq) for 24 h, (B) after ultrasonication in distilled H_2O for 1 h, and (C) after ultrasonication in 10% HCl (aq) for 1 h.

3.4. Gas Separation Analysis. Figure 5 shows the mixed gas permeances of H_2, CO_2, N_2, CH_4, C_2H_6, and C_3H_8 for equimolar H_2/X (X = N_2, CO_2, CH_4, C_2H_6, C_3H_8) gas mixtures through the oriented UiO-66 membrane as a function of the kinetic gas diameter. It is obvious that the permeance of hydrogen through the UiO-66 membrane is much higher compared to the other gases (N_2, CO_2, CH_4, C_2H_6, C_3H_8) and the permeance decreases steeply with increasing kinetic gas diameter. This order seems to be in good accordance with the concept of molecular sieving, since hydrogen (2.9 Å) is the smallest gas with a size clearly below the estimated pore size of 6 Å of UiO-66. However, since the pore size of 6 Å is larger than the kinetic diameter of all gases under study, the UiO-66 membrane works like a "soft" molecular sieve for N_2, CH_4, C_2H_6, and C_3H_8, which shows selectivities of H_2/N_2 = 4.7, H_2/CH_4 = 12.9, H_2/C_2H_6 = 22.4, and H_2/C_3H_8 = 28.5, respectively. These selectivities are higher than their corresponding Knudsen selectivities of α_{ideal} (A/B) 3.7, 2.8, 3.9, and 4.7, which can be calculated by the following eq 2:

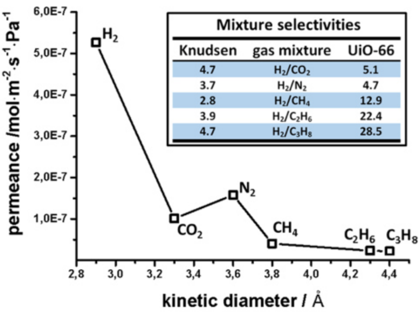

Figure 5. Neat UiO-66 single layer membrane: Gas mixture permeances for CO_2, N_2, CH_4, C_2H_6, and C_3H_8, in binary mixtures with H_2 as a function of the kinetic diameter at 25 °C and 1 bar for both the feed and the sweep side. Inset shows the comparison between the measured mixture separation factors and the corresponding Knudsen values for the binary gas mixtures.

$$\alpha_{ideal}(A/B) = \frac{\sqrt{M(B)}}{\sqrt{M(A)}} \qquad (2)$$

Since CO_2 (3.3 Å) has the second smallest kinetic diameter and shows a specific interaction with the hydroxylated Zr_6 cluster of the inorganic subunit,[55] the mixture separation factor of H_2/CO_2 = 5.1 is found to be close to its Knudsen selectivity of 4.7. In summary, although there are a lot of publications with membranes that outperform the represented layer in terms of the aforementioned gas pairs,[56−58] the UiO-66 membrane shows a good gas separation performance, which is comparable to several other 3D MOF membranes, such as those reported in refs 59 and 60.

In a previous paper, we developed the concept that an additional polymer layer on top of the MOF layer can drastically enhance the separation performance.[61] We prepared, therefore, a multilayer membrane by coating a Matrimid layer (≈15 μm) on top of the UiO-66 membrane. This polymer top layer can (i) heal present defects in the MOF layer, (ii) modify the pore entrance size at the MOF−polymer interface, or (iii) reduce the bulk framework flexibility of the MOF in contact with the polymer, thus resulting in a modified behavior as shown for other MOF/polymer pairs.[61,62] Another crucial point, affecting the overall capabilities of such materials in general and in our composite in particular, is the direct compatibility between the composite's components.[63−65] The smaller the points of contact, the more important this compatibility becomes. The latter can be adjusted or improved

DOI: 10.1021/acsami.7b02105
ACS Appl. Mater. Interfaces 2017, 9, 12878−12885

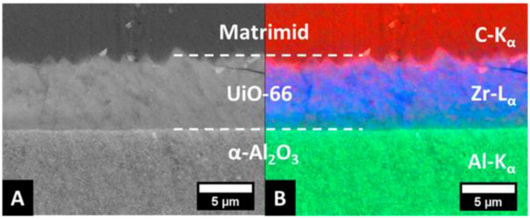

Figure 6. Cross section SEM image (A) and the corresponding EDXS mapping (B) of the Matrimid/UiO-66 multilayer membrane.

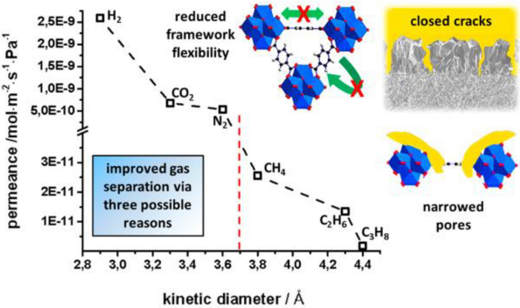

Figure 7. Matrimid/UiO-66 multilayer membrane. Gas mixture permeances for CO_2, N_2, CH_4, C_2H_6, and C_3H_8 in an equimolar mixture with H_2 as a function of the kinetic diameter at 25 °C and 1 bar for both the feed and the sweep side. Insets demonstrate suggested reasons for improved performance.

by several measures such as functionalization with appropriate groups[66] or even direct coupling.[67]

Figure 6A,B shows the results of the SEM/EDXS investigations for the multilayer membrane. They indicate a continuous MOF/polymer interface without any detectable voids and a good contact between the two different layers. Furthermore, it is obvious that the UiO-66 layer did not suffer from the coating process and looks unchanged (cf. Figure 3B). Therefore, one can expect a modified separation behavior in comparison to the neat MOF layer. As shown in Figure 7, the permeances for all investigated gases are indeed at least two magnitudes lower in comparison to the neat UiO-66 membrane (cf. Figure 5). At first sight, this seems plausible and in line with expectations, since the polymer Matrimid used for the preparation of the multilayer membrane has relative low fluxes. However, the decrease of the permeance values is especially strong for those gases with a kinetic diameter larger than the minimum estimated pore size (CH_4, C_2H_6, C_3H_8). The mixture separation factors for H_2/CO_2 and H_2/N_2 are comparable to the neat UiO-66 membrane, whereas the mixture separation factors for H_2/CH_4, H_2/C_2H_6, and H_2/C_3H_8 are increased to a high degree, as shown in Figure 8A, making this multilayer competitive to other state of the art materials.[68,69] The increase in selectivity might have different explanations: (i) the coating with Matrimid "heals" present defects in the MOF layer, thus resulting in improved separation capabilities; (ii) the coating narrows the pore size by penetrating into the framework structure to a certain degree; (iii) the polymer layer modulates/hinders the linker mobility within the UiO-66 framework. The latter would also affect the minimum pore size for a certain

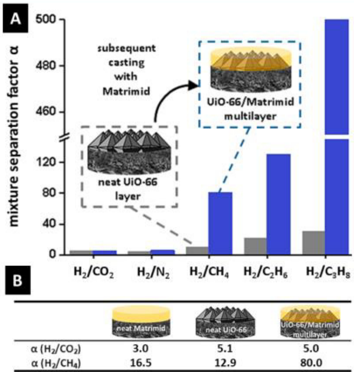

Figure 8. (A) Comparison of the mixture separation factors α for the neat UiO-66 membrane and the Matrimid/UiO-66 multilayer. (B) Exemplary clarification of the interplay between both materials (UiO-66 and Matrimid) with respect to the separation performance for two gaseous probe systems.

DOI: 10.1021/acsami.7b02105
ACS Appl. Mater. Interfaces 2017, 9, 12878−12885

orientation of the 3 benzene rings (cf. Figure 1C). However, also a combination of the three aforementioned effects is imaginable. Despite published results, which show Matrimid as a membrane with great H_2/CH_4 selectivity,[70] our neat supported layer shows lower gas separation capabilities (cf. Figure 8B). This lower performance is most probably caused by improper handling, thus resulting in bubbles within the polymeric matrix. In conclusion from this experimental finding, one can deduce that a "soft" porous MOF molecular sieve layer can be transferred to a membrane with better separation performance by coating it with a thin polymer top layer. Although the permeances for the presented composite membrane are substantially decreased compared to the noncoated UiO-66 layer, this could fairly be fixed by reducing the thickness of the polymer cover layer.

4. CONCLUSIONS

In summary, the present study describes the synthesis of a 3D supported, oriented UiO-66 membrane layer on flat ceramic supports. The orientation of the octahedrons to the support was characterized via CPOs and approximated via Rietveld refinement. Furthermore, the stability as well as the adherence of the prepared layer was investigated in different stressful conditions. Regarding the mixed gas separation performance, the neat UiO-66 layer exhibits reasonable gas selectivity with separation factors higher than the corresponding Knudsen selectivity. Due to the framework flexibility and the relatively large pore size of 6 Å, no sharp molecular sieving was observed. However, this soft porous MOF material UiO-66 was transferred to a membrane with better separation performance by coating the MOF layer with a thin Matrimid polymer top layer. The latter can be a result of a plethora of different reasons. Nevertheless, we believe that the additional polymer layer most likely has three ramifications: (i) it fills present defects in the MOF layer; (ii) it reduces the pore size by extending into the framework to a certain degree; (iii) it affects the framework flexibility at the polymer−MOF interface. Consequently, the UiO-66/Matrimid multilayer membrane shows improved separation performance and better molecular sieving. Our finding raises the question of the effect's origin and whether this could be conferred or even be multiplied by incorporating (nano)particles of UiO-66 or other MOFs completely in a polymeric matrix as a so-called mixed-matrix membrane. Corresponding studies are on the way.

■ ASSOCIATED CONTENT

Supporting Information

The Supporting Information is available free of charge on the ACS Publications website at DOI: 10.1021/acsami.7b02105.

Synthesis of the UiO-66 seeding crystals; XRD and SEM data for the UiO-66 seeding crystals; Rietveld-fit of the oriented UiO-66 membrane layer; exemplary counting of *c*-axis tilting angle within the oriented membrane (PDF)

■ AUTHOR INFORMATION

Corresponding Author

*E-mail: Sebastian.friebe@pci.uni-hannover.de.

Notes

The authors declare no competing financial interest.

■ ACKNOWLEDGMENTS

The authors of this work are grateful for the financial support from the EU 7th Framework project M_4CO_2 (Grant Agreement No. 608490), organized by F. Kapteijn and J. Gascon.

■ REFERENCES

(1) Batten, S. R.; Champness, N. R.; Chen, X.-M.; Garcia-Martinez, J.; Kitagawa, S.; Öhrström, L.; O'Keeffe, M.; Suh, M. P.; Reedijk, J. Coordination Polymers, Metal-Organic Frameworks and the Need for Terminology Guidelines. *CrystEngComm* **2012**, *14*, 3001−3004.

(2) Sun, Y.; Zhou, H.-C. Recent Progress in the Synthesis of Metal-Organic Frameworks. *Sci. Technol. Adv. Mater.* **2015**, *16*, 054202.

(3) Ferey, G. Hybrid Porous Solids: Past, Present, Future. *Chem. Soc. Rev.* **2008**, *37*, 191−214.

(4) Zhong, R.; Xu, Z.; Bi, W.; Han, S.; Yu, X.; Zou, R. A Charged Metal-Organic Framework for CO_2/CH_4 and CO_2/N_2 Separation. *Inorg. Chim. Acta* **2016**, *443*, 299−303.

(5) Pentyala, V.; Davydovskaya, P.; Ade, M.; Pohle, R.; Urban, G. Carbon Dioxide Gas Detection by Open Metal Site Metal Organic Frameworks and Surface Functionalized Metal Organic Frameworks. *Sens. Actuators, B* **2016**, *225*, 363−368.

(6) Friebe, S.; Mundstock, A.; Unruh, D.; Renz, F.; Caro, J. NH_2-MIL-125 as Membrane for Carbon Dioxide Sequestration: Thin Supported MOF Layers contra Mixed-Matrix-Membranes. *J. Membr. Sci.* **2016**, *516*, 185−193.

(7) Li, J.-R.; Kuppler, R. J.; Zhou, H.-C. Selective Gas Adsorption and Separation in Metal-Organic Frameworks. *Chem. Soc. Rev.* **2009**, *38*, 1477−1504.

(8) Betard, A.; Fischer, R. A. Metal-Organic Framework Thin Films: From Fundamentals to Applications. *Chem. Rev.* **2012**, *112*, 1055−1083.

(9) Gascon, J.; Kapteijn, F. Metal-Organic Framework Membranes-High Potential, Bright Future? *Angew. Chem., Int. Ed.* **2010**, *49*, 1530−1532.

(10) Bradshaw, D.; Garai, A.; Huo, J. Metal-Organic Framework Growth at Functional Interfaces: Thin Films and Composites for Diverse Applications. *Chem. Soc. Rev.* **2012**, *41*, 2344−2381.

(11) Coronas, J. Present and Future Synthesis Challenges for Zeolites. *Chem. Eng. J.* **2010**, *156*, 236−242.

(12) Caro, J. Are MOF Membranes Better in Gas Separation Than Those Made of Zeolites? *Curr. Opin. Chem. Eng.* **2011**, *1*, 77−83.

(13) Yao, J.; Wang, H. Zeolitic Imidazolate Framework Composite Membranes and Thin Films: Synthesis and Application. *Chem. Soc. Rev.* **2014**, *43*, 4470−4493.

(14) Bux, H.; Feldhoff, A.; Cravillon, J.; Wiebcke, M.; Li, Y.-S.; Caro, J. Oriented Zeolitic Imidazolate Framework-8 Membrane with Sharp H_2/C_3H_8 Molecular Sieve Separation. *Chem. Mater.* **2011**, *23*, 2262−2269.

(15) Mao, Y.; Li, J.; Cao, W.; Ying, Y.; Sun, L.; Peng, X. Pressure-Assisted Synthesis of HKUST-1 Thin Film on Polymer Hollow Fiber at Room Temperature Toward Gas Separation. *ACS Appl. Mater. Interfaces* **2014**, *6*, 4473−4479.

(16) Huang, K.; Li, Q.; Liu, G.; Shen, J.; Guan, K.; Jin, W. A ZIF-71 Hollow Fiber Membrane Fabricated by Contra-Diffusion. *ACS Appl. Mater. Interfaces* **2015**, *7*, 16157−15660.

(17) Zhang, X.; Liu, Y.; Li, S.; Kong, L.; Liu, H.; Li, Y.; Han, W.; Yeung, K. L.; Zhu, W.; Yang, W.; Qiu, J. New Membrane Architecture with High Performance: ZIF-8 Membrane Supported on Vertically Aligned ZnO Nanorods for Gas Permeation and Separation. *Chem. Mater.* **2014**, *26*, 1975−1981.

(18) Li, J.-R.; Sculley, J.; Zhou, H.-C. Metal-Organic Frameworks for Separations. *Chem. Rev.* **2012**, *112*, 869−932.

(19) Mundstock, A.; Böhme, U.; Barth, B.; Hartmann, M.; Caro, J. Propylen/Propan-Trennung im Festbettadsorber und durch Membranpermeation. *Chem. Ing. Tech.* **2013**, *85*, 1694−1699.

(20) Knebel, A.; Friebe, S.; Bigall, N. C.; Benzaqui, M.; Serre, C.; Caro, J. Comparative Study of MIL-96(Al) as Continuous Metal-

Organic Frameworks Layer and Mixed-Matrix Membrane. *ACS Appl. Mater. Interfaces* **2016**, *8*, 7536−7544.
(21) Huang, A.; Bux, H.; Steinbach, F.; Caro, J. Molecular-Sieve Membrane with Hydrogen Permselectivity: ZIF-22 in LTA Topology Prepared with 3-Aminopropyltriethoxysilane as Covalent Linker. *Angew. Chem.* **2010**, *122*, 5078−5081.
(22) Herm, Z. R.; Wiers, B. M.; Mason, J. A.; van Baten, J. M.; Hudson, M. R.; Zajdel, P.; Brown, C. M.; Masciocchi, N.; Krishna, R.; Long, J. R. Separation of Hexane Isomers in a Metal-Organic Framework with Triangular Channels. *Science* **2013**, *340*, 960−964.
(23) Gutov, O. V.; Bury, W.; Gomez-Gualdron, D. A.; Krungleviciute, V.; Fairen-Jimenez, D.; Mondloch, J. E.; Sarjeant, A. A.; Al-Juaid, S. S.; Snurr, R. Q.; Hupp, J. T.; Yildrim, T.; Farha, O. K. Water-Stable Zirconium-Based Metal-Organic Framework Material with High-Surface Area and Gas-Storage Capacities. *Chem. - Eur. J.* **2014**, *20*, 12389−12393.
(24) Mondloch, J. E.; Bury, W.; Fairen-Jimenez, D.; Kwon, S.; DeMarco, E. J.; Weston, M. H.; Sarjeant, A. A.; Nguyen, S. T.; Stair, P. C.; Snurr, R. Q.; Farha, O. K.; Hupp, J. T. Vapor-Phase Metalation by Atomic Layer Deposition in a Metal-Organic Framework. *J. Am. Chem. Soc.* **2013**, *135*, 10294−10297.
(25) Guillerm, V.; Ragon, F.; Dan-Hardi, M.; Devic, T.; Vishnuvarthan, M.; Campo, B.; Vimont, A.; Clet, G.; Yang, Q.; Maurin, G.; Ferey, G.; Vittadini, A.; Gross, S.; Serre, C. A Series of Isoreticular, Highly Stable, Porous Zirconium Oxide Based Metal-Organic Frameworks. *Angew. Chem.* **2012**, *124*, 9401−9405; *Angew. Chem., Int. Ed.* **2012**, *51*, 9267−9271.
(26) Van de Voorde, B.; Borges, D. D.; Vermoortele, F.; Wouters, R.; Bozbiyik, B.; Denayer, J.; Taulelle, F.; Martineau, C.; Serre, C.; Maurin, G.; De Vos, D. Isolation of Renewable Phenolics by Adsorption on Ultrastable Hydrophobic MIL-140 Metal-Organic Frameworks. *ChemSusChem* **2015**, *8*, 3159−3166.
(27) Kandiah, M.; Nilsen, M. H.; Usseglio, S.; Jakobsen, S.; Olsbye, U.; Tilset, M.; Larabi, C.; Quadrelli, E. A.; Bonino, F.; Lillerud, K. P. Synthesis and Stability of Tagged UiO-66 Zr-MOFs. *Chem. Mater.* **2010**, *22*, 6632−6640.
(28) Piscopo, C. G.; Polyzoidis, A.; Schwarzer, M.; Loebbecke, S. Stability of UiO-66 Under Acidic Treatment: Opportunities and Limitations for Post-Synthetic Modifications. *Microporous Mesoporous Mater.* **2015**, *208*, 30−35.
(29) Liu, J.; Canfield, N.; Liu, W. Preparation and Characterization of a Hydrophobic Metal-Organic Framework Membrane Supported on a Thin Porous Metal Sheet. *Ind. Eng. Chem. Res.* **2016**, *55*, 3823−3832.
(30) Katz, M. J.; Brown, Z. J.; Colon, Y. J.; Siu, P. W.; Scheidt, K. A.; Snurr, R. Q.; Hupp, J. T.; Farha, O. K. A Facile Synthesis of UiO-66, UiO-67 and Their Derivatives. *Chem. Commun.* **2013**, *49*, 9449−9451.
(31) Stassen, I.; Styles, M.; Van Assche, T.; Campagnol, N.; Fransaer, J.; Denayer, J.; Tan, J.-C.; Falcaro, P.; De Vos, D.; Ameloot, R. Electrochemical Film Deposition of the Zirconium Metal-Organic Framework UiO-66 and Application in a Miniaturized Sorbent Trap. *Chem. Mater.* **2015**, *27*, 1801−1807.
(32) Zhang, C.; Zhao, Y.; Li, Y.; Zhang, X.; Chi, L.; Lu, G. Defect-Controlled Preparation of UiO-66 Metal-Organic Framework Thin Films with Molecular Sieving Capability. *Chem. - Asian J.* **2016**, *11*, 207−210.
(33) Goesten, M. G.; de Lange, M. F.; Olivos-Suarez, A. I.; Bavykina, A. V.; Serra-Crespo, P.; Krywka, C.; Bickelhaupt, F. M.; Kapteijn, F.; Gascon, J. Evidence for a Chemical Clock in Oscillatory Formation of UiO-66. *Nat. Commun.* **2016**, *7*, 11832.
(34) Wu, H.; Yildirim, T.; Zhou, W. Exceptional Mechanical Stability of Highly Porous Zirconium Metal-Organic Framework UiO-66 and Its Important Implications. *J. Phys. Chem. Lett.* **2013**, *4*, 925−930.
(35) Valenzano, L.; Civalleri, B.; Chavan, S.; Bordiga, S.; Nilsen, M. H.; Jakobsen, S.; Lillerud, K. P.; Lamberti, C. Disclosing the Complex Structure of UiO-66 Metal Organic Framework: A Synergic Combination of Experiment and Theory. *Chem. Mater.* **2011**, *23*, 1700−1718.
(36) Øien, S.; Wragg, D.; Reinsch, H.; Svelle, S.; Bordiga, S.; Lamberti, C.; Lillerud, K. P. Detailed Structure Analysis of Atomic Positions and Defects in Zirconium Metal-Organic Frameworks. *Cryst. Growth Des.* **2014**, *14*, 5370−5372.
(37) Cavka, J. H.; Jakobsen, S.; Olsbye, U.; Guillou, N.; Lamberti, C.; Bordiga, S.; Lillerud, K. P. A New Zirconium Inorganic Building Brick Forming Metal Organic Frameworks with Exceptional Stability. *J. Am. Chem. Soc.* **2008**, *130*, 13850−13851.
(38) Devautour-Vinot, S.; Maurin, G.; Serre, C.; Horcajada, P.; Paula da Cunha, D.; Guillerm, V.; de Souza Costa, E.; Taulelle, F.; Martineau, C. Structure and Dynamics of the Functionalized MOF Type UiO-66(Zr): NMR and Dielectric Relaxation Spectroscopies Coupled with DFT Calculations. *Chem. Mater.* **2012**, *24*, 2168−2177.
(39) Barcia, P. S.; Guimaraes, D.; Mendes, P. A. P.; Silva, J. A. C.; Guillerm, V.; Chevreau, H.; Serre, C.; Rodrigues, A. E. Reverse Shape Selectivity in the Adsorption of Hexane and Xylene Isomers in MOF UiO-66. *Microporous Mesoporous Mater.* **2011**, *139*, 67−73.
(40) Kolokolov, D. I.; Stepanov, A. G.; Guillerm, V.; Serre, C.; Frick, B.; Jobic, H. Probing the Dynamics of the Porous Zr Terephthalate UiO-66 Framework Using 2H NMR and Neutron Scattering. *J. Phys. Chem. C* **2012**, *116*, 12131−12136.
(41) Gould, S. L.; Tranchemontagne, D.; Yaghi, O. M.; Garcia-Garibay, M. A. Amphidynamic Character of Crystalline MOF-5: Rotational Dynamics of Terephthalate Phenylenes in a Free-Volume, Sterically Unhindered Environment. *J. Am. Chem. Soc.* **2008**, *130*, 3246−3247.
(42) Kolokolov, D. I.; Jobic, H.; Stepanov, A. G.; Guillerm, V.; Devic, T.; Serre, C.; Ferey, G. Dynamics of Benzene Rings in MIL-53(Cr) and MIL-47(V) Frameworks Studied by 2H NMR Spectroscopy. *Angew. Chem., Int. Ed.* **2010**, *49*, 4791−4794.
(43) Schaate, A.; Roy, P.; Godt, A.; Lippke, J.; Waltz, F.; Wiebcke, M.; Behrens, P. Modulated Synthesis of Zr-Based Metal-Organic Frameworks: From Nano to Single Crystals. *Chem. - Eur. J.* **2011**, *17*, 6643−6651.
(44) Liu, Y.; Zeng, G.; Pan, Y.; Lai, Z. Synthesis of Highly C-Oriented ZIF-69 Membranes by Secondary Growth and Their Gas Permeation Properties. *J. Membr. Sci.* **2011**, *379*, 46−51.
(45) Lee, T.; Choi, J.; Tsapatsis, M. On the Performance of C-Oriented MFI Zeolite Membranes Treated by Rapid Thermal Processing. *J. Membr. Sci.* **2013**, *436*, 79−89.
(46) van der Drift, A. Evolutionary Selection, a Principle Governing Growth Orientation in Vapour-Deposited Layers. *Philips Res. Reports* **1967**, *22*, 267−288.
(47) Tsuruoka, T.; Furukawa, S.; Takashima, Y.; Yoshida, K.; Isoda, S.; Kitagawa, S. Nanoporous Nanorods Fabricated by Coordination Modulation and Oriented Attachment Growth. *Angew. Chem., Int. Ed.* **2009**, *48*, 4739−4743.
(48) Diring, S.; Furukawa, S.; Takashima, Y.; Tsuruoka, T.; Kitagawa, S. Controlled Multiscale Synthesis of Porous Coordination Polymer in Nano/Micro Regimes. *Chem. Mater.* **2010**, *22*, 4531−4538.
(49) Verduijn, J. P.; Bons, A.-J.; Anthonis, M. H. C. Molecular sieves and processes for their manufacture WO 1997025272 A1, 1997.
(50) Zolotoyabko, E. Determination of the Degree of Preferred Orientation within the March-Dollase Approach. *J. Appl. Crystallogr.* **2009**, *42*, 513−518.
(51) Zhao, J.; Lee, D. T.; Yaga, R. W.; Hall, M. G.; Barton, H. F.; Woodward, I. R.; Oldham, C. J.; Walls, H. J.; Peterson, G. W.; Parsons, G. N. Ultra-Fast Degradation of Chemical Warfare Agents Using MOF-Nanofiber Kebabs. *Angew. Chem., Int. Ed.* **2016**, *55*, 13224−13228.
(52) Zhao, J.; Losego, M. D.; Lemaire, P. C.; Williams, P. S.; Gong, B.; Atanasov, S. E.; Blevins, T. M.; Oldham, C. J.; Walls, H. J.; Shepherd, S. D.; Browe, M. A.; Peterson, G. W.; Parsons, G. N. Highly Adsorptive, MOF-Functionalized Nonwoven Fiber Mats for Hazardous Gas Capture Enabled by Atomic Layer Deposition. *Adv. Mater. Interfaces* **2014**, *1*, 1400040.
(53) Liu, J.; Canfield, N.; Liu, W. Preparation and Characterization of a Hydrophobic Metal-Organic Framework Membrane Supported on a Thin Porous Metal Sheet. *Ind. Eng. Chem. Res.* **2016**, *55*, 3823−3832.
(54) Liu, X.; Demir, N. K.; Wu, Z.; Li, K. Highly Water-Stable Zirconium Metal−Organic Framework UiO-66 Membranes Supported

on Alumina Hollow Fibers for Desalination. *J. Am. Chem. Soc.* **2015**, *137*, 6999−7002.

(55) Cmarik, G. E.; Kim, M.; Cohen, S. M.; Walton, K. S. Tuning the Adsorption Properties of UiO-66 via Ligand Functionalization. *Langmuir* **2012**, *28*, 15606−15613.

(56) Fu, J.; Das, S.; Xing, G.; Ben, T.; Valtchev, V.; Qiu, S. Fabrication of COF-MOF Composite Membranes and Their Highly Selective Separation of H_2/CO_2. *J. Am. Chem. Soc.* **2016**, *138*, 7673−7680.

(57) Kang, Z.; Xue, M.; Fan, L.; Huang, L.; Gou, L.; Wei, G.; Chen, B.; Qiu, S. Highly Selective Sieving of Small Gas Molecules by Using an Ultra-Microporous Metal-Organic Framework Membrane. *Energy Environ. Sci.* **2014**, *7*, 4053−4060.

(58) Jin, H.; Wollbrink, A.; Yao, R.; Li, Y.; Caro, J.; Yang, W. A Novel CAU-10-H MOF Membrane for Hydrogen Separation under Hydrothermal Conditions. *J. Membr. Sci.* **2016**, *513*, 40−46.

(59) Mao, Y.; Su, B.; Cao, W.; Li, J.; Ying, Y.; Ying, W.; Hou, Y.; Sun, L.; Peng, X. Specific Oriented Metal-Organic Framework Membranes and Their Facet-Tuned Separation Performance. *ACS Appl. Mater. Interfaces* **2014**, *6*, 15676−15685.

(60) Qiu, S.; Xue, M.; Zhu, G. Metal-Organic Framework Membranes: From Synthesis to Separation Application. *Chem. Soc. Rev.* **2014**, *43*, 6116−6140.

(61) Diestel, L.; Wang, N.; Schwiedland, B.; Steinbach, F.; Giese, U.; Caro, J. MOF Based MMMs with Enhanced Selectivity due to Hindered Linker Distortion. *J. Membr. Sci.* **2015**, *492*, 181−186.

(62) Mueller, R.; Zhang, S.; Zhang, C.; Lively, R.; Vasenkov, R. Relationship Between Long-Range Diffusion and Diffusion in the ZIF-8 and Polymer Phases of a Mixed-Matrix Membrane by High Field NMR Diffusometry. *J. Membr. Sci.* **2015**, *477*, 123−130.

(63) Gong, H.; Lee, S. S.; Bae, T.-H. Mixed-Matrix Membranes Containing Inorganically Surface-Modified 5A Zeolite for Enhanced CO_2/CH_4 Separation. *Microporous Mesoporous Mater.* **2017**, *237*, 82−89.

(64) Armstrong, M. R.; Shan, B.; Maringanti, S. V.; Zheng, W.; Mu, B. Hierarchical Pore Structures and High ZIF-8 Loading on Matrimid Electrospun Fibers by Additive Removal from a Blended Polymer-Precursor. *Ind. Eng. Chem. Res.* **2016**, *55*, 9944−9951.

(65) Rodenas, T.; Luz, I.; Prieto, G.; Seoane, B.; Miro, H.; Corma, A.; Kapteijn, F.; Llabres, I.; Xamena, F. X.; Gascon, J. Metal-Organic Framework Nanosheets in Polymer Composite Materials for Gas Separation. *Nat. Mater.* **2015**, *14*, 48−55.

(66) Guo, X.; Liu, D.; Han, T.; Huang, H.; Yang, Q.; Zhong, C. Preparation of Thin Film Nanocomposite Membranes with Surface Modified MOF for High Flux Organic Solvent Nanofiltration. *AIChE J.* **2017**, *63*, 1303−1312.

(67) Jiang, W. L.; Ding, L. G.; Yao, B. J.; Wang, J. C.; Chen, G.-J.; Li, Y. A.; Ma, J.-P.; Ji, J.; Dong, Y.; Dong, Y.-B. A MOF-Membrane Based on the Covalent Bonding Driven Assembly of a NMOF with an Organic Oligomer and Its Application in Membrane Reactors. *Chem. Commun.* **2016**, *52*, 13564−13567.

(68) Tien-Binh, N.; Vinh-Thang, H.; Chen, X. Y.; Rodrigue, D.; Kaliaguine, S. Crosslinked MOF-Polymer to Enhance Gas Separation of Mixed Matrix Membranes. *J. Membr. Sci.* **2016**, *520*, 941−950.

(69) Erucar, I.; Keskin, S. Computational Assessment of MOF Membranes for CH_4/H_2 Separations. *J. Membr. Sci.* **2016**, *514*, 313−321.

(70) Xiao, Y.; Guo, X.; Huang, H.; Yang, Q.; Huang, A.; Zhong, C. Synthesis of MIL-88B(Fe)/Matrimid Mixed-Matrix Membranes with High Hydrogen Permselectivity. *RSC Adv.* **2015**, *5*, 7253−7259.

DOI: 10.1021/acsami.7b02105
ACS Appl. Mater. Interfaces 2017, 9, 12878−12885

2.4 Comparative Study of MIL-96 (Al) as Continuous Metal-Organic Frameworks Layer and Mixed-Matrix Membrane

A. Knebel, S. Friebe, N.C. Bigall, M. Benzaqui, C. Serre, J. Caro

ACS Applied Materials and Interfaces **2016**, 8, 7536-7544.

ACS APPLIED MATERIALS & INTERFACES

Research Article

www.acsami.org

Comparative Study of MIL-96(Al) as Continuous Metal–Organic Frameworks Layer and Mixed-Matrix Membrane

Alexander Knebel,[†] Sebastian Friebe,[*,†] Nadja Carola Bigall,[†] Marvin Benzaqui,[‡] Christian Serre,[‡] and Jürgen Caro[†]

[†]Institute of Physical Chemistry and Electrochemistry, Leibniz Universität Hannover, Callinstraße 3A, D-30167 Hannover, Germany

[‡]Institut Lavoisier de Versailles, Université de Versailles St-Quentin-de-Yvelines, 45 avenue des Etats-Unis, 78035 Versailles cedex, France

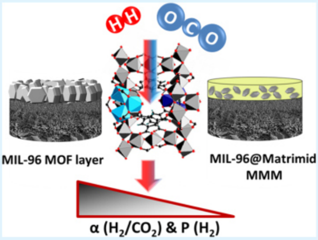

ABSTRACT: MIL-96(Al) layers were prepared as supported metal–organic frameworks membrane via reactive seeding using the α-alumina support as the Al source for the formation of the MIL-96(Al) seeds. Depending on the solvent mixture employed during seed formation, two different crystal morphologies, with different orientation of the transport-active channels, have been formed. This crystal orientation and habit is predefined by the seed crystals and is kept in the subsequent growth of the seeds to continuous layers. In the gas separation of an equimolar H_2/CO_2 mixture, the hydrogen permeability of the two supported MIL-96(Al) layers was found to be highly dependent on the crystal morphology and the accompanied channel orientation in the layer. In addition to the neat supported MIL-96(Al) membrane layers, mixed-matrix membranes (MMMs, 10 wt % filler loading) as a composite of MIL-96(Al) particles as filler in a continuous Matrimid polymer phase have been prepared. Five particle sizes of MIL-96(Al) between 3.2 μm and 55 nm were synthesized. In the preparation of the MIL-96(Al)/Matrimid MMM (10 wt % filler loading), the following preparation problems have been identified: The bigger micrometer-sized MIL-96(Al) crystals show a trend toward sedimentation during casting of the MMM, whereas for nanoparticles aggregation and recrystallization to micrometer-sized MIL-96(Al) crystals has been observed. Because of these preparation problems for MMM, the neat supported MIL-96(Al) layers show a relatively high H_2/CO_2 selectivity (≈9) and a hydrogen permeance approximately 2 magnitudes higher than that of the best MMM.

KEYWORDS: *MIL-96(Al), MOF membrane, hydrogen/carbon dioxide separation, mixed-matrix membrane (MMM), crystal morphology*

1. INTRODUCTION

Current politics and industry are interested in materials for environmentally friendly,[1] economical,[2] and energy-efficient processes, especially with respect to gas purification and CO_2 capture.[3] Established materials like zeolites or novel materials like metal–organic frameworks (MOFs), hybrid inorganic–organic solids, and one of the latest class of porous crystalline solids are possible candidates to solve these problems of CO_2 capture.[4] MOFs that exhibit a permanent porosity, tunable composition, and pore and cage sizes show high inner surfaces and are often found to have adsorption properties favoring gas uptake.[5] For use in gas separation, the MOF has to be water-stable and heat-resistant and has to feature appropriate pore sizes or functional groups.[6] The investigated MOF in this study—both the neat MOF layer as well as the powder filler in mixed-matrix membranes (MMMs)—is MIL-96(Al).[7] Like most Al-carboxylate-based MOFs, it shows good hydrothermal stability and is stable in air up to about 300 °C.[8,9] The alumina octahedral building units show a very rare structure, containing corner-sharing chains of metal octahedra bridged by three μ-oxo centered trinuclear units in the *c*-direction of the hexagonal unit cell as characteristic element. The pores connect three types of cavities with different free volumes

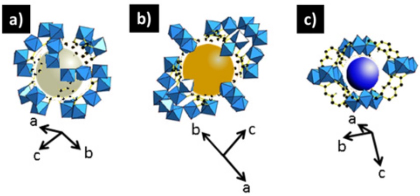

Figure 1. Schematic structure of MIL-96(Al) and its three main cavities with volumes of approximately (a) 420 Å^3, (b) 635 Å^3, and (c) ≤100 Å^3. Drawn with the software Diamond.

(cf. Figure 1a–c).[10,11] The three-dimensional (3D) MOF structure has a unique feature since there is no direct connection between two equal cavities. Cavity (c) acts as a junction between

Received: December 22, 2015
Accepted: February 17, 2016
Published: February 17, 2016

DOI: 10.1021/acsami.5b12541
ACS Appl. Mater. Interfaces 2016, 8, 7536–7544

the other cavities. However, the window size between cavity (a) and cavity (c) is very narrow, close to 1 Å, thus sealing this path gastight in some degree. In contrast, the window size between cavity (b) and cavity (c) is around 3.5 Å. This results in a virtual two-dimensional (2D) pore network, which allows a "zigzag" gas transport for CO_2 and H_2 between cavities (b) and (c).

As a consequence of the features of MIL-96 mentioned above, it could be optimal for hydrogen separation in precombustion CO_2 capture technologies.[12,13] Precombustion hydrogen separation means that the carbonaceous fuel (e.g., natural gas, coal) is transformed by several partial oxidation and reforming steps in a H_2/CO_2 mixture. The separated hydrogen can be used energetically (combustion in a turbine or fuel cell) whereas the captured CO_2 can be sequestrated.

Therefore, two types of MIL-96(Al) membranes have been developed here and evaluated in the H_2/CO_2 mixed gas separation: (i) Neat continuous MIL-96(Al) layers of a few micrometers thickness on ceramic alumina supports and (ii) MIL-96(Al) powder in Matrimid as MMM, also casted as layers on alumina supports.

For the preparation of MMMs, MIL-96 crystals of different sizes had to be prepared. Regarding the synthesis of MIL-96, several groups have already investigated the adjustment of MIL-96 particle sizes and shapes by various modulation routes, like different solvents and solvent mixture ratios[14] and pH adjustment and competing reactions.[15−17] As shown recently in ref 18, following the MMMs concept, the good permselectivity of an inorganic filler material (MOFs like zeolitic imidazolate frameworks (ZIFs) and Materials Institute Lavoisier (MILs) and zeolites) and the mechanical properties of the polymeric material can be combined in the composite material called MMM.[19−21] These studies reveal all the positive features of MMMs, for example, easy and low-cost production as well as favorable mechanical properties of the polymer (flexibility, long-term stability, and reproducibility). Additionally, by incorporating separation-active filler materials, one can also overcome the negative aspects of the neat polymer membranes, especially of low fluxes.[19,22−24] It is assumed that MMMs may close the gap between neat MOF layers and neat polymer membranes.[25−28] Regarding the MMM fabrication, the use of Matrimid seems to be a good choice since it shows high thermal and chemical stability and easy processability.[29,30] Despite all the positive features mentioned above for the MMMs, several problems might occur, for example, low interaction between filler and polymer[31] as a result of a mismatch in polarity, sedimentation, and also aggregation phenomena,[32] depending on the nature, particle size, and shape of the filler.

2. MATERIALS AND METHODS

2.1. Materials. The chemicals in this work were obtained from commercial vendors and used without further purification. The chemicals in this work were $Al(NO_3)_3{\cdot}9H_2O$ (Merck, Darmstadt, Germany, 98.5%), benzene tricarboxylic acid (H_3BTC) (Sigma-Aldrich, Schnelldorf, Germany 95%), acetic acid (Sigma-Aldrich, 99.7%), dimethylformamide (DMF) (Sigma-Aldrich, 99.8%), toluene (Carl Roth, Karlsruhe, Germany, 99.9%), methanol (Sigma-Aldrich, 99.8%), and dichloromethane (DCM) (Sigma-Aldrich 99.9%).

2.2. Particle Synthesis. MIL-96(Al) particles were produced by hydrothermal synthesis following a synthesis of Sindoro et al.[33] with slight modifications. In this work we for the first time report a synthesis for monodisperse nanometer-sized MIL-96(Al) particles. Particles with average sizes of 3.2 μm, 1.1 μm, 160 nm, 116 nm, and 55 nm were produced. In the first step 0.42 g of aluminum nitrate nonahydrate was dissolved in 4, 4.5, 5.25, 6, and 8 mL of deionized water at 80 °C, respectively. In parallel, 0.21 g of H_3BTC was dissolved in 4, 4.5, 5.25, 6, and 8 mL of DMF at 80 °C in an ultrasonication bath. The clear solutions were put together in a Teflon-lined autoclave at 80 °C and 0.5 mL of a 10 mM acetic acid solution was added. The autoclave was sealed and put in an oven at 210 °C for 2 h. After the reaction the particles were washed with methanol in the first step and deionized water in a second step using a centrifuge at 10 000 rpm and an ultrasonication bath to redisperse the particles. After that, the particles were dried at 150 °C for 2 h and stored in a sealed bottle for further use.

2.3. Mixed-Matrix Membranes. The supported 10 wt % MMM and the neat Matrimid membranes were produced by a simple drop-casting approach. Therefore, the evacuated MOF powder and the Matrimid 5218 were weighed in a glass bottle under an inert gas atmosphere in the desired ratio (10 mg of MOF, 90 mg of polymer). After that, 1 mL of DCM was added, the glass bottle was closed, and the resulting mixture was stirred overnight. On the following day, the mixture was thickened to 500 μL by evaporation and casted on an Al_2O_3 support (2.5 μm pores; Fraunhofer IKTS, former Hermsdorfer HITK, Germany) with the help of an Eppendorf-Pipette. After casting, the MMMs were dried in an atmosphere of DCM to allow a slow solvent evaporation. At the end, the membranes were activated at 100 °C in a drying oven for several hours.

2.4. Neat-MOF Membrane. MIL-96(Al) MOF layers in the thickness of only a few micrometers for mixed-gas separation measurements were produced using a slightly modified reactive-seeding procedure previously reported by Nan et al.[34] and Sindoro et al.,[33] respectively. Reactive seeding with toluene was carried out mixing 4 mL of a 0.02 mM aqueous H_3BTC solution with 4 mL of toluene and adding 68 μL of 10 mM acetic acid. In the case of the DMF seeding, 1.26 g of H_3BTC was dissolved in a 4 mL DMF and 4 mL water mixture.

The DMF and toluene seedings were performed on rough ceramic supports. These were put in the Teflon-lined autoclaves in a vertical orientation and heated up to 210 °C. The reaction time for the DMF seeding was 72 h, while it was 12 h for the toluene seeding.

For the actual membrane growth and achievement of a dense, defect-free layer the reaction temperature was 130 °C and the reaction time was 36 h. In both cases 3 mL of DMF and 12 mL of deionized water were used with 2.35 g of aluminum nitrate nonahydrate and 1.26 g of H_3BTC. Afterward, the membranes were rinsed with methanol and water and then dried, first for 4 h at 70 °C and second at 180 °C for another 4 h.

2.5. Characterization. Scanning electron microscopy (SEM) studies of the membranes were done with a field-emission SEM (JEOL JSM-6700F). Concerning the powder materials and the neat MOF layers, the accelerating voltage was set to 2 kV and the working distance was 8 mm. The MMMs were investigated at 5 kV and 15 mm working distance. All membranes were coated with a thin carbon film (Leica, EM SCD500) via evaporation to minimize surface charge effects.

Dynamic light scattering (DLS) measurements were performed on a Zetasizer Nano ZSP from Malvern Instruments. The measurement was made by dispersing the nanoparticles with ultrasonic treatment in DCM and the actual casting solution with Matrimid for 5 min. After that, the solutions were measured in a glass cuvette with a 633 nm laser at a laser position of 178° dependent on time up to a total time of 9 min. The integration time per measurement point was 10 s. Between ultrasonication and measurement start a delay of approximately 1 min occurred (attenuater adjustment and sample adjustment). The attenuator was 8 for all measurements. Refraction indices for DCM (1.42) and Al_2O_3 (1.77) were used for the analysis. The particle size was calculated as Z-average diameter, which is the harmonic intensity averaged particle diameter.

2.6. Permeation. The gas separation properties were evaluated by mixed gas separation measurements of an equimolar mixture of hydrogen (25 mL/min) and carbon dioxide (25 mL/min) as feed gas. The sweep side was rinsed with nitrogen (50 mL/min for the MOF membranes, 1 mL/min for the MMMs). The membranes were sealed in the permeation cell with Viton O-rings (FKM 70 Vi 370). The neat MOF layers were investigated at ambient conditions. The 10 wt % MMMs were investigated at 150 °C and varying feed pressures (3, 4, and 5 bar), thus simulating the precombustion process conditions. Gas chromatography (Agilent Technologies 7890B) was applied to investigate the permeated mixture.

DOI: 10.1021/acsami.5b12541
ACS Appl. Mater. Interfaces 2016, 8, 7536−7544

3. RESULTS AND DISCUSSION

MIL-96(Al) was prepared as powder with different crystal sizes for application in MMMs with Matrimid as continuous polymer phase and as thin continuous MOF membrane layer with different crystal orientation in the layer. Both the MMM and the neat MIL-96(Al) membrane layer have been evaluated as supported membrane to investigate their potential in gas separation of an equimolar H_2/CO_2 mixture as a practice-relevant probe system.

3.1. Preparation and Characterization of MIL-96-Matrimid MMM. Figure 2 shows the XRD patterns of the as-synthesized MIL-96(Al) powder with different particle sizes (3.2 μm, 1.1 μm, 160 nm, 116 nm, and 55 nm) and a simulated X-ray powder diffraction (XRPD) from a cif file for comparison. The insets reveal the SEM images of the corresponding particles, clarifying their particle shape. All XRPD are in good accordance with the simulated one, thus indicating the successful MIL-96(Al) synthesis for each particle size. In addition, a tendency to broader reflexes for smaller particle sizes according to the Scherrer Law is obvious. The sizes determined by SEM are in fair accordance with those calculated by Rietveld refinement (cf. Table 1). Depending on the fit (Gauss, Lorentz) of the XRD line, different particle sizes have been obtained. The average Ø corresponds roughly to the size derived from SEM. As expected, the formation of a distinctive crystal shape needs a certain minimal crystal size. Every particle shows the hexagonal morphology, but only the micrometer-sized particles show the truncated crystal shape characteristic of MIL-96(Al). This finding is very similar to crystallization processes of other MOFs. Recently, the controllable synthesis of MOF crystals with a desirable morphology and pore structure has been reviewed.[35] For ZIF-8 as an example, the shape and size of the crystals can be controlled by adding the surfactant hexadecyltrimethylammonium bromide which adsorbs selectively to the hydrophobic ZIF-8 as a capping agent.[36] The formation of ZIF-8 nano- and microcrystals can be controlled by modifying the reactivity of different zinc salts[37] and the ZIF-8 crystal morphology develops with time from cubes to the rhombic dodecahedrons as equilibrium morphology.[38]

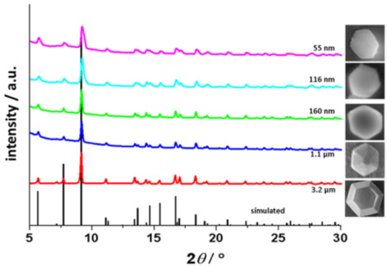

Figure 2. XRPDs and SEM images of the MIL-96(Al) particles of different size and morphology. A simulated XRD of MIL-96(Al) from a cif file is added.[12] CCDC 622598.

Table 1. Particle Size from SEM and the Corresponding Calculated Particle Sizes from Rietveld Refinement[a]

particle size via SEM	Gauss	Lorentz	Ø
55 nm	42	55	48.5
116 nm	87	154	120.5
160 nm	93	175	134
1.1 μm	n.c.[b]	n.c.	
3.2 μm	n.c.	n.c.	

[a]Ø is the arithmetic average of the crystal size calculated by the programm TOPAS fitting the XRD line by a Gaussian or a Lorentzian line shape. [b]n.c.: not calculated, due to physical correctness.

The MIL-96(Al) particles have been used for the fabrication of 10 wt % MIL-96(Al) in Matrimid MMMs to study binary gas permeation to identify a possible size dependence and polymer−filler interaction. The MMM in Figure 3 was prepared with the 3.2 μm sized MIL-96(Al) particles, then thermally conditioned at 150 °C under nitrogen flow for 24 h, and used for H_2/CO_2 permeation measurements at 150 °C. The corresponding SEM image (Figure 3a) indicates that the thickness of the supported MMM is approximately 140 μm. The two insets (Figure 3b,c) show two interesting phenomena. One can first derive from Figure 3b that the MIL-96(Al) particles are hosted in cavelike holes of the polymer Matrimid, thus indicating a low polymer−filler interaction as already found for another filler−polymer pair (Udel/Zeolite 4A).[39] This can be assigned to the high amount of inorganic component compared to the organic linker molecules of the MOF. In the other inset (Figure 3c), one can see an ca. 15 μm thick sedimented layer of the MIL-96(Al) particles in the Matrimid on top of the support. Obviously, this sedimentation took place between homogenization by ultrasonication of the MIL-96 powder in the Matrimid/DCM mixture and the evaporation of the solvent DCM.

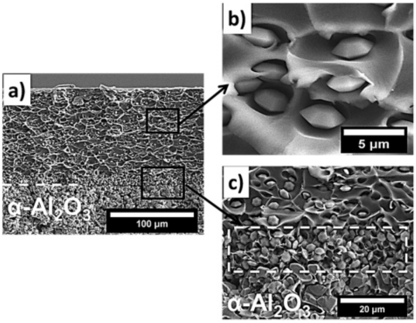

Figure 3. (a) SEM cross section of 10 wt % MIL-96(Al)@Matrimid MMM with 3.2 μm particles. (b) Embedded MIL-96(Al) particles in cavelike holes due to a poor MIL-96(Al)-Matrimid interaction. (c) Sedimented MIL-96(Al) particles near the support surface as an ca. 15 μm thick layer.

While MMMs with micrometer-sized particles can suffer from sedimentation, the MMMs with nanometer-sized particles (55 nm, 116 nm) might face other issues. The as-synthesized MIL-96(Al) nanoparticles, used for the casting solution for the MMM preparation, are initially comprised of a well-dispersed powder with little aggregation. From SEM analysis, a maximum diameter around 116 nm was found, as shown in Figure 4a. This size distribution was achieved by counting a total amount of approximately 150 particles. As indicated by time-dependent dynamic light scattering (DLS) measurements in Figure 4b, the

DOI: 10.1021/acsami.5b12541
ACS Appl. Mater. Interfaces 2016, 8, 7536−7544

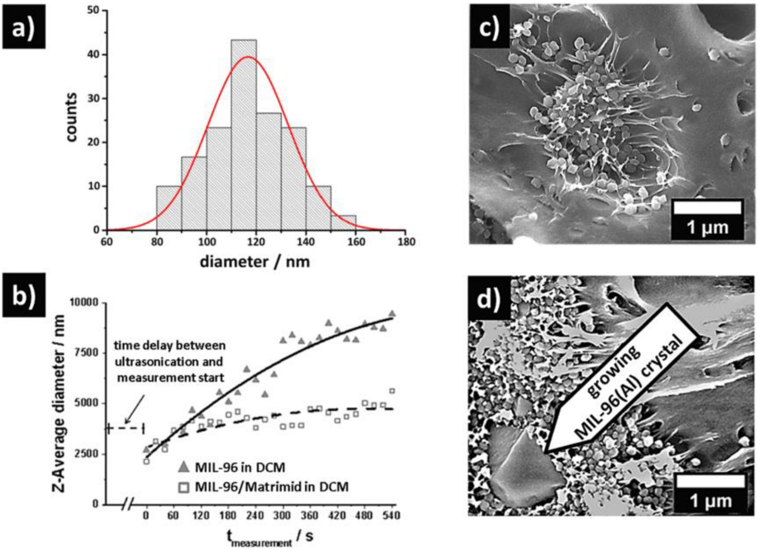

Figure 4. (a) Particle size distribution by counting 150 MIL-96(Al) particles on an SEM image with a maximum crystal size at 116 nm, including a Gaussian fit (red line). (b) Dynamic light scattering of nanometer-sized MIL-96 particles in pure DCM and in the actual MMM casting solution (mixture of Matrimid and DCM) as a function of time. (c) Agglomerates of 116 nm MIL-96(Al) in the MMM. (d) Micrometer-sized MIL-96(Al) crystal grown in the center of the aggregated 116 nm MIL-96 in Matrimid as shown in (c) after 36 h at 150 °C.

nanoparticles tend to aggregate to bigger micrometer-sized aggregates in DCM and also in a diluted actual casting solution (DCM/Matrimid). This diluted casting solution is far from the reality when the MMM is prepared. Nevertheless, one has to deduce from this measurement that the particles show a tendency toward aggregation in the polymeric solution since it is impossible to measure the nondiluted casting solution via DLS. We explain the slower aggregation for the latter solution by a hindrance through the polymer chains of the Matrimid, which results in a higher viscosity, thus slowing down the aggregation kinetics of the suspended MIL-96(Al) particles. The polymer chains may stabilize the colloidal solution, thus resulting in a limited aggregation. From comparison of the particle sizes as-derived from SEM and DLS, one can conclude that the aggregation shall occur right after the end of the homogenization by ultrasonication, casting, and evaporation of the solvent DCM. Consequently, the micrometer-sized aggregates made from initial nanometer-sized MIL-96(Al) as detected for the DCM/Matrimid casting solution in the DLS can also be found in the MMM (cf. Figure 4c). However, a ripening of these aggregates into micrometer-sized MIL-96(Al) crystals (cf. Figure 4d) occurs at higher temperatures, in our case at 150 °C in the MMM. A similar finding of an Ostwald ripening was also previously found for ZIF-8 nanosized crystals during the homogenization of the MMM casting solution by intense ultrasonic treatment.[40] Therefore, a stable dispersion of the nanometer-sized MOFs in the continuous polymer phase seems important to avoid aggregation and crystal growth. As shown recently in various publications, the polymer−filler interaction and the resulting MMM quality can be enhanced by chemical or thermal modification to some degree.[41−46]

3.2. Preparation and Characterization of Neat MIL-96 Membrane Layers. Depending on the solvent and the crystallization conditions, the MIL-96(Al) crystals can exhibit various shapes, as shown recently.[34] For instance, MIL-96(Al), grown in DMF/water, shows truncated hexagonal crystals, whereas crystallization of MIL-96(Al) in toluene/water results in c-elongated crystals. The third crystal shape of MIL-96(Al) is the hexagonal-bipyramidal shape which can be obtained at low DMF concentrations.

Inspired by these studies, we prepared supported MIL-96(Al) membranes with different shapes of the crystals in the layer. In the reactive seeding step, the crystal facets orientation and crystal shape of the future MIL-96(Al) membrane was predefined. Reactive seeding means that the alumina support served as Al source for the MIL-96(Al) seed crystals, as already shown for several Al-based MOF structures.[47] When the reactive seeding was done in DMF/water, truncated hexagonal bipyramidal MIL-96(Al) seeds were obtained, whereas the use of the solvent mixture toluene/water gives hexagonal MIL-96(Al) platelike seed crystals (cf. Figure 5). In the following step the seeded supports were grown to continuous MOF layers in identical DMF/water mixture. However, the cross sections of the MIL-96 layers show that the two membranes are of different thicknesses (cf. Figure 5). The MIL-96 layer seeded in DMF and grown in DMF is about 2 μm thick, and the MIL-96 layer seeded in toluene and grown in DMF is about 8 μm thick.

DOI: 10.1021/acsami.5b12541
ACS Appl. Mater. Interfaces 2016, 8, 7536−7544

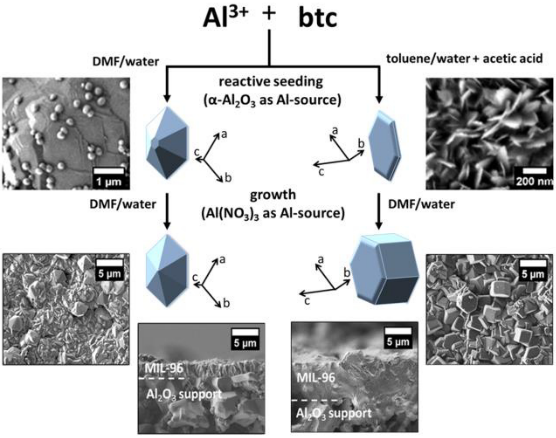

Figure 5. Reaction scheme for the synthesis of differently shaped and oriented seed crystals and MOF layers. The solvent mixture DMF/water results in hexagonal-truncated bipyramidal seed crystals, whereas toluene/water gives hexagonal platelike seeds. These seeds grow to continuous layers in the DMF/water mixture, keeping their crystallographic orientation and habit.

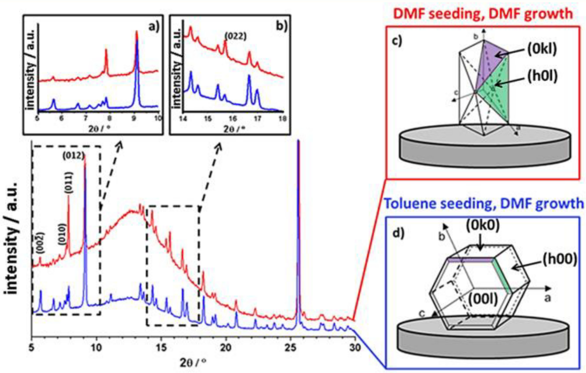

Figure 6. X-ray diffractograms of the two neat supported MIL-96(Al) membranes under study. Insets (a) and (b) show the differences between the two layers. (c) and (d) schematically clarify the crystal orientation relative to the support and the different crystal habit. The broad hump around $2\theta = 13°$ results from the amorphous polymer holder used for the XRD measurement. Because of the different thicknesses of the MIL-96(Al) layers (2 and 8 μm, respectively), the intensities of both XRDs have been normalized to the (012) reflex. CCDC 622598.

In addition to the SEM, from XRD in θ–θ geometry detailed information on the crystal orientation in the MIL-96 layer relative to the support and the crystal habit in the layers can be extracted, as shown in Figure 6. The seeding solvent mixtures—DMF/water or toluene/water/acetic acid—clearly affect the preferential growth direction of MIL-96(Al) seeds. Afterward, this seed crystal preference is maintained in the growth of the oriented MIL-96 seeds to a continuous layer of crystals with different outward facets. The $(00\bar{2})$ reflex is smaller for the MIL-96 layer seeded and grown in DMF, while it is quite intense in the case of the layer seeded in toluene and grown in DMF (cf. Figure 6a). It has to be clarified that the crystals in both layers are oriented with the *c*-direction parallel to the support. However, reflex intensity differences between the two XRDs are visible, thus indicating the preferential growth of lattice directions. This is in fact attributed to the different shapes of the crystals. In the case of the MIL-96 layer grown on the toluene-seeded support, the reflexes for the lattice planes (*h*00), (0*k*0), and (00*l*) are more intense (cf. Figure 6a). In contrast, the layer grown on DMF seeded supports shows more intense reflexes for the lattice planes forming the trigonal facets, especially (011) and (022) (cf. Figure 6b). The outward facets in the layer have an influence

DOI: 10.1021/acsami.5b12541
ACS Appl. Mater. Interfaces 2016, 8, 7536−7544

ACS Applied Materials & Interfaces Research Article

on the gas transport through the membrane since the blocked cavity mentioned above acts like a barrier (cf. Figure 1c). The two reflexes between 15 and 16° 2θ have reversed intensities, thus indicating a directional influence of the crystal growth toward the (0*kl*) or the equivalent (*h*0*l*) lattice planes as an effect of the crystal shape (cf. Figure 6b). The crystal shape resulting from toluene/water/acetic acid seeding is elongated in the *c*-direction (cf. Figure 6d), which was previously reported for MIL-96(Al) particles grown under toluene/water influence,[34] whereas the crystal morphology resulting from DMF/water seeding (cf. Figure 6c) is truncated bipyramidal. In summary, from XRD analysis one can say, on the whole, that the seeding procedure (DMF, toluene) results, on one hand, in a preferential crystal orientation. On the other hand, these seeding crystals subsequently grow to continuous layers in DMF/water, under conservation of the preferred habit of the seed crystals.

Also in other studies, oriented MOF layers on solid supports have recently been obtained. With use of the layer-by-layer liquid phase epitaxial growth, oriented MOF layers can be prepared on very smooth surfaces such as gold,[48,49] Si wafer,[50] or indium tin oxide.[51] Since the surface of a porous support is rather rough, only in a few cases oriented membrane layers have been obtained such as for ZIF-8[52] and ZIF-69.[53]

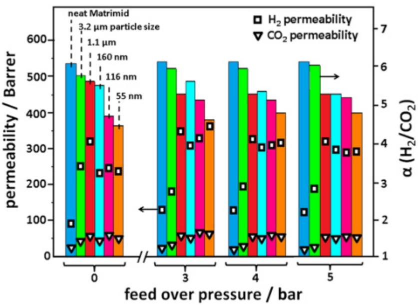

Figure 7. Permeation measurements for the MIL-96(Al)@Matrimid MMMs at 150 °C. Left: H_2 (□) and CO_2 (▽) permeabilities in Barrer. (One Barrer = 3.347×10^{-16} mol·m^{-1}·s^{-1}·Pa^{-1}.) Right: H_2/CO_2 mixed gas separation factor α (columns). Before permeation, all MMMs were treated for 24 h at 150 °C under nitrogen. The sweep side was at 1 bar for all measurements.

3.3. Gas Permeation Tests for the H_2/CO_2 Mixture. Both the MIL-96(Al)/Matrimid MMMs and the neat MIL-96(Al) membrane layers have been evaluated in the separation of an equimolar mixture of H_2 and CO_2. Therefore, the mixture was permeated through the neat MOF layers at room temperature and ambient pressure and through the MMMs at 150 °C and different feed pressures. The permeation measurements for the different MMMs containing 10 wt % MIL-96(Al) of different sizes are shown in Figure 7. Before the measurements, the membranes have been conditioned under nitrogen flux at 150 °C for 24 h. Because of the (i) aggregation and (ii) the tendency of the aggregates to crystallize into large crystals (cf. Figure 4a and b), one could not expect a superior separation performance for the MMMs containing the nanometer-sized MIL-96(Al) particles (116 and 55 nm). Because of the shrinking due to the crystallization of the aggregates of nanometer-sized MIL-96(Al) into micrometer-sized MIL-96(Al) crystals, new unselective cavities are formed. The newly formed micrometer-scale MIL-96(Al) crystals are found inside cavity-like holes in the Matrimid phase, without contact with the polymer phase as already seen for the MMM prepared with 3.2 μm sized particles (cf. Figure 3b). In complete accordance with this expectation, the MMMs prepared with nano-MIL-96(Al) (55 and 116 nm MIL-96(Al)) show indeed a slightly lower H_2/CO_2 selectivity than MMMs prepared with the larger micrometer-sized MIL-96 particles and Matrimid itself. But also the micrometer-sized

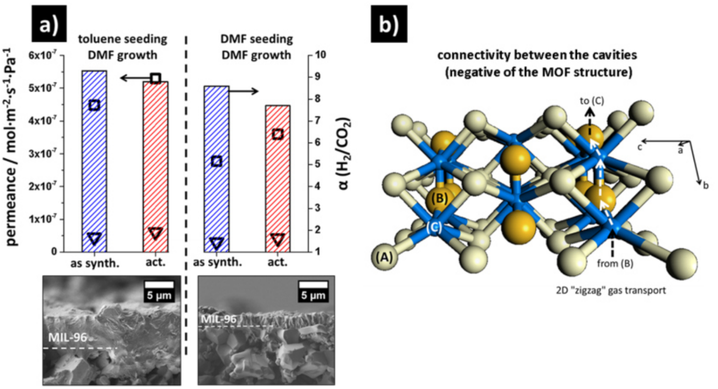

Figure 8. (a) H_2/CO_2 mixture separation factor α (columns) and H_2 (□) and CO_2 (▽) permeances for the two neat supported MIL-96(Al) membranes (left, toluene/water seeding; right, DMF/water seeding) at room temperature. Measurements carried out directly after synthesis (as synth.) and after 24 h activation at 150 °C in a nitrogen flow (act.). (b) Schematic connectivity between the three different cavities (A), (B), and (C), showing that the 3D pore structure is a virtual 2D pore structure since the gas transport is limited to a "zigzag" pathway (arrows) between the two cavities (B) and (C).

DOI: 10.1021/acsami.5b12541
ACS Appl. Mater. Interfaces 2016, 8, 7536−7544

MIL-96(Al) particles do not improve the separation performance of Matrimid because of the poor contact between MIL-96(Al) and Matrimid and additionally because of sedimentation (see Figure 3c). In summary, it was found that, (i) at an only slightly decreased H_2/CO_2 selectivity, the permeabilities of the MMMs increased by the factor of 2−3 and (ii) the permselectivity shows no dependence on the used particle size for our MMM samples.

Figure 8 shows the permeation measurement of the two neat supported MIL-96(Al) layers. However, Figure 8a indicates, surprisingly, that the permeance for the 2 μm thick membrane is lower compared to that of the 8 μm membrane layer. This experimental finding is explained by the different shape of the MIL-96(Al) crystals in the membrane layer as previously clarified in Figure 6. The formed (0*k*0)-equivalent facets of the MIL-96(Al) membrane from the toluene/water seeding allow a significantly faster transport through the membrane. The permeance of the thicker membrane (toluene/water seeded) is 100% higher than the permeance of the thinner MIL-96(Al) membrane (DMF/water seeded). This is caused by the variation of aspect ratio of the crystals (as discussed above). The outer lattice planes in the pathway of the gas molecules from the DMF/water-seeded MIL-96 layer block the gas-transport path since this MOF is a virtual 2D network. In the MIL-96(Al) system, diffusion in the *a*-direction (perpendicular to *b*−*c* planes) and *b*-direction (perpendicular to *a*−*c* planes) is much easier compared to that in the *c*-direction (perpendicular to *a*−*b* planes), as mentioned above. Similar findings of gas transport depending on the differently exposed facets with different pore sizes were recently observed for various classes of porous materials (e.g., MOFs and ZIFs).[54−56]

These data clarify that the permeation flux can be strongly dependent on the direction of the outward facing crystal facets. The crystals with elongated (00l), thus exposed (0*k*0) planes from the toluene-seeded membrane, have shown a significantly higher flux, while maintaining a good H_2/CO_2 permselectivity of about 9.

4. CONCLUSIONS

Two kinds of MIL-96(Al) membranes have been prepared: a few micrometer thick continuous "neat" layers on top of asymmetric α-Al_2O_3 supports, and mixed-matrix membranes (MMM) with MIL-96(Al) powder of different crystal sizes in Matrimid, also supported by porous asymmetric α-Al_2O_3 discs.

For the preparation of the neat supported MIL-96(Al) membranes, two different layer types, depending on the solvent during seeding, could be obtained. Reactive seeding led to different orientations of the outward facing lattice planes and thus crystal shapes. As a consequence of the virtual 2D network and the varying crystal habits, two different separation behaviors for the binary H_2/CO_2 mixture were found. The reactive seeding in toluene/water and later grown in DMF/water to the continuous layer led to a membrane with a doubled H_2 permeance compared to the layer fabricated by reactive seeding in DMF/water and later grown in DMF/water. This finding could be explained by different channel orientation and the outward facing of gastight transport-ineffective cavities.

For the preparation of MMM, MIL-96(Al) powders of different crystal sizes have been synthesized and mixed with Matrimid in DCM, and were homogenized by ultrasonication. However, during solvent evaporation two effects took place: (i) when the MIL-96(Al) powder is micrometers in size, the crystals sediment resulting in an inhomogeneous MMM; (ii) when nanometer-size MIL-96(Al) are used, these tend to form 5−10 μm sized aggregates which upon thermal activation at 150 °C merge into micrometer-sized MIL-96(Al) crystals. The resulting MIL-96/Matrimid MMMs show higher H_2 permeabilities at only slightly reduced H_2/CO_2 selectivities in comparison with the neat Matrimid membranes.

On comparing the performance of the MIL-96(Al) membranes for the H_2/CO_2 separation, we can state that the mixed gas separation factor α (H_2/CO_2) for the neat supported MIL-96(Al) layer is about 10, which is approximately 2 times higher than the separation values obtained for the best MMMs of MIL-96(Al) in Matrimid. Also, the hydrogen flux through the supported MOF membranes is higher, due to the reasons mentioned above.

However, despite the high performance of the neat supported MOF layers as membranes, especially of their high fluxes, "there's plenty of room at the bottom" to prepare practice-relevant, cheap, nonbrittle MMMs with acceptable thermal expansion coefficients with well-dispersed and, therefore, stabilized nanosized MOFs as filler.

■ AUTHOR INFORMATION

Corresponding Author

*E-mail: Sebastian.friebe@pci.uni-hannover.de (S.F.).

Notes

The authors declare no competing financial interest.

■ ACKNOWLEDGMENTS

The authors of this work are thankful to the EU 7th Framework project M_4CO_2 (Energy efficient MOF-based mixed-matrix membranes for CO_2 capture, Grant Agreement No. 608490) for financial support. N. C. Bigall is grateful for financial support from BMBF (NanoMatFutur support code 03X5525). F. Kapteijn and J. Gascon (TU Delft) are thanked for stimulating discussions. Furthermore, B. Geppert is thanked for technical assistance.

■ REFERENCES

(1) Casas, N.; Schell, J.; Joss, L.; Mazzotti, M. A Parametric Study of a PSA Process for Pre-combustion CO_2 Capture. *Sep. Purif. Technol.* **2013**, *104*, 183−192.

(2) Davison, J. Performance and Costs of Power Plants with Capture and Storage of CO_2. *Energy* **2007**, *32*, 1163−1176.

(3) Belaissaoui, B.; Le Moullec, Y.; Hagi, H.; Favre, E. Energy Efficient Oxygen Enriched Air Production Technologies: Cryogeny vs Membranes. *Sep. Purif. Technol.* **2014**, *125*, 142−150.

(4) Rangnekar, N.; Mittal, N.; Elyassi, B.; Caro, J.; Tsapatsis, M. Zeolite Membranes − A Review and Comparison with MOFs. *Chem. Soc. Rev.* **2015**, *44*, 7128−7154.

(5) Batten, S. R.; Champness, N. R.; Chen, X.-M.; Garcia-Martinez, J.; Kitagawa, S.; Ohrstrom, L.; O'Keeffe, M.; Suh, M. P.; Reedijk, J. Coordination Polymers, Metal-Organic Frameworks and the Need for Terminology Guidelines. *CrystEngComm* **2012**, *14*, 3001−3004.

(6) Sumida, K.; Rogow, D. L.; Mason, J. A.; McDonald, T. M.; Bloch, E. D.; Herm, Z. R.; Bae, T.-H.; Long, J. R. Carbon Dioxide Capture in Metal − Organic Frameworks. *Chem. Rev.* **2012**, *112*, 724−781.

(7) Loiseau, T.; Lecroq, L.; Volkringer, C.; Marrot, J.; Ferey, G.; Haouas, M.; Taulelle, F.; Bourrelly, S.; Llewellyn, P. L.; Latroche, M. MIL-96 a Porous Aluminium Trimesate 3D Structure Constructed from a Hexagonal Network of 18-Membred Rings and μ_3-Oxo-Centred Trinuclear Units. *J. Am. Chem. Soc.* **2006**, *128*, 10223−10230.

(8) Ahnfeldt, T.; Guillou, N.; Gunzelmann, D.; Margiolaki, I.; Loiseau, T.; Ferey, G.; Senker, J.; Stock, N. $[Al_4(OH)_2(OCH_3)_4(H_2N\text{-bdc})_3] \cdot x H_2O$: A 12-Connected Porous Metal-Organic Framework with an Unprecedented Aluminium-Containing Brick. *Angew. Chem.* **2009**, *121*, 5265−5268.

(9) Loiseau, T.; Serre, C.; Huguenard, C.; Fink, G.; Taulelle, F.; Henry, M.; Bataille, T.; Ferey, G. A Rationale for the Large Breathing of the

Porous Aluminium Terephthalate (MIL-53) Upon Hydration. *Chem. - Eur. J.* **2004**, *10*, 1373−1382.
(10) Volkringer, C.; Loiseau, T. A New Indium Metal-Organic 3D Framework with 1,3,5-Benzenetricarboxylate, MIL-96 (In), Containing μ_3-Oxo-Centred Trinuclear Units and a Hexagonal 18-Ring Network. *Mater. Res. Bull.* **2006**, *41*, 948−954.
(11) Volkringer, C.; Loiseau, T.; Ferey, G.; Morais, C. M.; Taulelle, F.; Montouillout, V.; Massiot, D. Synthesis, Crystal Structure and ^{71}Ga Solid State NMR of a MOF-Type Gallium Trimesate (MIL-96) with μ_3-Oxo Bridged Trinuclear Units and a Hexagonal 18-Ring Network. *Microporous Mesoporous Mater.* **2007**, *105*, 111−117.
(12) Kanniche, M.; Gros-Bonnivard, R.; Jaud, P.; Valle-Marcos, J.; Amann, J.-M.; Bouallou, C. Pre-Combustion, Post-Combustion and Oxy-Combustion in Thermal Power Plant for CO_2 Capture. *Appl. Therm. Eng.* **2010**, *30*, 53−62.
(13) Li, T.; Pan, Y.; Peinemann, K. V.; Lai, Z. Carbon Dioxide Selective Mixed Matrix Composite Membrane Containing ZIF-7 Nano-Fillers. *J. Membr. Sci.* **2013**, *425*−*426*, 235−242.
(14) Sarawade, P.; Tan, H.; Anjum, D.; Cha, D.; Polshettiwar, V. Size-and Shape-Controlled Synthesis of Hexagonal Bipyramidal Crystals and Hollow Self-Assembled Al-MOF Spheres. *ChemSusChem* **2014**, *7*, 529−535.
(15) Seoane, B.; Dikhtiarenko, A.; Mayoral, A.; Tellez, C.; Coronas, J.; Kapteijn, F.; Gascon, J. Metal-Organic Framework Synthesis in the Presence of Surfactants: Towards Hierarchical MOFs? *CrystEngComm* **2015**, *17*, 1693−1700.
(16) Liu, D.; Liu, Y.; Dai, F.; Zhao, J.; Yang, K.; Liu, C. Size- and Morphology-Controllable Synthesis of MIL-96 (Al) by Hydrolysis and Coordination Modulation of Dual Aluminium Source and Ligand Systems. *Dalton Trans.* **2015**, *44*, 16421−16429.
(17) Lin, Y.; Kong, C.; Chen, L. Facile Synthesis of Aluminium-Based Metal-Organic Frameworks with Different Morphologies and Structures through and OH^--Assisted Method. *Chem. - Asian J.* **2013**, *8*, 1873−1878.
(18) Seoane, B.; Coronas, J.; Gascon, I.; Benavides, M. E.; Karvan, O.; Caro, J.; Kapteijn, F.; Gascon, J. Metal-Organic Framework Based Mixed Matrix Membranes: A Solution for Highly Efficient CO_2 Capture? *Chem. Soc. Rev.* **2015**, *44*, 2421−2454.
(19) Goh, P. S.; Ismail, A. F.; Sanip, S. M.; Ng, B. C.; Aziz, M. Recent Advances of Inorganic Fillers in Mixed Matrix Membranes for Gas Separation. *Sep. Purif. Technol.* **2011**, *81*, 243−264.
(20) Bastani, D.; Esmaeili, N.; Asadollahi, M. Polymeric Mixed Matrix Membranes Containing Zeolites as a Filler for Gas Separation Applications: A Review. *J. Ind. Eng. Chem.* **2013**, *19*, 375−393.
(21) Diestel, L.; Wang, N.; Schwiedland, B.; Steinbach, F.; Giese, U.; Caro, J. MOF based MMMs with Enhanced Selectivity due to Hindered Linker Distortion. *J. Membr. Sci.* **2015**, *492*, 181−186.
(22) Rezakazemi, M.; Amooghin, A. E.; Montazer-Rahmati, M. M.; Ismail, A. F.; Matsuura, T. State-of-the-art Membrane Based CO_2 Separation using Mixed Matrix Membranes (MMMs): An Overview on Current Status and Future Directions. *Prog. Polym. Sci.* **2014**, *39*, 817−861.
(23) Lin, R.; Ge, L.; Liu, S.; Rudolph, V.; Zhu, Z. Mixed-Matrix Membranes with Metal−Organic Framework-Decorated CNT Fillers for Efficient CO_2 Separation. *ACS Appl. Mater. Interfaces* **2015**, *7*, 14750−14757.
(24) Ulbricht, M. Advanced Functional Polymer Membranes. *Polymer* **2006**, *47*, 2217−2262.
(25) Noble, R. D. Perspectives on Mixed Matrix Membranes. *J. Membr. Sci.* **2011**, *378*, 393−397.
(26) Tanh Jeazet, H. B.; Staudt, C.; Janiak, C. Metal-Organic Frameworks in Mixed-Matrix Membranes for Gas Separation. *Dalton Trans.* **2012**, *41*, 14003−14027.
(27) Rodenas, T.; van Dalen, M.; Serra-Crespo, P.; Kapteijn, F.; Gascon, J. Mixed Matrix Membranes Based on NH_2-functionalized MIL-type MOFs: Influence of Structural and Operational Parameters on the CO_2/CH_4 Separation Performance. *Microporous Mesoporous Mater.* **2014**, *192*, 35−42.
(28) Rodenas, T.; van Dalen, M.; Garcia-Perez, E.; Serra-Crespo, P.; Zornoza, B.; Kapteijn, F.; Gascon, J. Visualizing MOF Mixed Matrix Membranes at the Nanoscale: Towards Structure-Performance Relationships in CO_2/CH_4 Separation over NH_2-MIL-53(Al)@PI. *Adv. Funct. Mater.* **2014**, *24*, 249−256.
(29) Shishatskiy, S.; Nistor, C.; Popa, M.; Nunes, S. P.; Peinemann, K. V. Polyimide Asymmetric Membranes for Hydrogen Separation: Influence of Formation Conditions on Gas Transport Properties. *Adv. Eng. Mater.* **2006**, *8*, 390−397.
(30) Loloei, M.; Omidkhah, M.; Moghadassi, A.; Amooghin, A. E. Preparation and Characterization of Matrimid®5218 Based Binary and Ternary Mixed Matrix Membranes for CO2 Separation. *Int. J. Greenhouse Gas Control* **2015**, *39*, 225−235.
(31) Mahajan, R.; Burns, R.; Schaeffer, M.; Koros, W. J. Challenges in Forming Successful Mixed Matrix Membranes with Rigid Polymeric Materials. *J. Appl. Polym. Sci.* **2002**, *86*, 881−890.
(32) Hooper, J. B.; Schweizer, K. S. Contact Aggregation, Bridging, and Steric Stabilisation in Dense Polymer-Particle Mixtures. *Macromolecules* **2005**, *38*, 8858−8869.
(33) Sindoro, M.; Jee, A.-Y.; Granick, S. Shape-Selected Colloidal MOF Crystals for Aqueous Use. *Chem. Commun.* **2013**, *49*, 9576−9578.
(34) Nan, J.; Dong, X.; Wang, W.; Jin, W. Formation Mechanism of Metal-Organic Framework Membranes Derived from Reactive Seeding Approach. *Microporous Mesoporous Mater.* **2012**, *155*, 90−98.
(35) Yao, J.; He, M.; Wang, H. Strategies for Controlling Crystal Structure and Reducing Usage of Organic Ligand and Solvents in the Synthesis of Zeolitic Imidazolate Frameworks. *CrystEngComm* **2015**, *17*, 4970−4976.
(36) Pan, Y.; Heryadi, D.; Zhou, F.; Zhao, L.; Lestari, G.; Su, H.; Lai, Z. Tuning the crystal morphology and size of zeolitic imidazolate framework-8 in aqueous solution by surfactants. *CrystEngComm* **2011**, *13*, 6937−6940.
(37) Schejn, A.; Balan, L.; Falk, V.; Aranda, L.; Medjahdi, L.; Schneider, R. Controlling ZIF-8 Nano-and Microcrystal Formation and Reactivity through Zinc Salt Variations. *CrystEngComm* **2014**, *16*, 4493−4500.
(38) Cravillon, J.; Schröder, C. A.; Bux, H.; Rothkirch, A.; Caro, J.; Wiebcke, M. Formate modulated solvothermal synthesis of ZIF-8 investigated using time-resolved *in situ* X-ray diffraction and scanning electron microscopy. *CrystEngComm* **2012**, *14*, 492−498.
(39) Moore, T. T.; Koros, W. J. Non-Ideal Effects in Organic-Inorganic Materials for Gas Separation Membranes. *J. Mol. Struct.* **2005**, *739*, 87−98.
(40) Thompson, J. A.; Chapman, K. W.; Koros, W. J.; Jones, C. W.; Nair, S. Sonication-Induced Ostwald Ripening of ZIF-8 Nanoparticles and Formation of ZIF-8/Polymer Composite Membranes. *Microporous Mesoporous Mater.* **2012**, *158*, 292−299.
(41) Lin, R.; Ge, L.; Hou, L.; Strounina, E.; Rudolph, V.; Zhu, Z. Mixed Matrix Membranes with Strengthened MOFs/Polymer Interfacial Interaction and Improved Membrane Performance. *ACS Appl. Mater. Interfaces* **2014**, *6*, 5609−5618.
(42) Xin, Q.; Ouyang, J.; Liu, T.; Li, Z.; Li, Z.; Liu, Y.; Wang, S.; Wu, H.; Jiang, Z.; Cao, X. Enhanced Interfacial Interaction and CO_2 Separation Performance of Mixed Matrix Membrane by Incorporation Poly-ethylenimine-Decorated Metal−Organic Frameworks. *ACS Appl. Mater. Interfaces* **2015**, *7*, 1065−1077.
(43) Amooghin, A. E.; Omidkhah, M.; Kargari, A. The Effects of Aminosilane Grafting on NaY Zeolite−Matrimid®5218 Mixed Matrix Membranes for CO_2/CH_4 Separation. *J. Membr. Sci.* **2015**, *490*, 364−379.
(44) Chen, X. Y.; Nik, O. G.; Rodrigue, D.; Kaliaguine, S. Mixed Matrix Membranes of Ami-nosilanes Grafted FAU/EMT Zeolite and Cross-linked Polyimide for CO_2/CH_4 Separation. *Polymer* **2012**, *53*, 3269−3280.
(45) Nik, O. G.; Chen, X. Y.; Kaliaguine, S. Amine-Functionalized Zeolite FAU/EMT-Polyimide Mixed Matrix Membranes for CO_2/CH_4 Separation. *J. Membr. Sci.* **2011**, *379*, 468−478.
(46) Song, Q.; Cao, S.; Pritchard, R. H.; Qiblawey, H.; Terentjev, E. M.; Cheetham, A. K.; Sivaniah, E. Nanofiller-Tuned Microporous

DOI: 10.1021/acsami.5b12541
ACS Appl. Mater. Interfaces 2016, 8, 7536−7544

Polymer Molecular Sieves for Energy and Environmental Processes. *J. Mater. Chem. A* **2016**, *4*, 270−279.

(47) Hu, Y.; Dong, X.; Nan, J.; Jin, W.; Ren, X.; Xu, N.; Lee, Y. M. Metal-Organic Framework Membranes Fabricated *via* Reactive Seeding. *Chem. Commun.* **2011**, *47*, 737−739.

(48) Liu, B.; Shekhah, O.; Arslan, H. K.; Liu, J.; Wöll, C.; Fischer, R. A. Enantiopure Metal-Organic-Fraumework Thin Films: Oriented SURMOF Growth and Enantioselective Adsorption. *Angew. Chem., Int. Ed.* **2012**, *51*, 807−810.

(49) Shekhah, O.; Eddaoudi, M. The Liquid Phase Epitaxy Method for the Construction of Oriented ZIF-8 Thin Films with Controlled Growth on Functionalized Surfaces. *Chem. Commun.* **2013**, *49*, 10079−10081.

(50) So, M. C.; Jin, S.; Son, H.-J.; Wiederrecht, G. P.; Farha, O. K.; Hupp, J. T. Layer-by-Layer Fabrication of Oriented Porous Thin Films Based on Porphyrin-Containing Metal-Organic-Frameworks. *J. Am. Chem. Soc.* **2013**, *135*, 15698−15701.

(51) Hou, C.; Xu, Q.; Peng, J.; Ji, Z.; Hu, X. (110)-Oriented ZIF-8 Thin Films on ITO with Con-trollable Thickness. *ChemPhysChem* **2013**, *14*, 140−144.

(52) Bux, H.; Feldhoff, A.; Cravillon, J.; Wiebcke, M.; Li, Y.-S.; Caro, J. Oriented Zeolitic Imidazolate Framework-8 Membrane with Sharp H_2/C_3H_8 Molecular Sieve Separation. *Chem. Mater.* **2011**, *23*, 2262−2269.

(53) Liu, Y.; Zeng, G.; Pan, Y.; Lai, Z. Synthesis of Highly c-Oriented ZIF-69 Membranes by Secondary Growth and their Permeation Properties. *J. Membr. Sci.* **2011**, *379*, 46−51.

(54) Mao, Y.; Su, B.; Cao, W.; Li, J.; Ying, Y.; Ying, W.; Hou, Y.; Sun, L.; Peng, X. Specific Oriented Metal−Organic Framework Membranes and Their Facet-Tuned Separation Performance. *ACS Appl. Mater. Interfaces* **2014**, *6*, 15676−15685.

(55) Zhong, Z.; Yao, J.; Chen, R.; Low, Z.; He, M.; liu, J. Z.; Wang, H. Oriented two-Dimensional Zeolitic Imidazolate Framework-L Membranes and their Gas Permeation Properties. *J. Mater. Chem. A* **2015**, *3*, 15715−15722.

(56) Motevalli, B.; Wang, H.; Liu, J. Z. Cooperative Reformable Channel System with Unique Recognition of Gas Molecules in a Zeolitic Imidazolate Framework with Multilevel Flexible Ligands. *J. Phys. Chem. C* **2015**, *119*, 16762−16768.

DOI: 10.1021/acsami.5b12541
ACS Appl. Mater. Interfaces 2016, 8, 7536−7544

2.5 On Comparing Permeation through Matrimid®-based Mixed Matrix and Multilayer Sandwich FAU Membranes: H_2/CO_2 Separation, Support Functionalization and Ion Exchange

A. Mundstock, S. Friebe, J. Caro

International Journal of Hydrogen Energy **2017**, 42, 279-288.

INTERNATIONAL JOURNAL OF HYDROGEN ENERGY 42 (2017) 279–288

Available online at www.sciencedirect.com

ScienceDirect

journal homepage: www.elsevier.com/locate/he

On comparing permeation through Matrimid®-based mixed matrix and multilayer sandwich FAU membranes: H_2/CO_2 separation, support functionalization and ion exchange

Alexander Mundstock **, *Sebastian Friebe*, *Jürgen Caro* *

Institute of Physical Chemistry and Electrochemistry, Leibniz University Hannover, Callinstr. 3A, 30167 Hannover, Germany

ARTICLE INFO

Article history:
Received 19 April 2016
Received in revised form
31 August 2016
Accepted 15 October 2016
Available online 9 December 2016

Keywords:
H_2/CO_2 separation
FAU/Matrimid® MMMs
Ion exchange
FAU membrane
Support modification

ABSTRACT

A series of supported membranes with zeolite FAU either as a thin layer or as powder in Matrimid as Mixed Matrix Membrane (MMM) have been prepared and evaluated in the H_2/CO_2 separation. In addition to neat NaX membrane layers, we developed two novel composite materials, namely FAU/Matrimid® Mixed Matrix Membranes (MMMs) as well as NaX/Matrimid® multilayer/sandwich membranes, all of them supported by porous alumina plates. The influence of different pre-synthetic support modifications (APTES = 3-aminopropyltrietoxysilane, PDA = polydopamine) on the quality of neat supported NaX membranes grown as layer on these modified supports has been investigated studying the H_2/CO_2 separation performance. It could be shown that NaX membrane layers grown on modified supports show an remarkably increased quality and correspondingly higher H_2/CO_2 separation factors α (H_2/CO_2) ($\alpha = 8.0$ for neat NaX, $\alpha = 8.9$ for NaX/APTES and $\alpha = 10.3$ for NaX/PDA). In the preparation of MMMs, the separation performance could be improved by ion exchanged Na-FAU powders. Exchanging the Na^+ of the as-synthesized NaX particles for metal ions with higher ionic potentials like Co^{2+}, results in enhanced mixed gas separation factors α in the H_2/CO_2 separation (NaX/Matrimid® MMM $\alpha = 4.0$ and CoX/Matrimid® MMM $\alpha = 5.6$).

Introduction

In academic literature on can find a wide variety of CO_2- and H_2-selective membranes for syngas purification at different pressures like e.g. FAU [1], ZIF-8/Matrimid® Mixed Matrix Membranes (MMM) [2] and polyvinylalcohol-polysiloxan/fumed silica MMMs [3], but their problems are insufficient selectivity and/or stability. Prominent examples for this issue are palladium based membranes, which are known for permeating H_2 at an almost infinite selectivity [4]. However, they suffer from sulfur poisoning, hydrogen embrittlement and the difficult scale up of [5]. These problems triggered

* *Corresponding author*. Fax: +49 51176219121.
** *Corresponding author*. Fax: +49 51176219121.
E-mail addresses: alexander.mundstock@pci.uni-hannover.de (A. Mundstock), Juergen.caro@pci.uni-hannover.de (J. Caro).
http://dx.doi.org/10.1016/j.ijhydene.2016.10.161

increased research and development efforts towards alternative materials with a special focus on polymers and MMMs [1,6,7]. Even though the polymers show lower selectivities than inorganic membranes, their commercially far more viable upscalability, high degree of variability (different polymers/fillers) and high mechanical-/pressure-stability more than compensate for this. Especially MMMs ingeniously combine the processability of polymers and the superior gas separation properties of inorganic materials. The key challenge now is to find the right materials.

One of the more promising candidates is zeolite faujasite (FAU) – either as filler in MMM or as supported membrane layer. Zeolite FAU is usually synthesized as NaX with Si/Al ratio of 1.2–1.5. Consisting of sodalite cages which are connected through hexagonal prisms, NaX features 12-membered oxygen ring pores (pore diameter ≈ 7.4 Å) in a 3D pore system. Of special interest for a desired H_2/CO_2 separation are metal ions in the activated de-hydrated state (CO_2 - ion interactions), the possibility of an ion exchange (e.g. Co^{2+}, Ni^{2+}, Cu^{2+}), high gas capacity as well as the overall high stability (chemical, thermal) inherent to zeolites. Potential applications for supported NaX membranes are e.g. H_2/CO_2 separation [1], propane/propene separation [8], dehydration of organic solvents by steam permeation [9] and separating large molecules which cannot be handled by other zeolite membranes [10,11]. Growing neat, phase-pure dense NaX membranes without cracks, pinholes or other defects is very demanding due to inhomogeneous nucleation on the support surface and the electrostatic rejection between the negatively charged precursor species and the often used alumina (α-Al_2O_3) supports [1,8]. This problem can be solved by pre-synthetic support surface modifications with "molecular binders" like e.g. polydopamine (PDA) [1,12] and 3-aminopropyltriethoxysilane (APTES) [1,8]. Both serve as molecular binder to chemically anchor NaX precursors on the support surface during hydrothermal synthesis, resulting in dense and phase-pure zeolite membranes. In this work, to get a complete picture, we evaluated both, the impact of these modifications on the membrane quality as well as on the H_2/CO_2 separation capabilities of supported NaX membranes.

Among the polymers frequently used for commercial gas separation (e.g. polysulfones, polycarbonates, poly (arylethers), poly (arylketones) [13,14]), polyimides are of particular interest because of their high chemical, thermal and mechanical stability and high gas selectivity [15,16]. Especially Matrimid®, one of the most frequently studied polyimides, shows permeability and selectivity properties falling close to upper bound regions of various Robeson plots [17,18]. Therefore, Matrimid® is a suitable basis for MMMs with different filler materials e.g. carbon molecular sieves [19], carbon nanotubes [20] as well as metal–organic frameworks [21,22] which have been implemented so far for various tasks, including the H_2/CO_2 separation [2,6,7,23]. Recent progress in ZIF-enabled membranes and the barriers that must be overcome to advance ZIF-enabled membranes beyond the laboratory level are discussed in the reviews [24,25]. In this work we prepared and evaluated novel FAU/Matrimid® MMMs using ion exchanged FAU particles as inorganic filler and investigated their impact/influence on the H_2/CO_2 separation performance.

Recently, there have been reports on how coating ZIF (–8 and –90) membranes with an additional Matrimid® top layers dramatically increases their H_2/CH_4 selectivity [26]. This improvement is most like due to a suppressed linker distortion in the ZIF/polymer contact zone and the accompanying enhanced sieving capabilities. To verify whether a similar enhancement can be achieved in the case of zeolite membranes, maybe due to a "defect healing" or synergistic effects, we additionally coated several of the NaX/PDA membranes with a layer of neat Matrimid® and measured the H_2/CO_2 separation capabilities of this multilayer/sandwich membrane.

Experimental

Unless otherwise noted, all procedures were performed under ambient atmosphere. All reagents were obtained from commercial vendors at reagent grade purity or higher and used without further purification.

Depending on the task at hand, two different kinds of porous α-Al_2O_3 supports (Fraunhofer IKTS Hermsdorf, diameter d = 18 mm, thickness h = 1 mm) have been used in this work, featuring either a medium top layer pore diameter of d_{50} = 2.5 μm (called rough/large-pored (r)) or d_{50} = 70 nm (called fine/fine-pored (f)).

Support modifications

As described in the following, the supports (f) with the fine top layer have been functionalized by APTES and PDA:

(i) 3-aminopropyltriethoxysilane (APTES) functionalized α-Al_2O_3 supports were prepared according to a previously reported [27] but slightly modified procedure. Two of the porous supports were placed in an APTES (460 mg) toluene (10 mL) mixture within a sealable reaction vial (Schott Duran Bottle) and heated up to 120 °C for 30 min. After subsequently drying in an oven at 60 °C for about 20 min and cooling down in ambient air, the modified supports were ready for further utilization.

(ii) Polydopamine (PDA) functionalized α-Al_2O_3 supports were also prepared according to a published procedure [28]. Dopamine (DPA) (2 mg/mL) was completely dissolved in 50 mL of 10 mM Tris–HCl (pH 8.5) in an open watch glass (d = 180 mm). The neat supports were simply immersed in this buffered aqueous solution for 24 h at room temperature under continuous stirring. After drying in the ambient atmosphere, the now dark brown supports were used for further membrane preparations.

Preparation of supported NaX and multilayer sandwich membranes

The crystallization of NaX membrane layers on the modified as well as unmodified α-Al_2O_3 supports has been achieved by following a previously reported but again slightly modified procedure by Huang et al. [27]. A synthesis solution with a specific molar ratio of $70Na_2O$:$1Al_2O_3$:$20SiO_2$:$2000H_2O$ was prepared by mixing a silicate and an aluminate solution at room temperature. The latter one was obtained by dissolving 7.78 g sodium hydroxide (>99%, Merck) and 0.075 g of aluminum foil (Fisher Scientific) as Al source in 25 g deionized water in a sealable reaction vial under stirring. In a second vial the silicate solution was prepared by mixing 4.17 g LUDOX AS-40 colloidal silica (40% SiO_2 in water, Aldrich) as Si source and 22.22 g deionized water. The resulting solution was then vigorously stirred for 2 h at 60 °C. After this period of time the still hot silicate solution was poured into the aluminum solution and the resulting mixture was stirred in the closed vial at room temperature till a colorless, clear and homogeneous solution was obtained (ca. 12 h). This was then transferred into a Teflon-lined stainless steel autoclave (Parr Instruments Germany). The treated or non-treated α-Al_2O_3 supports were jammed into special Teflon-holders and placed face down in the autoclave/solution too. After in situ growth for 24 h at 75 °C in an oven, the solution was decanted of and the resulting membranes were transferred into a sealed vial filled with deionized water for 24 h (washing step). Subsequently they were dried in ambient air at 60 °C in an air conditioned oven for about 2 h. In this membrane synthesis, also NaX powder has been formed which sedimented at the bottom of the autoclave. This powder has been used for ion exchange and MMM preparation.

The preparation of the FAU sandwich membranes was done as follows. First of all Matrimid® 5218 was solved in Dichloromethane. This mixture was stirred overnight and sonicated at the following day to remove air bubbles. After the sonification, the polymer solution was casted on top of the neat FAU membrane with the help of an Eppendorf pipette. This sandwich membrane was stored under dichloromethane atmosphere and activated as described below.

Ion exchange of NaX powder for MMM preparation

All ion exchanges were done, respectively, with Cobalt (II) nitrate hexahydrate, Nickel (II) nitrate hexahydrate, Copper (II) nitrate trihydrate and Lead (II) nitrate as "ion sources".

The liquid state ion exchanges were done by suspending the FAU powders (100 mg each) in an aqueous solution of the metal salts (100 mg of salt in 20 ml distilled water) for 24 h at room temperature. Afterward, the solutions were decanted, and the powders were washed with water a few times and dried in an oven at 60 °C for 2 h.

Preparation of supported mixed matrix membranes (MMM) with ion exchanged FAU powder

The supported Mixed Matrix Membranes (MMMs) were produced by a simple casting approach. Therefore, the Matrimid® 5218 and the dried (still hydrated) ion-exchanged FAU (Na^+, Pb^{2+}, Co^{2+}, Ni^{2+}, Cu^{2+}) powders (10 wt%) were weighed in a glass bottle. After that 1 mL Dichloromethane was added, the glass bottle was closed and the resulting mixture was stirred overnight. At the following day the mixture was casted on a rough α-Al_2O_3 support (2.5 μm pores; Fraunhofer IKTS, former Hermsdorfer HITK, Germany) with the help of an Eppendorf pipette. After casting, the MMMs were stored in an atmosphere of Dichloromethane to allow a slow solvent evaporation. At the end the membranes were activated at 180 °C in vacuum for several hours and subsequently stored in a glove box (Ar).

Activation and permeation measurements

A full dehydration/activation of membranes and powders was achieved by heating (180 °C) under vacuum over 2 h followed by storage in a sealed Schlenk flask in a glove box (Ar). The assembly of the permeation cells, including the mounting of the membranes, was done under protective gas atmosphere within the glove box.

For the actual permeation measurements, the assembled cells were transferred to sealable vials filled with argon and discharged from the glove box. The installation into the permeation apparatus took place under a nitrogen current to prevent a deactivation of the membranes. All permeation measurements carried out for this work, single gas as well as equimolar H_2/CO_2 mixtures, were done with a modified Wicke-Kallenbach-apparatus at room temperature following the Wicke Kallenbach principle with equal gas pressure on feed and permeate side of the membrane. As feed we used an equimolar 50 ml/min stream (25 mL H_2 and 25 mL CO_2). As sweep we used N_2 with a flow rate of 50 ml/min. Since the flux of the polymer-based MMMs is only 1/50 of the flux of the neat NaX membrane, the sweep gas rate was adjusted accordingly (1 ml/min N_2 for polymer-based membranes).

XRD and SEM

The XRD patterns of the Na-X samples (powder and membranes) were obtained on a Bruker D8 Advance X-ray Diffractometer using Cu K_α (λ = 1.54 Å) radiation. All shown Scanning Electron Microscopy (SEM) micrographs were taken on a JEOL JSM-6700F with a cold field emission gun operating at 2 kV and 10 μA.

Results and discussion

Support modification by APTES and PDA, NaX membrane layer preparation

As shown in a previous paper [8], there are huge problems to prepare defect-free NaX membranes on our standard α-Al_2O_3 supports – even when using identical synthesis protocols. All NaX membrane preparations on the neat supports resulted in a ca. 2 μm thick and defect-rich membrane layer. These defects include all kinds of cracks, pinholes and other flaws which are counter-productive for gas separation and stem most probably from the electrostatic rejection between the negatively charged NaX precursor macro molecules (≈ −43 mV [8]) and the also negatively charged α-alumina (≈ −32 mV [8]) support at the pH 11 (NaX preparation condition) as for the first time shown by our group in Refs. [1,8]. The quantity and quality of the defect occurrence seems to be highly erratic, what results in the widely fluctuating membrane quality mentioned above. Eventually, only approximately 1 out of 10 preparations resulted in relatively dense neat NaX membranes, which were used for the permeation studies in this work (Table 1).

In comparison, all membranes grown on Al_2O_3 supports which had been pre-synthetically functionalized with APTES (from now on called NaX/APTES) are dense and nearly defect-free (no cracks, pinholes or other defects could be observed, see Fig. 1A). This is most probably due to the fact that APTES-modified α-Al_2O_3 has, in stark contrast to the unmodified/neat material, a nearly neutral surface charge (Zeta potential of APTES/$Al_2O_3 \approx -3$ mV at pH 11 [8]), minimizing the electrostatic rejection between the negatively charged FAU precursor species and the modified Al_2O_3 support. This then greatly benefits the homogeneous nucleation and growth of the Na-X membranes and, subsequently, their capability for separating H_2 from CO_2 and results also in a slightly thicker (ca. 3 μm) NaX layer.

Also support modification by a PDA layer was successful. A little bit contradictory at the first glance is that an enhanced membrane quality (Fig. 1B) and the improved H_2/CO_2 selectivity (Table 1) are achieved despite the Al_2O_3/PDAs highly negative Zeta potential (≈ -43 mV at pH 11 [8]) and the subsequent electrostatic rejection between the modified support and NaX, which is even higher than the one between the neat support and the NaX zeolite. The positive effect of PDA coating of the support for the subsequent growth of the NaX layer is probably due to one of PDAs special features, namely the ability to chelate metal ions. Along with the abundance of metal ions within the synthesis solution, which enables PDA to effectively shield its charge and consequently minimize or even equalize the otherwise disruptive electrostatic forces between the functionalized support and the charged FAU precursor species. Because most of the chelated metal ions are also NaX building blocks, the functionalized support surface now additionally features more direct nucleation points for the zeolite layer growth. Together, these two phenomena facilitate an unobstructed growth and almost defect-free membranes [8].

The NaX powder, later on used for ion exchange and MMM preparations, was obtained as a sedimentation by-product from the membrane syntheses. It consists of polycrystalline microparticles with a size range of ≈ 1–4 μm (diameter) which are distinguished by their high crystallinity and overall quality, as proven by accompanying XRD measurements (Fig. 3 black line).

Multilayer membrane preparation

The preparation of the multilayer sandwich membranes, consisting of an NaX membrane layer grown on a PDA-functionalized support and subsequently covered with a Matrimid® layer, turned out to be rather challenging due to a lack of interaction between polymer and zeolite. In most cases, the Matrimid® cover completely peels off from the supported NaX membrane during the drying, thus partially damaging the latter in the process. Various adjustments to the polymer casting procedure eventually enabled us to prepare several intact multilayer sandwich membranes of the desired composition, as shown in Fig. 2A.

The greatly differing thickness of the individual layers (crystalline NaX $\approx$ 2–3 μm and Matrimid® $\approx$ 10–15 μm) is due to the applied preparation techniques and their accompanying problems as described earlier. Fig. 2B shows that, despite the improved casting procedure, the overall adherence between polymer and zeolite layers is still limited to a small number of “anchor points” scattered throughout the “cavernous” border region. Obviously, the inorganic NaX layer and the Matrimid® – despite the latter's hydrophilicity – do not match. This finding differs from known published results which showed that polymer coatings easily adhere on MOF (Metal–Organic Framework) layers [26].

The mentioned few “anchor points” (see Fig. 2B left side), where a much better interaction between zeolite and polymer can be found, are possibly due to small defects (cracks and pinholes) and impurities within the surface of the zeolite membrane. Those “former” defect sites, now sealed by a plug of Matrimid®, could provide a better “grip” for the polymer (e.g. a filled crack) and consequently a much needed minimum of interaction between the two layers.

Ion exchange of the NaX powder for MMM preparation

Ion exchanged FAU particles have been used as inorganic filler phase in mixed matrix membranes (MMM). The ion exchanged particles show, apart from the expected color changes according to the ion source, no significant changes in XRD patterns (Fig. 3). However, all ion exchanged FAU powders seem to suffer from a slight loss of crystallinity compared to the NaX source material, as indicated by the overall decrease in signal intensity, due to the forced exchange of monovalent sodium ions for multivalent metal ions.

Mixed matrix membrane preparation

The hydrated ion exchanged FAU powder crystals have been used as inorganic filler phase (10 wt%) in supported (pressure

Table 1 – Mixed gas permeation data on supported (fine α-Al_2O_3, top-layer pore $d_{50} = 70$ nm) for an equimolar H_2/CO_2 mixture (Knudsen separation factor $\approx$ 4.7) at 1 bar (Wicke Kallenbach technique), room temperature and 50 ml/min N_2 sweep.

Support	Al_2O_3	Al_2O_3	Al_2O_3	Al_2O_3	Al_2O_3	Al_2O_3
Modification	–	–	APTES	APTES	PDA	PDA
Membrane	–	NaX	–	NaX	–	NaX
Mixed gas α (H_2/CO_2)	4.6	8.0	5.7	8.9	6.3	10.3
Flux H_2 mL min^{-1} cm^{-2}	6.3	4.5	5.8	0.7	0.0042	0.09
Flux CO_2 mL min^{-1} cm^{-2}	1.4	0.6	1.0	0.08	0.0007	0.009
Permeance H_2 mol/m^2 s Pa	$4.4 \cdot 10^{-7}$	$3.1 \cdot 10^{-7}$	$4.0 \cdot 10^{-7}$	$5.1 \cdot 10^{-8}$	$2.9 \cdot 10^{-10}$	$6.4 \cdot 10^{-9}$
Permeance CO_2 mol/m^2 s Pa	$9.8 \cdot 10^{-8}$	$3.9 \cdot 10^{-8}$	$7.1 \cdot 10^{-8}$	$5.7 \cdot 10^{-9}$	$4.6 \cdot 10^{-11}$	$6.2 \cdot 10^{-10}$

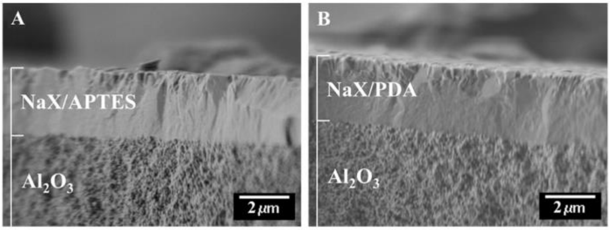

Fig. 1 – SEM cross sections of supported NaX membranes grown on α-alumina supports which have been treated with (A) 3-aminopropyltriethoxysilane (APTES) and (B) with polydopamine (PDA).

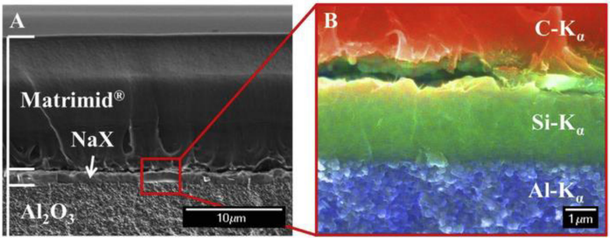

Fig. 2 – SEM images (A) of Matrimid®/FAU multilayer membrane and magnified cameo (EDX) (B) of the border regions.

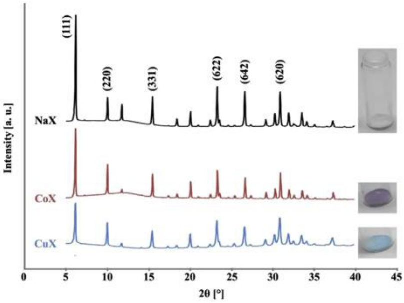

Fig. 3 – XRD patterns and photos of the original NaX as well as ion exchanged FAU powders (obtained by liquid state ion exchange). The hump at low 2θ angles is due to the amorphous plastic XRD sample holder.

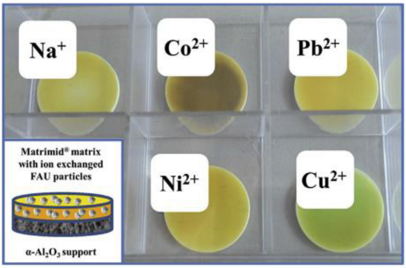

Fig. 4 – Photo of the Matrimid®-based MMMs prepared with ion exchanged FAU particles (10 wt%).

stability) Matrimid®-based MMMs. The results of the MMM preparations (casting and drying), thin glassy looking polymer layers with distinct discolorations (compared to the pure yellow of neat Matrimid®) due to the differently colored embedded FAU particles on top of the white corundum supports, are shown in Fig. 4. At first glance, the particles appear to be evenly distributed over the entire area, with exception of the fringe.

The average thickness of these casted MMM layers on top of the alumina support, as estimated respectively from several SEM cross section images, is around 100 μm. Fig. 5 exemplarily shows the transitional area between loaded polymer layer and support for a CoX/Matrimid® MMM. The majority of the embedded FAU particles seem to be located at exactly that border (see Fig. 5A). This is probably due to the sedimentation by gravity forces during the long drying time (2 h).

The corresponding element map (Fig. 5B) is further proof that the performed ion exchange was successful. By utilizing the element distribution obtained via EDX measurements, we were additionally able to determine that, in the special case of

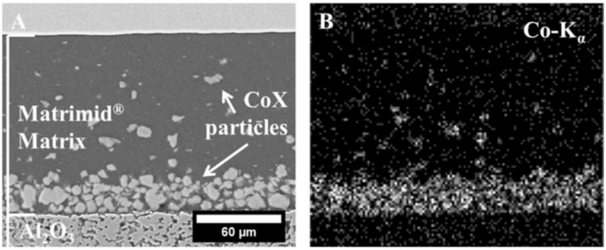

Fig. 5 – SEM image (A) of CoX/Matrimid® MMM and the corresponding Co element map (EDX) (B).

CoX as an example, around 75% of the initial Na^+ ions were exchanged with Co^{2+} ion during the fluid state ion exchange (atomic % of $Na^+ \approx 0.28$ and $Co^{2+} \approx 0.41$ after ion exchange). This value is in good agreement with literature data [29,30].

Permeation measurements on supported NaX and multilayer membranes

An examination of the results summarized in Table 1, regarding the mixed gas permeation studies done with supported NaX membranes, clearly reflects the known trend that APTES and PDA treatments of the support can not only decisively improve the quality of the resulting NaX membranes but also subsequently ensure a distinct improvement in the H_2/CO_2 separation capability compared to the NaX membranes grown on non-treated supports (e.g. Ref. [10]) (fine-pored α-Al_2O_3 ceramic discs exhibit their own basic gas separation capability (Knudsen, see Table 1)). All membranes under study are hydrogen-selective, i.e. they more or less hold back the CO_2, what is in accordance with the well-known rule of thumb: Permeation Selectivity $\approx$ Adsorption Selectivity $\times$ Diffusion Selectivity [1,31–34]. This behavior is basically due to the strong electrostatic potential of the FAU structure as well as the easily accessible site II (SII) sodium ions located near the six-membered oxygen rings, which are able to interact with various polar molecules [1,33]. In the special case of CO_2, these adsorption complexes are due to quadrupole–monopole interactions between it and single unsaturated Na^+ ions within the super-cages of the activated FAU structure. A strong adsorption like this inevitably entails

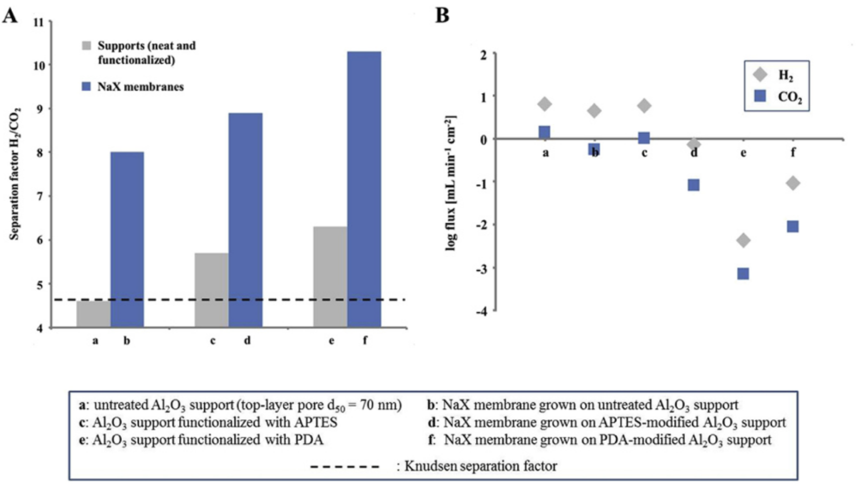

Fig. 6 – Neat supported NaX layer membranes prepared on the untreated as well as PDA and APTES functionalized supports in comparison with the untreated and modified supports without NaX layer: (A) H_2/CO_2 mixed gas (50:50) separation factors (derived from Table 1), and (B) their H_2 and CO_2 mixed gas fluxes (derived from Table 1) in logarithmic representation.

Table 2 – Mixed gas permeation data of supported (rough α-Al_2O_3, pore d_{50} = 2.5 μm in top layer) Matrimid®-based MMMs (thickness ≈ 100 μm) containing ion exchanged MeX crystals for an equimolar H_2/CO_2 mixture at 1 bar (Wicke Kallenbach technique), room temperature and 1 ml/min N_2 sweep.

Support	Al_2O_3	Al_2O_3	Al_2O_3	Al_2O_3	Al_2O_3	Al_2O_3	Al_2O_3
Matrix	–	Matrimid®	Matrimid®	Matrimid®	Matrimid®	Matrimid®	Matrimid®
Filler	–	–	NaX	PbX	CuX	NiX	CoX
Mixed gas α (H_2/CO_2)	1.0	3.0	4.0	4.8	5.2	5.6	5.6
Permeance H_2 mol/m² s Pa	$4.8 \cdot 10^{-08}$	$5.7 \cdot 10^{-11}$	$1.7 \cdot 10^{-10}$	$7.1 \cdot 10^{-11}$	$9.8 \cdot 10^{-11}$	$8.7 \cdot 10^{-11}$	$7.7 \cdot 10^{-11}$
Permeance CO_2 mol/m² s Pa	$4.7 \cdot 10^{-08}$	$1.9 \cdot 10^{-11}$	$4.3 \cdot 10^{-11}$	$1.5 \cdot 10^{-11}$	$1.9 \cdot 10^{-11}$	$1.6 \cdot 10^{-11}$	$1.4 \cdot 10^{-11}$
Ionic radius[a]	–	–	Na^+	Pb^{2+}	Cu^{2+}	Ni^{2+}	Co^{2+}
pm			102	119	73	69	75
Ionic potential e/pm	–	–	0.0098	0.0168	0.0274	0.0290	0.0267

[a] Empirical ionic radii of the exchanged two-valent metal ions (coordination number 6, derived by the comparison of bond length in ionic, metallic and covalent crystals and molecules) [39].

a decreased diffusion, causing lower CO_2 permeation than found for other small molecules like H_2, N_2 or CH_4 [1,35]. Besides these well-known one-on-one interactions (cation-CO_2), CO_2 additionally seems to be able to simultaneously adsorb on two neighboring cations at once (cation–CO_2–cation) [36,37], creating an even stronger adsorption.

All in all, NaX/PDA turned out to be the best supported FAU membrane for separating H_2 from CO_2 from the neat supported NaX membranes under study with a mixed gas separation factor (α H_2/CO_2) of 10.3 (Table 1 and Fig. 6A), which is not only higher than the ones for neat supported NaX (α (H_2/CO_2) = 8.0) and NaX/APTES (α (H_2/CO_2) = 8.9), but also exceeds the known literature values (see Table 3). This superiority of Na-X/PDA is caused, on the one hand, by the improved membrane quality due to the PDA functionalization, as mentioned above. The second reason for the higher separation capabilities of NaX/PDA in comparison with the other membranes under study, is possibly the residual PDA within the support pores itself. As one can see in Table 1, even the PDA-modified support, without a NaX membrane layer grown on top, shows a clearly increased selectivity compared to the Knudsen separation factor of the microporous neat support. This phenomenon is most likely due to strong interactions between CO_2 and PDA (free amine groups [38]) on the one hand and a furthermore reduced CO_2 permeability because of the 1–2 μm thick polymeric top layer (small chaotic pores) and narrowed top layer support pores (due to intruded PDA (d_{50} = 70 nm without)) on the other hand. The latter two aspects are also responsible for the very low (lowest measured) fluxes (Fig. 6B).

While lacking the mentioned PDA top layer, which was dissolved during membrane preparation, NaX/PDA still features the PDA residue within the topmost support pores in addition to the highly selective zeolite membrane. This combination results in the high H_2/CO_2 separation capability with α (H_2/CO_2) = 10.3 and low fluxes.

The slightly improved gas separation capabilities of the APTES-modified support in comparison with the neat support can also be attributed to extra interactions between free amine groups and CO_2. But in contrast to PDA, the APTES monolayer isn't able to seal hermetically the support pores. This is clearly proven by the very similar gas fluxes through both supports (see Table 1 and a/c in Fig. 6B).

As mentioned before, the sole purpose of adding a Matrimid® top layer to the NaX/PDA membranes was to use possible "defect healing" effects like sealed cracks to further enhance their the H_2/CO_2 separation performance. Unfortunately, adding a polymeric top layer nearly halfed the separation factor (multilayer membrane α (H_2/CO_2) = 5.4, see Table 3) compared to the starting membrane (NaX/PDA α (H_2/CO_2) = 10.3) rather than increasing it. Possible explanations for this are the previously mentioned very weak interaction between Matrimid® and NaX as well as further defects in the zeolite membrane caused during the casting and drying/shrinking of the polymeric top layer. The "defect healing" could also have a negative effect in the form of not only sealing existent cracks and pinholes but also widening them in the process. The permeances of the multilayer membranes (H_2 = $1.9 \cdot 10^{-10}$ mol/m² s Pa, see Table 3) are, as expected, lower than the ones of the starting NaX/PDA (H_2 = $6.4 \cdot 10^{-9}$ mol/m² s Pa) membranes due to the additional dense polymeric top layer.

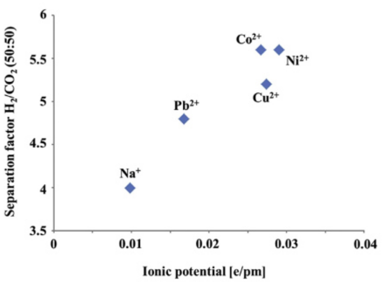

Fig. 7 – Influence of the ionic potential (derived from Table 2) on the H_2/CO_2 separation factor of Matrimid®-based MMMs containing different ion exchanged MeX particles as filler.

Permeation measurements on FAU/Matrimid® mixed matrix membranes

The second series of H_2/CO_2 separation tests, this time performed with supported FAU/Matrimid® MMMs (large-pore α-Al_2O_3 ceramic discs without own gas separation capability (see Table 2)), clearly show, on the one hand, that the separation performance of the neat polymer Matrimid® can easily be enhanced by embedding NaX particles. On the other hand, one can see that using ion exchanged FAU particles (Pb^{2+}, Co^{2+}, Ni^{2+}, Cu^{2+}) instead of the source zeolite (Na^+) to prepare those MMMs always (in all studied cases) resulted in improved separation capabilities (Table 2). These improvements in H_2/CO_2 selectivity are anything but random and follow a clear trend: α (H_2/CO_2): $Na^+ < Pb^{2+} < Cu^{2+} < Ni^{2+} \approx Co^{2+}$.

The decisive factor, which determines whether one ion exchanged FAU crystal is better suited for H_2/CO_2 separation than another, seems to be the so called "ionic potential". This indicator for the charge density at the surface of an ion (ionic charge/ionic radius see Table 2 and Fig. 7) provides evidence for how strong the interaction between the ion in question and gases like CO_2 may be. In the special case of H_2/CO_2 separation, this stronger interaction between carbon dioxide and the zeolite within the matrix in turn should induce a higher H_2 selectivity.

The veracity of this assumption is shown in Fig. 7. As one can see, the H_2/CO_2 separation factor of the FAU/Matrimid® MMMs rises, as expected, with increasing ionic potential of the exchanged bivalent metal ions in the FAU filler, and ions with similar ionic potentials show comparable influences. Similar observations, but with other ions, have already been reported in the literature [37,40]. Due to the dense glassy Matrimid® matrix, all MMMs displayed very similar, regardless of the used ions within the inorganic phase, very low fluxes/permeances and comparable only with the PDA layer mentioned earlier (Table 2).

A comparison between the H_2/CO_2 separation performances of our Matrimid®-based MMM and literature data shows that our approach is quite promising. Although our FAU/Matrimid MMM system is not quite the best yet in terms

Table 3 – Comparison of H_2/CO_2 separation performances of different supported membrane types.

Membrane	Temperature °C	Feed pressure bar	Permeance H_2 mol/m^2 s Pa	Separation factor H_2/CO_2	Reference
Supported NaX[a]	20	1.0	$6.4 \cdot 10^{-9}$	10.3	This study
Supported FAU[b]	100	1.0	$5.0 \cdot 10^{-7}$	8.0[c]	[1]
Supported LTA	20	1.0	$2.3 \cdot 10^{-7}$	6.7	[41]
Supported MFI	25	3.0	$7.9 \cdot 10^{-6}$	1.7	[42]
CoX/Matrimid® (10 wt% CoX)	20	1.0	$7.7 \cdot 10^{-11}$	5.6	This study
MOF-5/Matrimid® (5 wt% MIL-53)	25	6.0	$7.9 \cdot 10^{-11}$	0.9[b]	[6]
MIL-53/Matrimid® (37.5 wt% MIL-53)	35	2.0	$3.3 \cdot 10^{-10}$	2.0[b]	[7]
ZIF-8/Matrimid® (60 wt% ZIF-8)	35	2.7	$1.1 \cdot 10^{-10}$	7.0	[2]
Zeolite 4A/PDMS (40 wt% Zeolite 4A)	35	7.0	[d]	3.5[c]	[43]
NaX/PDA with Matrimid® cover	20	1.0	$1.9 \cdot 10^{-10}$	5.4	This study

[a] Prepared on PDA-modified supports.
[b] Prepared on APTES-modified supports.
[c] Ideal separation factor.
[d] 10,000 Barrer.

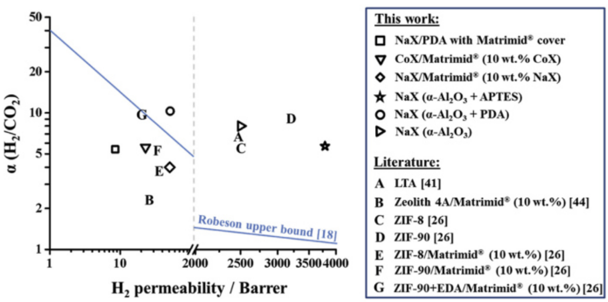

Fig. 8 – Hydrogen permeabilities and separation factors α (H_2/CO_2) for all membranes under study relative to an assortment of comparative membranes and the Robeson upper bound [18,44].

of separation factor and permeance (see e.g. ZIF-8/Matrimid® in Table 3) it offers a lot of potential and room for improvement. Some possible ways to enhance the current separation performances are e.g. smaller FAU particles for a better distribution within the matrix, a higher ion exchange rate, higher particle crystallinity after ion exchange as well as an increased volume fraction of the inorganic phase within the matrix to maximize the occurring effects.

For an even better comparison and benchmarking of our membranes, we use the established Robeson plot [18]. It follows from Fig. 8 that some of our preparations are above the upper bond. In the field of high-permeability membranes, the NaX layer grown on APTES-modified alumina supports, as well as the NaX layer grown on the non-modified alumina supports show a much better performance than the existing polymers. The MMMs show medium permeability and medium H_2/CO_2 selectivity, but their advantage is a cheap preparation and easy scale up.

Conclusions

Different types of supported FAU membranes have been prepared: (i) neat NaX membrane layers on chemically supported Al_2O_3 carriers, (ii) multilayer NaX/Matrimid® sandwich membranes, and (iii) FAU/Matrimid® Mixed Matrix Membranes (MMM). Said membranes have been evaluated in the H_2/CO_2 separation. They all showed a certain H_2 selectivity, that is to say they hold back CO_2 because of differently pronounced internal interactions. We found that the NaX membrane quality highly depends on the kind of pre-synthetic alumina support functionalization (no treatment, APTES or PDA functionalization). Both PDA and APTES coating of the alumina supports result in higher selectivity of the FAU membrane and a better reproducibility of FAU membrane formation. Compared with the pure Matrimid®, the Matrimid®-based MMM containing 10 wt% cation exchanged FAU powder as filler showed an almost doubled mixed gas separation factor α (H_2/CO_2), which seems to be proportional to the ionic potential of the ions in the FAU filler.

Acknowledgements

Financial support by DFG priority program 1570 "Porous media with defined pore structure in chemical engineering – modeling, application, synthesis" (CA 147/17-1 and 2) (organized by F. Keil, TU Hamburg-Harburg) and by the EU for financing the project M^4CO_2 (Energy efficient MOF-based mix matrix membranes for CO_2 capture, organized by F. Kapteijn and J. Gascon, Delft) under the 7th Framework Program, Grant agreement No. 608490 is acknowledged.

REFERENCES

[1] Huang A, Wang N, Caro J. Seeding-free synthesis of dense zeolite FAU membranes on 3-aminopropyltriethoxysilane-functionalized alumina supports. J Membr Sci 2012;389:272–9.

[2] Ordonez JC, Balkus KJ, Ferraris JP, Musselman IH. Molecular sieving realized with ZIF-8/Matrimid® mixed-matrix membranes. J Membr Sci 2010;361:28–37.

[3] Xin R, Ho WSW. Crosslinked polyvinylalcohol–polysiloxane/fumed silica mixed matrix membranes containing amines for CO_2/H_2 separation. J Membr Sci 2011;367:91–102.

[4] Ramasubramanian K, Zhao Y, Ho WSW. CO_2 capture and H_2 purification: prospects for CO_2-selective membrane processes. AlChE J 2013;59:1033–45.

[5] Gabitto J, Tsouris C. Sulfur poisoning of metal membranes for hydrogen separation. Int Rev Chem Eng 2009;1:394–411.

[6] Ren H, Jin J, Hu J, Liu H. Affinity between metal–organic frameworks and polyimides in asymmetric mixed matrix membranes for gas separations. Ind Eng Chem Res 2012;51:10156–64.

[7] Hsieh JO, Balkus KJ, Ferraris JP, Musselman IH. MIL-53 frameworks in mixed-matrix membranes. Micropor Mesopor Mater 2014;196:165–74.

[8] Mundstock A, Wang N, Friebe S, Caro J. Propane/propene permeation through Na-X membranes: the interplay of separation performance and pre-synthetic support functionalization. Micropor Mesopor Mater 2015;215:20–8.

[9] Zhu G, Li Y, Zhou H, Liu J, Yang W. Microwave synthesis of high performance FAU-type zeolite membranes: optimization, characterization and pervaporation dehydration of alcohols. J Membr Sci 2009;337:47–54.

[10] Nikolakis V, Xomeritakis G, Abibi A, Dickerson M, Tsapatsis M, Vlachos DG. Growth of a faujasite-type zeolite membrane and its application in the separation of saturated/unsaturated hydrocarbon mixtures. J Membr Sci 2001;184:209–19.

[11] Jeong BH, Hasegawa Y, Sotowa KI, Kuskabe K, Morooka S. Separation of mixtures of benzene and *n*-alkanes using an FAU-type zeolite membrane. J Chem Eng Jpn 2002;35:167–72.

[12] Lee H, Dellatore SM, Miller WM, Messerschmith PB. Mussel-inspired surface chemistry for multifunctional coatings. Science 2007;318:426–30.

[13] Robeson LM. Polymer membranes for gas separation. Curr Opin Solid State Mater Sci 1999;4:549–52.

[14] Mohamad IN, Rohani R, Mastar@Mastar MS, Nor MTM, Jahim J Md. Permeation properties of polymeric membranes for biohydrogen purification. Int J Hydrogen Energy 2016;41:4474–88.

[15] Ceceopieri-Gomez ML, Palacios-Alquisira J, Domingues JM. On the limits of gas separation in CO_2/CH_4, N_2/CH_4 and CO_2/N_2 binary mixtures using polyimide membranes. J Membr Sci 2007;293:53–65.

[16] Powell CE, Qiao GG. Polymeric CO_2/N_2 gas separation membranes for the capture of carbon dioxide from power plant flue gases. J Membr Sci 2006;211:1–49.

[17] Lang LY, Chung T-S, Li DF, Cao C, Kulprathipanja S. Fabrication of Matrimid/polyethersulfone dual-layer hollow fiber membranes for gas separation. J Membr Sci 2004;240:91–103.

[18] Robeson LM. The upper bound revisited. J Membr Sci 2008;320:390–400.

[19] Vu DQ, Koros WJ, Miller SJ. Mixed matrix membranes using carbon molecular sieves: I. Preparation and experimental results. J Membr Sci 2003;211:311–34.

[20] Kim S, Chen L, Johnson JK, Marand E. Polysulfone and functionalized carbon nanotube mixed matrix membranes for gas separation: theory and experiment. J Membr Sci 2007;284:147–58.

[21] Zhang Y, Musselman IH, Ferraris JP, Balkus Jr KJ. Gas permeability properties of Matrimid® membranes containing

the metal-organic framework Cu–BPY–HFS. J Membr Sci 2008:170–81.
[22] Fan H, Xia H, Kong C, Chen L. Synthesis of thin amine-functionalized MIL-53 membrane with high hydrogen permeability. Int J Hydrogen Energy 2013;38:10795–801.
[23] Abedini R, Omidkhah M, Dorosti F. Hydrogen separation and purification with poly (4-methyl-1-pentyne)/MIL 53 mixed matrix membrane based on reverse selectivity. Int J Hydrogen Energy 2014;39:7897–909.
[24] Seoane B, Coronas J, Gascon I, Benavides ME, Karvan O, Caro J, et al. Metal–organic framework based mixed matrix membranes: a solution for highly efficient CO_2 capture? Chem Soc Rev 2015;44:2421–54.
[25] Zhang C, Koros WJ. Zeolitic imidazolate framework-enabled membranes: challenges and opportunities. J Phys Chem Lett 2015;6:3841–9.
[26] Diestel L, Wang N, Schwiedland B, Steinbach F, Giese U, Caro J. MOF based MMMs with enhanced selectivity due to hindered linker distortion. J Membr Sci 2015;492:181–6.
[27] Huang A, Liang F, Steinbach F, Caro J. Preparation and separation properties of LTA membranes by using 3-aminopropyltriethoxysilane as covalent linker. J Membr Sci 2010;350:5–9.
[28] Lui R, Mahurin M, Li C, Unocic RR, Gao HJ, Pennycook SJ, et al. Dopamine as a carbon source: the controlled synthesis of hollow carbon spheres and yolk-structured carbon nanocomposites. Angew Chem Int Ed 2011;50:6799–802.
[29] Nibou D, Amokrane S, Lebaili N. Use of NaX porous materials in the recovery of iron ions. Desalination 2010;250:459–62.
[30] Maes A, Cremers A. Ion exchange of synthetic zeolite X and Y with Co^{2+}, Ni^{2+}, Cu^{2+} and Zn^{2+} ions. J Chem Soc Faraday Trans 1975;71:265–77.
[31] Chmelik C, Bux H, Voß H, Caro J. Adsorption and diffusion–basis for molecular understanding of permeation through molecular sieve membranes. Chem Ing Tech 2011;83:104–12.
[32] Bux H, Chmelik C, Krishna R, Caro J. Ethene/ethane separation by the MOF membrane ZIF-8: molecular correlation of permeation, adsorption, diffusion. J Membr Sci 2011;369:284–9.
[33] Krishna R. Describing the diffusion of guest molecules inside porous structures. J Phys Chem C 2009;113:19756–81.
[34] Go Y, Lee JH, Shamsudin IK, Kim J, Othman MR. Microporous ZIF-7 membranes prepared by *in-situ* growth method for hydrogen separation. Int J Hydrogen Energy 2016;41:10366–73.
[35] Weh K, Noack M, Sieber I, Caro J. Permeation of single gases and gas mixtures through faujasite-type molecular sieve membranes. Micropor Mesopor Mater 2002;54:27–36.
[36] Pulido A, Nachtigall P, Zukal A, Domimguez I, Cejka J. Adsorption of CO_2 on sodium-exchanged ferrierites: the bridged CO_2 complexes formed between two extraframework cations. J Phys Chem C 2009;112:2928–35.
[37] Pirngruber GD, Raybaud P, Cejka J, Zukal A. The role of the extra-framework cations in the adsorption of CO_2 on faujasite Y. Phys Chem Chem Phys 2010;12:13534–46.
[38] Pan F, Jia H, Qiao S, Jiang Z, Wang J, Wang B, et al. Bioinspired fabrication of high performance composite membranes with ultrathin defect-free skin layer. J Membr Sci 2009;341:279–85.
[39] Huheey JE, Keiter EA, Keiter RL. Anorganische Chemie: Prinzipien von Struktur und Reaktivität. 5th ed. De Gruyter; 2014.
[40] Yu L, Gong J, Zeng C, Zhang L. Synthesis of binderless zeolite X microspheres and their CO_2 adsorption properties. Sep Purif Technol 2013;118:188–95.
[41] Huang A, Caro J. Facile synthesis of LTA molecular sieve membranes on covalently functionalized supports by using diisocyanates as molecular linkers. J Mater Chem 2011;21:11424–9.
[42] Algieri C, Bernado P, Golemme G, Barbieri G, Drioli E. Permeation properties of a thin silicalite-1 (MFI) membrane. J Membr Sci 2003;222:181–90.
[43] Rezakamezi M, Shahidi K, Mohammadi T. Hydrogen separation and purification using crosslinkable PDMS/zeolite A nanoparticles mixed matrix membranes. Int J Hydrogen Energy 2012;37:14576–89.
[44] Ahmad J, Hägg A-B. Development of matrimid/zeolite 4A mixed matrix membranes using low boiling point solvent. Sep Purif Technol 2013;115:190–7.

3. New Membrane Concepts for Hydrogen Purification

3.1 Summary

As mentioned in chapter 1.3.5, MOF or zeolite membranes are quite difficult to prepare and the up-scale is still the bottleneck in terms of their usage in practice-relevant separation processes. Furthermore, among the diversity of available materials, the search for membranes or their corresponding composites - such as MMMs as mentioned in chapter 1.4 - with great selectivities and high fluxes is still a challenging task. Therefore, the development of new membrane concepts is an inevitable task for modern membrane science. The publication in this chapter reports a new revolutionary membrane concept for hydrogen purification from different simulated waste gases with 100 % selectivity.

A commercial short-circuited Nafion based PEM fuel cell is introduced as membrane in chapter 3.2. Since Nafion works like a doorkeeper for anything but hydrogen, the purification of the latter from different simulated waste gases is demonstrated. Furthermore, by applying a resistive cascade, the hydrogen flux can be switched in dependence of the used resistor. Lastly, the fuel cell is reported as catalytic membrane reactor for olefin hydration.

3.2 Inverted Fuel Cell: Room Temperature Hydrogen Separation from an Exhaust Gas by Using a Commercial Short-Circuited PEM Fuel Cell without Applying any Electrical Voltage

S. Friebe, B. Geppert, J. Caro

Angewandte Chemie International Edition **2015**, 54, 7790-7794.

Angewandte Communications

Hydrogen Separation | Hot Paper

International Edition: DOI: 10.1002/anie.201500751
German Edition: DOI: 10.1002/ange.201500751

Inverted Fuel Cell: Room-Temperature Hydrogen Separation from an Exhaust Gas by Using a Commercial Short-Circuited PEM Fuel Cell without Applying any Electrical Voltage**

*Sebastian Friebe, Benjamin Geppert, and Jürgen Caro**

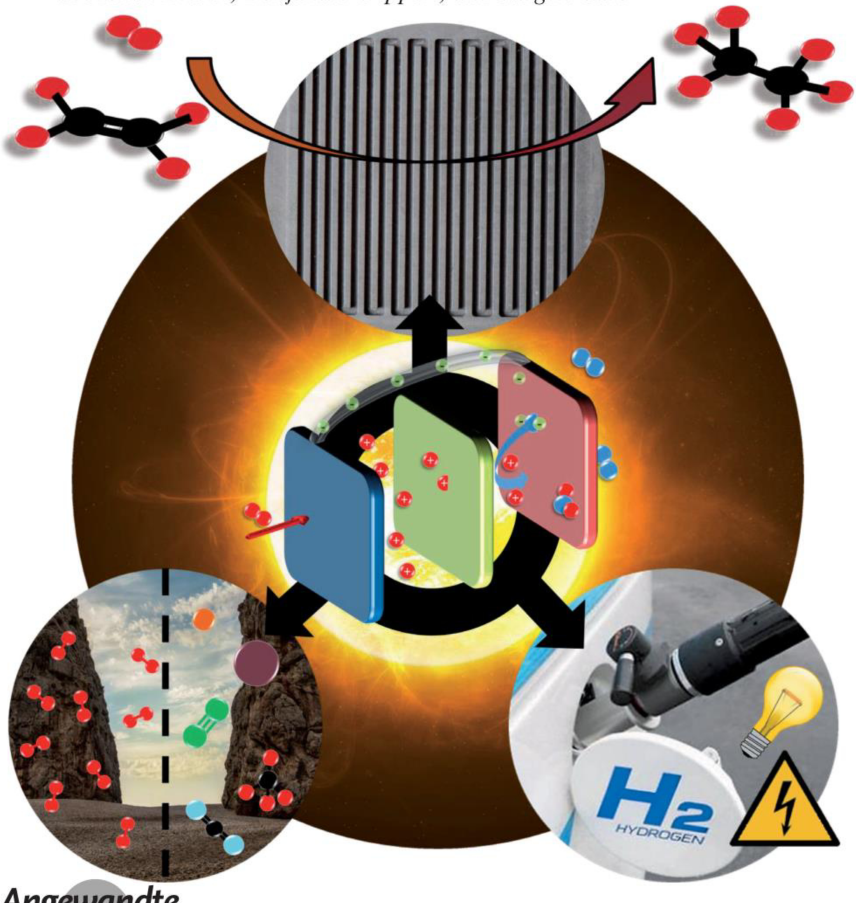

Angewandte International Edition Chemie

Angewandte International Edition Chemie

Abstract: *A short-circuited PEM fuel cell with a Nafion membrane has been evaluated in the room-temperature separation of hydrogen from exhaust gas streams. The separated hydrogen can be recovered or consumed in an in situ olefin hydrogenation when the fuel cell is operated as catalytic membrane reactor. Without applying an outer electrical voltage, there is a continuous hydrogen flux from the higher to the lower hydrogen partial pressure side through the Nafion membrane. On the feed side of the Nafion membrane, hydrogen is catalytically split into protons and electrons by the Pt/C electrocatalyst. The protons diffuse through the Nafion membrane, the electrons follow the short-circuit between the two brass current collectors. On the cathode side, protons and electrons recombine, and hydrogen is released.*

Hydrogen is a high-demand product that is mainly produced by steam reforming and used for ammonia and methanol synthesis. Hydrogen is also used in oil reforming for the production of high-grade petrol and to remove sulfur compounds. Hydrogen is becoming increasingly attractive as an energy carrier because it can be combusted with oxygen (from air) to water. A proton-exchange membrane fuel cell (PEM FC) with a Nafion proton-exchange membrane (PEM) is usually applied to transform the chemical energy liberated during the electrochemical hydrogen combustion into electrical energy. The heart of the PEM FC is the proton-conducting Nafion membrane. Hydrogen is split on the anode side at the Pt/C electrocatalyst of the PEM FC into protons and electrons. The protons diffuse through the Nafion membrane, and the electrons follow the outer circuit and perform "work". On the cathode side of the PEM FC, water is formed from the protons, electrons, and oxygen from the air (Supporting Information, Figure S1). For the function of the PEM FC it is crucial that the Nafion membrane conducts only protons and no electrons because this would result in an "inner short-circuit". In our concept of a reverse PEM FC for hydrogen separation, we have deliberately caused this short-circuit by connecting the two brass current collectors which are attached to the Pt/C electrocatalyst layers on both sides of the Nafion membrane by a cable (Figure 1 a).

Herein we study a new principle to separate hydrogen from an exhaust gas that contains a few vol% hydrogen through a Nafion membrane using a commercial PEM FC with an external short-circuit. Our concept is similar in a way to oxygen or hydrogen high-temperature permeation through mixed conducting ceramics. Mixed conductivity means that these ceramic membranes show at their working temperature of about 800 °C sufficient oxygen-ion/electron[1–3] or proton/electron[4–6] conductivity in the case of oxygen and hydrogen transport, respectively. There are some attempts to increase the oxygen or hydrogen transport by an external short-circuit between the feed and the sweep side. For instance, Zhang et al. investigated the permeation of the above mentioned gases through short-circuited ceramics at high temperatures. However, the short-circuit was realized with silver paste and the fluxes of oxygen and hydrogen could be slightly improved at temperatures between 800 and 900 °C.[7–11]

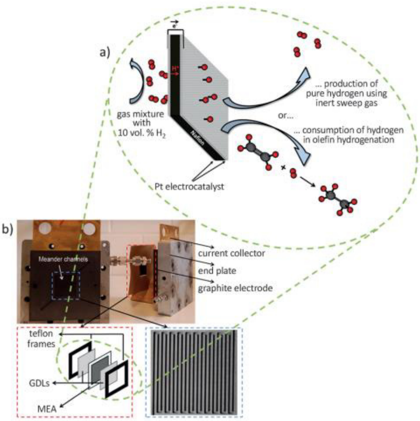

Figure 1. Principle of a reverse fuel cell for hydrogen recovery and olefin hydrogenation. a) Voltage-free hydrogen production and olefin hydrogenation in a fuel cell with an external short-cut. b) Setup of the fuel cell.

Our concept for the hydrogen separation from exhaust gases works with a Nafion membrane in a commercial PEM FC at room temperature. As Nafion only conducts protons, the nascent electrons are conducted to the other side of the Nafion membrane via a cable between the two brass current collectors. The driving force for hydrogen transport is the concentration gradient of hydrogen between the two sides of the Nafion membrane. The steady-state concentration gradient is formed by supplying new hydrogen-containing gas to the feed side and using a sweep gas such as nitrogen to remove the permeated hydrogen from the cathode side. We could also reduce the hydrogen partial pressure on the anode side by consuming the hydrogen in a chemical reaction such as the ethylene hydrogenation to ethane. Additionally we analyzed the hydrogen permeance as a function of an adjustable resistor between the two brass current collectors, thus controlling the hydrogen flux by the electron flow as limiting parameter. Furthermore we calculated the proton conductivity across the membrane with the help of the Nernst–Einstein equation.

First of all we investigated the hydrogen separation from binary gas mixtures hydrogen/methane with different hydro-

[*] S. Friebe, B. Geppert, Prof. Dr. J. Caro
Institute of Physical Chemistry and Electrochemistry
Leibniz University Hannover
Callinstrasse 22, 30167 Hannover (Germany)
E-mail: caro@pci.uni-hannover.de

[**] We thank A. Bayer and E. Lerbs from SolviCore GmbH & Co. KG in Hanau for supplying the Nafion membranes and Dr. G. Hübner from Volkswagen Technologiezentrum Isenbüttel for supplying the fuel cell. PEM = proton exchange membrane.

Supporting information for this article is available on the WWW under http://dx.doi.org/10.1002/anie.201500751.

gen concentrations between 0 and 100 vol% (Figure 2). Figure 2a shows the hydrogen permeance for two operation modes: When nitrogen is used as a sweep gas to reduce the hydrogen partial pressure on the permeate side of the membrane, a remarkable hydrogen flux can be observed even for a gas mixture containing 5 vol%. This hydrogen flux comes to saturation with increasing hydrogen concentration in the feed. In a second experiment, air has been used as reactive sweep gas. In this experiment, the permeated hydrogen is burnt at the Pt/C electrocatalyst with the oxygen from air. Since in this operation mode the hydrogen partial pressure is reduced drastically on the permeate side by hydrogen combustion, the concentration gradient as driving force for hydrogen transport increases, and correspondingly the hydrogen permeance is doubled in comparison with the inert sweep gas nitrogen. We also studied the separability of hydrogen from other gases, namely N_2, CO_2, helium, and argon. For this we analyzed the permeances of the hydrogen in equimolar gas mixtures with the above-mentioned gases and checked if hydrogen is the only signal in the gas chromatograph. Figure 2b shows the results for the different gas mixtures.

Since the proton conductivity depends strongly on the moisture of the Nafion, small variations of the moisture can lead to even larger variations in the proton conductivity. Additionally, varying compression of the Nafion membrane can lead to changes in performance.[12] Nevertheless there were no other signals except the hydrogen signal in the gas chromatograph, meaning that the separation of hydrogen from other gases is also possible with a short-circuited fuel cell.

The idea behind these experiments was to identify the rate-limiting step of our hydrogen separation. Along with the measurements above, we analyzed the hydrogen permeance as a function of an adjustable resistor. Therefore, we placed a resistor in the "short-circuit way" and changed its resistance between 0 and 100 kΩ. Figure 3a indicates that the proton conductivity is rate limiting for the hydrogen permeance. If the resistance of the adjustable resistor is zero, the hydrogen permeance is identical to the measurements without resistor. With increasing resistance, the hydrogen permeance decreases. Already a resistance of 100 Ω decreases the permeance to 10% of its starting value, meaning that the electron transport becomes more and more the limiting parameter. With even higher resistances than 1 kΩ the permeance is approximately zero. This measurement clarifies that not only the proton conductivity through the Nafion is important to understand the mechanism of this process but also the flow of electrons.

Figure 3b shows the proton conductivity of the Nafion membrane as a function of the hydrogen concentration in the binary mixture hydrogen/methane. Therefore, we used different ratios between hydrogen and methane and calculated the proton conductivity by using the Nernst–Einstein Equation (1).

The PEM FCs work with Nafion membranes.[13] Nafion as a sulfonated tetrafluoroethylene polymer (Supporting Information, Figure S3) is known as a cation conductor and as an anion barrier. The highly selective proton exchange across the membrane proceeds over the sulfonic acid groups. The proton conductivity σ_{H^+} depends strongly on the moisture of the polymer membrane. Investigations on the influence of the moisture showed that more wet membranes lead to higher proton conductivity, but it should be annotated that an excessive moisture can also inhibit the protons to cross the membrane.[14–16] The conductivity of the dense polymer can be concluded with the help of the Nernst–Einstein equation (1):

$$\sigma_{H^+} = \frac{J_{H_2}\, z_{H^+}\, e\, L}{\Delta\phi} \quad (1)$$

where J_{H_2} is the hydrogen flux, z_{H^+} the proton charge, e the elementary charge, L the membrane thickness, and $\Delta\phi$ the potential gradient.

Figure 3b clarifies that the proton conductivity is nearly constant over the whole range of hydrogen concentration in the mixed gas which recommends Nafion as a separating membrane also for low hydrogen concentrations. This means that if hydrogen is available in the gas mixture, the proton transport through the Nafion membrane is almost the same for any hydrogen concentration. This result is in good agreement with Figure 2a, which shows the fast saturation

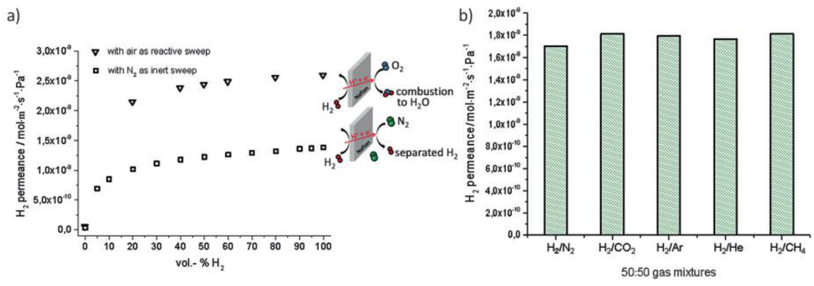

Figure 2. Hydrogen purification from a simulated waste gas. a) Hydrogen permeance as a function of the hydrogen concentration in a binary gas mixture with methane at room temperature. b) Hydrogen separation from different simulated waste gases at room temperature. Nitrogen was used as sweep gas except for the binary mixture of H_2/N_2, where argon was the sweep gas.

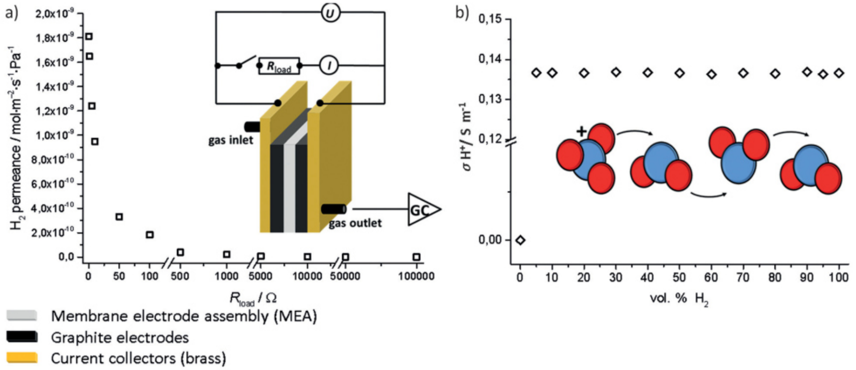

Figure 3. Influence of electron transport and hydrogen concentration in the feed. a) Influence of a limiting electron flux caused about by an adjustable resistor on the hydrogen permeance in a binary, equimolar mixture with methane (N_2 as inert sweep). Inset: the setup for the limiting electron flux. b) Proton conductivity as a function of the hydrogen concentration in a binary mixture with methane (N_2 as inert sweep). Inset: the common Grotthus proton-transport mechanism through the Nafion membrane.[17,18]

of the hydrogen permeance with increasing hydrogen concentration in the gas mixture.

Along with the hydrogen separation and purification processes, we tested our short-circuited PEM FC as catalytic membrane reactor for in situ ethylene hydrogenation at room temperature. In this case, ethylene on permeate side of the Nafion membrane (Figure 1 a) can be considered as a reactive sweep gas that consumes the permeated hydrogen, thus reducing its partial pressure. Fortunately, we can use for this hydrogenation the same Pt/C electrocatalyst as for the hydrogen liberation on the permeate side of the Nafion membrane by recombining the protons and electrons to atomic and molecular hydrogen. From the gas chromatogram in Figure 4 it follows that remarkable amounts of ethane have been formed by the in situ hydrogenation of ethylene. Moreover, from the absence of any hydrogen signal it can be concluded that all permeated hydrogen has been consumed in the catalytic ethylene hydrogenation. As expected, only the hydrated short-circuited Nafion membrane transports hydrogen, since only wet Nafion is an excellent proton conductor. These results are in good agreement with the dependence of the proton conductivity on the moisture.[13–15]

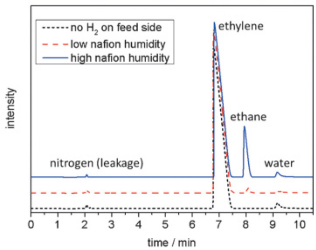

Figure 4. Gas chromatogram of the product gas for the olefin hydrogenation for Nafion membranes of different humidity.

In conclusion, we have shown the room-temperature separation of hydrogen from other gases by means of a short-circuited commercial proton exchange fuel cell with a Nafion membrane without applying an electrical voltage. If there is a gradient in the hydrogen partial pressure over the proton-transporting Nafion membrane, hydrogen can be separated from exhaust gases that contain a few vol% hydrogen. We separated hydrogen from different gases such as methane, carbon dioxide, nitrogen, argon, and helium. By using a vacuum pump or a condensable sweep gas on the permeate side, hydrogen can be recovered. The hydrogen partial pressure on the permeate side of the Nafion membrane can also be reduced by a hydrogen-consuming reaction. As a proof of principle, we showed the in situ hydrogenation of ethylene to ethane at room temperature operating our proton exchange fuel cell as catalytic membrane reactor. The hydrogen flux can be switched by a resistor that controls the electron flux in the short-circuit. The short-circuited fuel cell with proton exchange membrane is a good example of the combination of separation (hydrogen recovery), energy production (electric current), and catalysis (olefin hydrogenation).

Experimental Section

The experimental investigations focused on the hydrogen-separation performance and in situ olefin hydrogenation with the help of a Nafion-based PEM FC with an external short-circuit. We used a commercial Greenerity H600 STD MEA, gas-diffusion layers (GDLs; Supporting Information, Figure S2) and also Teflon frames from the company SolviCore GmbH & Co. KG to evaluate our principle. The active area on the MEA membranes was 10 cm^2 with a platin coating of 0.85 $mg\,cm^{-2}$. The thickness of the platin coating was around 8–15 μm. The fuel cell, the flow field of which consisted of 20 equally spaced meander like channels with a total distance of around 0.6 m between the gas inlet and the exit, was supplied by Volkswagen AG, Technology Center Isenbüttel (Figure 1b).

Before the measurements, the MEA was moistened with distilled water to enhance the proton conductivity, whereas the used gas mixtures were purged through a water reservoir to maintain the moisture. For gas analysis we used a gas chromatograph (Agilent Technologies 7890 B). For controlling the hydrogen flux via the electron flux in the short-circuit, a resistive cascade (CML R1-1000) was used.

Keywords: electrocatalysis · fuel cells · hydrogen · membrane · separation

How to cite: *Angew. Chem. Int. Ed.* **2015**, *54*, 7790–7794
Angew. Chem. **2015**, *127*, 7788–7904

[1] J. M. Serra, V. B. Vert, O. Büchler, W. A. Meulenberg, H. P. Buchkremer, *Chem. Mater.* **2008**, *20*, 3867–3875.
[2] X. Chen, L. Huang, Y. Wei, H. Wang, *J. Membr. Sci.* **2011**, *368*, 159–164.
[3] J. Sunarso, S. Baumann, J. M. Serra, W. A. Meulenberg, S. Liu, Y. S. Lin, J. C. Diniz da Costa, *J. Membr. Sci.* **2008**, *320*, 13–41.
[4] X. Qi, Y. S. Li, *Solid State Ionics* **2000**, *130*, 149–156.
[5] S. Ricote, A. Manerbino, N. P. Sullivan, *J. Mater. Sci.* **2014**, *49*, 4332–4340.
[6] J. W. Phair, S. P. S. Badwal, *Ionics* **2014**, *12*, 103–115.
[7] K. Zhang, J. Sunarso, G. H. Pham, S. Wang, S. Liu, *Ceram. Int.* **2014**, *40*, 791–797.
[8] K. Zhang, B. Meng, X. Tan, L. Liu, S. Wang, S. Liu, *J. Am. Ceram. Soc.* **2014**, *97*, 120–126.
[9] K. Zhang, Y. Zou, C. Su, Z. Shao, L. Liu, S. Wang, S. Liu, *J. Membr. Sci.* **2013**, *427*, 168–175.
[10] K. Zhang, L. Liu, J. Sunarso, H. Yu, V. Pareek, S. Liu, *Energy Fuels* **2014**, *28*, 349–355.
[11] K. Zhang, Z. Shao, C. Li, S. Liu, *Energy Environ. Sci.* **2014**, *5*, 5257–5264.
[12] W.-k. Lee, C.-H. Ho, J. W. Van Zee, M. Murthy, *J. Power Sources* **1999**, *84*, 45–51.
[13] V. Mehta, J. S. Cooper, *J. Power Sources* **2003**, *114*, 32–53.
[14] C. Yang, S. Srinivasan, A. B. Bocarsly, S. Tulyani, J. B. Benziger, *J. Membr. Sci.* **2004**, *237*, 145–161.
[15] Y.-S. Ye, J. Rick, B.-J. Hwang, *Polymers* **2004**, *4*, 913–963.
[16] U. Pasaogullari, C. Y. Wang, *J. Electrochem. Soc.* **2004**, *151*, A399–A406.
[17] N. Miyake, J. S. Wainright, R. F. Savinell, *J. Electrochem. Soc.* **2001**, *148*, A898–A904.
[18] G. A. Ludueña, T. D. Kühne, D. Sebastiani, *Chem. Mater.* **2011**, *23*, 1424–1429.

Received: January 27, 2015
Published online: May 26, 2015

4. Conclusion

4.1 Summary

This thesis gives insight into the comparison between neat MOF and zeolite membranes and their corresponding composite membranes as well as into the development of new membrane concepts for hydrogen purification.

The first part of this thesis was focused on the preparation and evaluation of several supported MOF (NH_2-MIL-125, UiO-66, MIL-96) and zeolite (FAU) membranes as well as some corresponding composite membranes (MMMs, multilayers) for hydrogen purification at praxis relevant conditions.

The synthesis of the supported NH_2-MIL-125 layers was done via a hydrothermal approach, while the corresponding Matrimid based MMMs were prepared via a simple casting procedure of the polymer-particle slurry. The attractive interaction between the amino functions and CO_2 as well as the direct coupling between filler and polymer in the MMM were approved with IR-spectroscopy. The neat MOF layers were evaluated from 25 °C up to 150 °C in single and mixed gas permeation of H_2/CO_2. The mixed gas selectivity showed a declining tendency at higher temperatures, due to the weaker interaction of CO_2 with the amino functions in the MOF framework, thus resulting in suppressed retardation of the latter ($\alpha\ (H_2/CO_2)_{25°C} \approx 8.0$; $\alpha\ (H_2/CO_2)_{150°C} \approx 6.0$). The corresponding MMMs with different weight fractions of the filler NH_2-MIL-125 (10/20 wt.-%) were evaluated in mixed gas permeation at 150 °C and varying feed pressures (0, 3, 4, 5 bar). Said membranes showed improved performance in comparison to the neat Matrimid membranes ($\alpha\ (H_2/CO_2)_{Matrimid} \approx 5.5$; $\alpha\ (H_2/CO_2)_{MMM} \approx 8.0$). Lastly, the performance results of all membranes were evaluated with the Maxwell-model. The deviations between predicted and real MMM performance were attributed to the good embedment, due to the direct coupling of NH_2-MIL-125 with the polymeric matrix via a ring opening polymerization reaction with the filler particles as bridging nodes between neighboring Matrimid polymer chains.

UiO-66 as oriented, dense supported layer was prepared via a benzoic acid modulated hydrothermal synthesis. The orientation of the layer was verified by comparing the CPOs of the statistic oriented powder with the crystallized layer. Furthermore, said layers showed great stability as well as sufficient adherence to the ceramic support in three different taxing conditions (e.g. sonication in water). This oriented membrane was then investigated in terms of its sieving properties for different binary gas mixtures (H_2/CO_2, H_2/N_2, H_2/CH_4, H_2/C_2H_6, H_2/C_3H_8) at room temperature. The mixture separation factors α for these gas pairs were determined as 5.1, 4.7, 12.9, 22.4 and 28.5, which displays the "soft" molecular sieve character without a sharp cut-off, due to the linker flexibility inside the framework. The "soft" molecular sieve membrane was then transferred into a membrane with a sharp cut-off at around 3.7 Å by a thin polymer top layer, which most likely suppressed the linker mobility, thus giving modified separation factors (5.0, 4.7, 80.0, 130.0, 500.0).

The third supported MOF layer - MIL-96 - was prepared via a reactive seeding approach with two different synthesis routes. Depending on the used solvent for the reactive seeding step, we were able to steer the orientation and the crystal morphology in the membrane layer. The crystal orientation and morphology was predefined through the different seed crystals and was kept during the growth process of the membrane. These two different membranes were then evaluated in terms of their separation performance for H_2/CO_2 separation in pristine and activated state. Said membranes showed a crystal facet depending gas transport behavior with constant selectivity of α (H_2/CO_2) ≈ 9.0 but different fluxes, which is a result of the virtual two-dimensional pore system with transport in-/active channels in the framework. As a result of this idiosyncracy, the four times thicker membrane showed, in contrary to popular belief, the greater permeation fluxes. In addition, MIL-96 was prepared in five different particle sizes for the fabrication of MMMs. We were able to identify several preparation problems, namely sedimentation, aggregation and even recrystallization in dependence of the used filler size. Consequently, the gas separation performance of the MMMs showed only enhanced permeabilities but no increase in selectivity.

As described in chapter 1.3.4, also zeolites can be used as membrane materials for hydrogen purification, due to their uniform pore structure and the possibility for post-synthetic modifications. Therefore, zeolite faujasite (FAU) was prepared as dense membrane layer on different pretreated supports. We were able to increase the membrane performance by using different pre-synthetic support treatments, namely functionalization with 3-APTES or PDA, from α (H_2/CO_2) ≈ 8.0 on the unmodified support to ≈ 9.0 (3-APTES) and ≈ 10.0 (PDA), respectively. This increase was brought into relation with zeta potential measurements, which explain the better interaction of FAU with the modified supports. In addition, Matrimid based MMMs with the pristine FAU powder (Na^+) as well as ion-exchanged (Co^{2+}, Ni^{2+}, Pb^{2+}, Cu^{2+}) counterparts were prepared and evaluated for the same separation process. All MMMs showed at least 25 % increased separation performance in comparison to the neat polymer layer. Furthermore, the separation behavior could be brought into relation with the ionic potential of the used cation for the ion-exchange.

The second part of this thesis was focused on the development of new membrane concepts. Therefore, a commercial Nafion based PEM fuel cell was successfully evaluated for hydrogen purification from different waste gases (He, Ar, CO_2, CH_4, N_2) with 100 % selectivity. The driving force was twice the high by using the reactive sweep gas oxygen instead of the inert gas N_2. The hydrogen flux became adjustable by inserting different resistors into the migration path of the electrons, thus making the electron mobility the rate-determining step instead of the proton conductivity through the Nafion. By using the Nernst-Einstein equation, the proton conductivity was demonstrated to be independent of the hydrogen concentration on the feed side. Lastly, the fuel cell was applied as catalytic membrane reactor for the hydration of ethylene. The whole setup for hydrogen purification as well as the ethylene conversion showed a drastically dependence on the Nafion humidity.

4.2 Outlook

This work presented four different kinds of supported membranes for hydrogen separation. Various Metal-Organic Framework and zeolite types with different pore sizes (3.2 Å, 6.0 Å, 6.0 Å and 7.4 Å) and unique features were prepared by different synthesis routes. Supported means that a zeolite or MOF layer of a few µm thickness is grown directly on a porous alumina support. Pre-synthetic support treatments (secondary growth, reactive seeding, 3-APTES, PDA) resulted in improved membrane layer quality and as a consequence in increased separation performance or in unique transport properties for the crystallized layers. Also post-synthetic modification, such as a polymer cover on top of the crystallized membranes resulted in modified separation performances. However, the reproducible synthesis and the handling of these membranes are still a difficult task. A simple cost evaluation of supported MOF and zeolite membrane shows that 1 m^2 of non-installed membrane area will be > 1000 €. About 60 - 80 % of the costs originate from the support. Since the composition of the latter is crucial for minimizing the flow resistance of the support, their graded fabrication has been developed in different countries. However, the high support costs are due to the fact that each layer of the support is fired before the next layer is added. Usually the supports must be fired at least three times: first the main coarse body (particle size of a few µm), than a microfiltration layer (particle and pore size of the order of 1 - 0.1 µm) and finally an ultrafiltration layer (particle and pore size of the order of 100 - 2 nm) is added and fired. Nevertheless, there are world-wide about 60 plants with hydrophilic LTA and FAU zeolite membranes in multi-channel/tube geometry in operation for the water removal from different solvents like (bio) ethanol, i-propanol, DMF, acetonitrile, ethylene glycol. The driving force for these membrane installations is a saving of the running energy costs of roughly 40 % but only when operating the plant in a combination of distillation (near to the azeotropic point) combined with steam permeation and of the order of minus 30 % for the combination of distillation and pervaporation. On the other hand, the investment costs for the process with membranes implemented is higher in comparison to an azeotrope distillation (25 %) or a pressure swing adsorber (10 %). A big problem with supported zeolite membranes is that in case of defects in the layer - or even worse - when one ceramic tube brakes, the whole module must be replaced. An in situ mending like in case of polymer hollow fibers is so far not possible for supported zeolite layers. Supported MOF membranes are far from an industrial implementation. The main bottleneck is their chemical instability in humid atmospheres. Lastly, a huge variety of promising materials is not even crystallizable as defect-free membrane layer.

Therefore, also Mixed-Matrix-Membranes with different MOF and zeolite filler materials were investigated, in addition. The incorporation of amino functionalized MOFs as well as ion-exchanged zeolite powders, for instance, improved the separation performance of the neat Matrimid polymer membrane in terms of permeability and selectivity. Furthermore, some occurring problems during MMM preparation, their impact on the separation performance and measures to avoid these problems were identified. The big expectation of Mixed-Matrix-Membranes is that established technologies for the preparation of polymer membranes such as hollow fiber spinning or casting for spiral wound module applications can be applied. Further, the polymer matrix can (if it is hydrophobic) stabilize the chemical stability of embedded MOF particles. Therefore, there are huge research activities in this field. We are active in the project M^4CO_2 under the auspices of the 7th Framework Program of the European Commission (cooperation with 7 companies and 8 universities). Furthermore, in 2016 we have started an R&D project with a big German company in gas separation on Mixed-Matrix-Membranes containing MOFs.

Despite all the effort, up to now, those membranes are not competitive enough in comparison to common methods like PSA or cryogenic distillation for gas separation, in general. Moreover, for industrial application the membranes should be manufacturable as hollow fibers or as coiled modules. The latter is easier to achieve by the concept of Mixed-Matrix-Membranes in my opinion. However, membranes should feature utopian selectivities of α (H_2/CO_2) $\geq$ 30 and permeabilities of P (H_2) $\approx$ 500 Barrer in order to replace the abovementioned used methods (PSA & distillation) with comparable or lower costs. Mixed-Matrix-Membranes will not trigger a revolution in gas separation, but evolutionary improvements. This is due to the fact that in general not more than 30 vol.-% of the polymer can be replaced by a filler (because of mechanical properties) and the resulting membrane performance is as a rough estimate a linear combination of polymer (90 to 70 vol.-%) and filler (10 to 30 vol.-%).

In my PhD work I followed indeed two “revolutionary” concepts. The newly developed concept of a Nafion based PEM fuel cell as membrane apparatus is an interesting approach for hydrogen purification, which may become competitive after certain challenges like, up-scale, implementation in existing processes and improvements of the present materials in terms of their conductance and operating temperature, are overcome in the future. Second, scientists should maybe try to think a bit more outside the box in terms of new preparation methods and cost-saving fabrications. I have developed and patented (H2110EP) a quite new and simple preparation for self-supporting molecular sieve membranes to overcome the abovementioned cost issues of common supported MOF and zeolite membranes as well as the non-producibility of promising separation active materials.

These Polymer Stabilized Percolation Membranes (PSPMs) consist of up to 95 % separation active filler, which is first pressed into the desired geometric shape followed by infiltration of a pore filling agent (un-/selective) and cured by temperature treatment. The resulting molded body features a comparable stability to commercial alumina supports and can be post-treated accorded to the desired application without losing the separation capability (e.g. polishing, drilling, cutting). This concept has maybe potential for a broad variety of applications but whether or not it will give a breakthrough to the field of membrane processes is still a long way off.

Appendix

Publications

Publications included in this thesis

1. **S. Friebe**, A. Mundstock, D. Unruh, F. Renz, J. Caro, NH_2-MIL-125 as membrane for carbon dioxide sequestration: Thin supported MOF layers contra Mixed-Matrix-Membranes. *J. Membr. Sci.*, **2016**, 516, 185-193.
2. **S. Friebe**, B. Geppert. F. Steinbach, J. Caro, Metal-Organic Framework UiO-66 Layer: A Highly Oriented Membrane with Good Selectivity and Hydrogen Permeance. *ACS Appl. Mater. Interfaces*, **2017**, 9, 12878-12885.
3. A. Knebel, **S. Friebe**, N. C. Bigall, M. Benzaqui, C. Serre, J. Caro, Comparative Study of MIL-96(Al) as Continuous MOF-Layer and Mixed-Matrix-Membrane. *ACS Appl. Mater. Interfaces,* **2016**, 8, 7536-7544.
4. A. Mundstock, **S. Friebe**, J. Caro, On Comparing Permeation through Matrimid®-based Mixed Matrix and Multilayer Sandwich FAU Membranes: H_2/CO_2 Separation, Support Functionalization and Ion Exchange. *Int. J. Hydrogen Energy*, **2017**, 42, 279-288.
5. **S. Friebe**, B. Geppert, J. Caro, Inverted Fuel Cell: Room Temperature Hydrogen Separation from an Exhaust Gas by Using a Commercial Short-Circuited PEM Fuel Cell without Applying any Electrical Voltage. *Angew. Chem. Int. Ed.*, **2015**, 54, 7790-7794.

Publications not included in this thesis

6. **S. Friebe**, N. Wang, L. Diestel, Y. Liu, A. Schulz, A. Mundstock, J. Caro, Deuterium/hydrogen permeation through different molecular sieve membranes: ZIF, LDH, zeolite. *Micropor. Mesopor. Mater.,* **2015**, 216, 127-132.
7. **S. Friebe**, L. Diestel, A. Knebel, A. Wollbrink, J. Caro, MOF-Based Mixed-Matrix Membranes in Gas Separation – Mystery and Reality. *Chem. Ing. Tech.*, **2016**, 88, 1788-1797.
8. S. Hurrle, **S. Friebe**, J. Wohlgemuth, C. Wöll, J. Caro, L. Heinke, Sprayable, Large-Area Metal-Organic Framework Films and Membranes of Varying Thickness. *Chem. Eur. J.*, **2017**, 23, 1-6.
9. A. Mundstock, N. Wang, **S. Friebe**, J. Caro, Propane/propene permeation through Na-X membranes: The interplay of separation performance and pre-synthetic support functionalization. *Micropor. Mesopor. Mater.,* **2015**, 215, 20-28.

10. J. Sanchez-Lainez, B. Zornoza, **S. Friebe**, J. Caro, S. Cao, A. Sabetghadam, B. Seoane, J. Gascon, F. Kapteijn, C. Le Guillouzer, G. Clet, M. Daturi, C. Tellez, J. Coronas, Influence of ZIF-8 particle size in the performance of polybenzimidazole mixed matrix membranes for pre-combustion CO_2 capture and its validation through interlaboratory test. *J. Membr. Sci.*, **2016**, 515, 54-53.
11. S. Sanchez-Paradinas, D. Dorfs, **S. Friebe**, A. Freytag, A. Wolf, N.C. Bigall, Aerogels from CdSe/CdS Nanorods with Ultra Long Exciton Lifetimes and High Fluorescence Quantum Yields. *Adv. Mater.*, **2015**, 27, 6152-6156.
12. A. Knebel. L. Sundermann, A. Mohmeyer, I. Strauß, **S. Friebe**, P. Behrens, J. Caro, Azobenzene Guest Molecules as Light-Switchable CO_2 Valves in an Ultrathin UiO-67 Membrane, *Chem. Mater.*, in revision.
13. **S. Friebe**, A. Mundstock, J. Caro, Europäische Patentanmeldung: Herstellungsverfahren für mechanisch stabile Perkolationsmembranen - Leibniz Universität Hannover. H1021EP, **2017**.

Contributions to Conferences

Oral Presentations

S. Friebe, J. Caro, Energy efficient MOF-based mixed-matrix membranes for CO_2 capture, M^4CO_2, 2nd status report, July 2014, Frankfurt.

S. Friebe, J. Caro, Energy efficient MOF-based mixed-matrix membranes for CO_2 capture, M^4CO_2, 3rd status report, December 2014, Zaragoza.

S. Friebe, J. Caro, Energy efficient MOF-based mixed-matrix membranes for CO_2 capture, M^4CO_2, 4th status report, June 2015, San Sebastian.

S. Friebe, B. Geppert, J. Caro, Fuel Cell turned on its head - Hydrogen from waste gas, Festkörpernachmittag, July 2015, Salzgitter Flachstahl GmbH.

S. Friebe, J. Caro, Energy efficient MOF-based mixed-matrix membranes for CO_2 capture, M^4CO_2, 6th status report, June 2016, Edinburgh.

S. Friebe, J. Caro, Up-scalable Ultrathin MOF-Membranes of Varying Thicknesses by Spray Coating, International Zeolite Membrane Meeting, August 2016, Dalian.

S. Friebe, A. Mundstock, A. Knebel, J. Caro, industry cooperation Evonik-Creavis, final report, September 2016, Marl.

S. Friebe, J. Caro, Energy efficient MOF-based mixed-matrix membranes for CO_2 capture, M^4CO_2, 7th status report, December 2016, Sofia.

Poster Presentations

S. Friebe, N. Wang, L. Diestel, Y. Liu, A. Schulz, A. Mundstock, J. Caro, Deuterium/hydrogen permeation through different molecular sieve membranes: ZIF, LDH, zeolite. Deutsche Zeolith-Tagung, March 2015, Oldenburg.

S. Friebe, A. Mundstock, D. Unruh, F. Renz, J. Caro, NH_2-MIL-125 as membrane for carbon dioxide sequestration: Thin supported MOF layers contra Mixed-Matrix-Membranes. Deutsche Zeolith-Tagung, March 2016, Gießen.

A. Knebel, **S. Friebe**, N. C. Bigall, M. Benzaqui, C. Serre, J. Caro, Comparative Study of MIL-96(Al) as Continuous MOF-Layer and Mixed-Matrix-Membrane. Deutsche Zeolith-Tagung, March 2016, Gießen.

S. Friebe, A. Mundstock, D. Unruh, F. Renz, J. Caro, NH_2-MIL-125 as membrane for carbon dioxide sequestration: Thin supported MOF layers contra Mixed-Matrix-Membranes. International Zeolite Membrane Meeting, August 2016, Dalian.